Design and Development of Polymer Optical Fiber Based Platforms for Glucose Detection

by

Mikel Azkune Ulla

A dissertation submitted to the School of Engineering of Bilbao in Partial fulfilment of the requirements for the degree of PhD in Engineering

Bilbo, March 2019

Polimerozko zuntz optikoetan oinarritutako plataformen diseinu eta garapena glukosa detektatzeko

Mikel Azkune Ullak egindako tesiaren txostena,
Euskal Herriko Unibertsitatean (UPV/EHU)
Ingeniaritzan Doktore titulua
eskuratzeko aurkeztua.

Bilbo, 2019ko martxoa

“…ezaren gudaz baietza sortuz,
ukazioa legetzat hartuz beti aurrera joatea…”
Izarren hautsa
Xabier Lete

Acknowledgments / Eskerrak

Lerro xume hauen bitartez, liburu honetan laburbiltzen den lan guztia aurrera eraman ahal izateko beharrezkoak izan diren pertsonei merezitako aitorpena egin nahiko nieke. Horien artean, nola ez, familia aurkitzen da, hitz-sorta honetan agertzen dena beraien harrotasun arrazoi izatea espero dudalarik. Lagunak ere, beti eskura egoteagatik eta pena zein poz guztiak pairatzeko prest izateagatik eskerretan agertzea ere merezi dute, noski. Hirugarren helduleku nagusi izanik, azken lau urte eta erdietan ezagutu eta laguntzeko prestutasuna aurkeztu duten ikerlari guztiak eskertu nahiko nituzke. Bilbon, Leioan zein Jenan laguntzeko prest dagoen jende eskuzabala besterik ez baitut topatu. Hainbeste izanik tesi honetan eskua sartu duten kideak, banan-bana izendatzea ezinezkoa litzatekela; horregatik, tesi hau zueri esker, zuentzat.

Bestetik, tesi-lan hau egitea ahalbidetu duten hainbat ikerkuntza talde zein erakunde eskertu nahiko nituzke. Lehenik eta behin, Euskal Herriko Unibertsitateko (UPV/EHU) Fotonika Aplikatuaren Taldea bere osotasunean. Esker horiek, gainera, Bilboko Ingeniaritza eskolako Komunikazion Ingeniaritza sailari zabaldu behar zaizkio. Horietaz gainera, Zientzia eta Teknologia fakultateko Kimika Fisikoa saileko Labquimac taldeari ere esker bero bat zor diot, tesiaren momentu zailenetako batean nire ikerkuntza bideratzeagatik.

Leibnizko IPHT zentroari eta Jürgen Popp zuzendariari eskerrik beroenak luzatu nahiko nizkieke, mundu mailan punta-puntako ikerkuntza egiten diharduten zentru eder honetan hiru hilabetez onartzeagatik.

Gainera, tesia aurrera eraman ahal izateko finantziazioa eskaini didan Euskararen eta Etengabeko Prestakuntzaren arloko Errektoreordetza derrigor eskertu behar dut, bekarik gabe ezinezko bailitzateke lau urteko lan hau.

Azkenik, eta modu berezian, Gotzon Aldabaldetreku Etxeberria eta Iñaki Bikandi Irazabal zuzendariek ere zor duten esker ona eta onarpena lerro hauetan idatzia egotea gustatuko litzaidake, bidean izandako zailtasun guztiak batera iragan ditugulako.

Index / Aurkibidea

Index of figures / Irudien aurkibidea

Index of tables / Taulen aurkibidea

Chapter 1/1. Kapitulua

Introduction

Sarrera

Abstract—In the first chapter, we make the introduction to the context in which this work is placed, together with the settlement of the main goals. In first place, biosensors and their historical evolution until the current state-of-art are described. Furthermore, optical fiber's basics, focusing on polymeric ones, are explained. The section is completed with the description of microstructured polymer optical fibers. After that, the experimental techniques used along this work are described, and finally, the main goals for this thesis are defined.

Laburpena—Lehenengo kapitulu honetan, tesia kokatzen den testuinguruaren sarrera egiten da, eta lan honen helburu nagusiak ezartzen dira. Lehenik eta behin, biosentsoreak zer diren eta heuren garapen historikoa azaltzen da, gaur egungo egoera azalduz. Bestetik, zuntz optikoek eta, bereziki, polimeroz eginikoek dituzten ezaugarriak sakonki azaltzen dira, polimerozko zuntz optiko mikroegituratuekin amaituz. Ondoren, tesian zehar erabili diren neurketa teknikak azaltzen dira, eta azkenik, tesi-lan honen helburu ezberdinak finkatzen dira.

Duela 50 urte inguru, telefono deiak kobrezko kable bikoitz kiribildu batetik transmititzeak zekartzan arazoez jabetuz, *Standard Telecommunication Laboratories*-eko (STL, Harlow Essex, Erresuma Batua) ikertzaileek teknologia alternatibo batean pentsatu zuten. Honela, *Charles Kao*-k eta *George Hockham*-ek argia beirazko geruza meheen bitartez transmititzeko lehen pausuak gauzatu zituzten. Bi ikerlari hauek, telekomunikazio sistema bat erakargarri izatera heltzeko, atenuazio-maila 20 dB/km-ko balio maximoan finkatu zuten. Garai horretan beira arina erabiliz 100 dB/km-ko atenuazioa lortzen zuten ikerlariek. Ordutik, beirazko zuntzen teknologia modu geldiezinean garatu da gaur egungo komunikazio gehienak beirazko zuntz optikoen bitartez izatera iritsi arte.

Bestalde, 60ko hamarkadan polimerozko zuntz optikoak (PZO) garatzen hasi ziren hainbat ikertzaile, beti ere argiztapen asmoetarako. Izan ere, polimeroen atenuazio

altua eta eskaera falta zirela medio, PZOen datu-transmisioetarako erabilera arakatu gabeko aukera izan zen. Lehen PZO komertzialek 650 nm-tan 500 dB/km-ko atenuazioa zuten, baina hau modu esanguratsuan hobetu zen maila-indizedun PZOak (MI-PZO) erabiltzetik indize-gradualeko PZOak (IG-PZO) erabiltzera pasa zirenean. Mota honetako PZOak *Koike* eta besteek aurkeztu zuten polimero amorfo perfluorinatuak (PF) erabiliz [1]–[3]. Aurkikuntza honek komunitate zientifikoren arreta PZOei bideratzea erakarri zuen; eta ordutik, mundu osoko ikerkuntza talde sendoak dabiltza lanean.

Hala ere, zuntz optikoen eta PZOen teknologia datu-komunikazioetarako erabiltzeaz gain, sentsore gisara erabiltzeak etorkizun handia du, eta gai honetan oinarrituko da tesi-lan honen ikerkuntza osoa. Dokumentu guztian zehar ikusiko den moduan, optika eta PZOen eremuak oso interesgarriak dira sentsore gisa erabiltzerako orduan, hainbat lan izanik horren erakusgarri [4]. Beirazko zein polimerozko zuntz optikoak hainbat fenomeno neurtzeko erabiltzen dira gaur egun, egituren osasun monitorizazioa egiteko edo tenperatura altuak ingurumen arrotzetan neurtzeko, besteak beste [5].

Gure kasuan PZOak erabiliz, glukosaren detekzio eta zenbatzean aritu gara biosentsoreen testuinguruan. Hori ahalbidetzeko, PZOetan oinarritzen diren hainbat detekzio eredu jorratu dira. Gizarteak duen eskaera handia dela eta, glukosa neurtzeko sentsoreek garrantzi handia dute. Azken urteotan diabetesa pairatzen duten gaixoen kopurua handitu egin da, *Osasunerako Mundu Erakundeak* (OME [6]) gaixoen kopurua 400 milioitan zenbatzen duelarik. Gainera, diabetesa lehen heriotza goiztiarren kausa izatera iritsi da eta zazpigarrena heriotza orokorrak kontuan izanik. Heriotzaz gain, itsutasuna, bihotzeko erasoak eta giltzurrunean kalte handiak sortzen ditu gaixotasun honek. Gaur egungo bizi estiloarengatik zenbaki hau igo egingo dela espero da; biztanleria helduaren herenak gehiegizko pisua eta hamarrenak obesitatea baitute.

Honenbestez, tesi-lan honetan glukosa helburu-molekula gisa hartuz, hau detektatzeko PZOetan oinarritzen diren bi detekzio plataforma aurkezten dira. Horren aurretik, ordea, eta testuinguru zabal bat aurkezteko asmoz, biosentsoreen zein PZOen historia eta denboran zehar izaneko bilakaerak azalduko dira. Ondoren, tesian zehar jorratu diren neurketa ereduak aztertuko dira, detekzio plataformek izan beharreko ezaugarriak definituz. Azkenik, tesi honetako helburuak finkatuko dira.

1.1 Biosentsoreak

International Union of Pure And Applied Chemistry (IUPAC) erakundearen arabera [7], biosentsore bat ondorengoan datza: seinale elektriko, termiko edo optiko bati, eta erreakzio biokimiko espezifiko bati esker, osagai kimikoak detektatzen dituen gailua, entzima isolatu, inmunosistema, ehun, organulu edo zelula oso batek bitartekari gisa jokatuz. Honenbestez, oinarrizko biosentsore batek honako hiru osagaiak izango ditu [8]:

- Lehenik eta behin, hautakortasuna aurkeztuko duen osagai bat izango du, helburu-molekula besteengandik banatuko duena. Normalean, gertaera honek lotura kimikoen osaketa sortuko du, eta hori dela eta, elementu biokimiko gisa ezagutzen da.
- Bigarrenez, transduktore bat ere agertuko da. Transduktoreak lotura kimiko horren sorrera seinale neurgarri batean bilakatu beharko du. Adibidez, errefrakzio-indizea (EI) edo eroankortasun elektrikoa aldatuko du.
- Azkenik, seinale aldaketa neurtuko duen metodo bat behar da. Honek aurreko puntuan esandako transduktorearen seinale aldaketa neurtuko du.

Hala ere, definizio eta ezaugarri zehatz hauek urte askotako garapenaren eta hainbat ikerkuntza eremuren baturaren ondorio izan direnez, definizio honen adostasuna lortzea ez da gauza erraza izan. Horregatik, ondorengo atalean biosentsoreen bilakaera historikoa azalduko da.

1.1.1 Biosentsoreen bilakaera historikoa

Azken 50 urteetako literatura aztertzen bada, *biosentsore* kontzeptua erakargarri edo itxaropentsu gisako ideiekin hertsiki lotuta egon dela ikusten da [9]. Hala ere, ikerkuntza eremu honetan zenbait jatorri ezberdinetako ikertzaileak aurki daitezke eta honek biosentsoreen definizioa hainbat ikuspuntu ezberdin kontuan izatera behartu du. Hala ere, argi dago biosentsore kontzeptuaren esanahia asko aldatu dela jatorrian eman zitzaionetik.

Orain dela 50 urte, biosentsore bat lagin biologikoetan aurkitzen zen osagai kimiko baten kontzentrazioari erantzuten zion gailu autonomoa zen. Definizio honi helduz, lagin biologiko batean darabilkigun eta fenomeno fisiko (termometroa) edo kimiko (ehun

biologikoetan inplantaturiko mikroelektrodoa) bat neurtzen duen edozein sentsore har daiteke biosentsore moduan. Gaur egungo ikuspuntutik, aitzitik, definizio hau ez da zuzena, besteak beste, transduktore zein hautakortsaunari buruzko aipurik ez baita egiten.

Gaur egun ezagutzen diren biosentsoreen aurrekaria 1956. urtean *Lelan C. Clark*-ek aurkezturiko *oxigeno zundan* datza. Honekin batera, sentsore elektrokimikoak adimendunago nola egin aurkeztu zuen 1962an New York-eko Zientzia Akademian eginiko konferentzia batean [10]. Horretarako, entzima transduktoreak sandwich-gisako geruzetan gehitzen zituen. Honenbestez, lehen biosentsore adibidea glukosa oxidasa atxikitzen zuen dialisi-mintz batetan oinarritu zen eta 1.1 irudian ikus daiteke aurkeztu zuen mota honetako lehen biosentsorearen eskema. Esan beharra dago gailu hau entzima elektrodo gisa argitaratu zuela [11]. Biosentsore honetan glukosa kontzentrazioa igotzean, oxigeno kontzentrazioa jaisten zen modu proportzionalean, eta azken hau neurtuz glukosa zenbatzen zen. 70. hamarkada aurretik, oinarri beretsua zuten hainbat argitalpen ere egin ziren [12], [13]. Hamarkada horretatik aurrera hasi zen biosentsoreen inguruan ikerkuntza sakonagoak egiten komunitate zientifikoa, beti ere entzimaren bat sentsore elektrokimiko bati gehituz. Gaur egun, hau kontsideratzen da biosentsoreen hasiera, sentsore elektrokimikoak eta osagai biologikoak batzen dituen eremua.

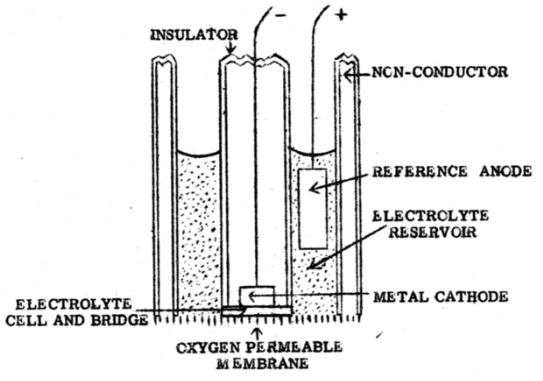

1.1 Irudia. *Lelan C. Clark*-ek aurkezturiko oxigeno zundaren eskema [11].

Aipaturiko mugarriek komunitate zientifikoaren interesa handiagotu eta ikerkuntza sendoen hasiera eragin zuten. Hasiera batean, biosentsore berriak elementu biologikoa eta transduktorea eraldatuz lortu ziren. Lehenik, gailu potentziometriko edo

anperemetrikoetan atxikitu ziren entzimak, organululak, bakteriak edo ehun biologikoak; horretarako entzima espezifikoak erabiliz. Ondoren, ikerkuntza korrontea gailu optiko, termometriko edo piezoelektrikoetara aldatu zen; azken berrikuntza gailu magnetikoena izanik. Entzimak eta hauetan oinarriturik dauden elementu biologiko guztiak osagaitzat dituzten biosentsoreak elementu katalitiko gisa ezagutzen dira. Hauetatik at, beste biosentsore klase ezagunena kidetasun elementuek osatzen dute eta antigorputz, lektina, azido-nukleiko (ADN zein RNA), eta azken urteotan garatutako estekatzaile sintetikoek osatzen dute.

Ondoren, biosentsoreen historian eman diren mugarri garrantzitsuenak azalduko dira, garapen historikoa hobeto ulertzeko asmoz.

1.1.2 Biosentsore-ikerkuntzan emandako mugarri garrantzitsuenak

Azken 30 urteetan emaniko mugarri garrantzitsuenak azaltzen dira ondorengo puntuetan. Hauek hiru gertakizunetan banandu arren, nahikoak dira biosentsoreen gaur egungo egoera nondik eratorria den jakiteko.

1.1.2.1 Glukosa arkatzaren kasua

1984. urtean, *Cass* eta bestek ferrozenoa eta antzerako substratu materialen erabilgarritasuna sentsore anperemetroko gisa frogatzen zuen artikulu bat argitaratu zuten [14]. Urte gutxiren buruan, *Medisense Exatech Glucose Meter* merkaturatu zen eta historian zehar izan den biosentsore salduena bilakatu zen. Hasiera batean, arkatzak elektrodoak inprimaturik eta erabilera bakarreko pantaila txiki bat zituen, 1.2 irudian ikusten den kaxatxoetan saltzen zelarik.

Gailu honek sekulako aurrerapausoa eragin zuen biosentsoreen merkatuan. Lehenik eta behin, bere salmenta-bilgarria arkatza itxurako gailu txiki bat zen odoleko glukosa kontzentrazioa azaltzeko gai zena, eroso eta sinplea. Bestetik, erabilera bakarreko elektrodoa inprimatuta zuen pantailak kalibrazio fasea saihestea ahalbidetzen zuen. Biosentsoreen munduan, hau aurrerapauso itzela izan zen, ordura arteko sentsore guztiak kalibratu egin behar baitziren erabili baino lehen (pH elektrodoak, ISE sentsoreak, …). Honenbestez, gailu komertzial erabilerraz hau diabetesa pairatzen zuten hainbat herritarrengana oso erraz hedatu zen, merkatu andana sortuz. Lehen merkaturatze

honetatik, oinarri beretsuko hainbat produktu ere kaleratu dira, glukosaren detekzioa eta neurketa baitira biosentsoreen artean merkatu handiena duena.

1.2 Irudia. Medisense Exatech Glucose Meter-a.

1.1.2.2 *BIAcore*-ren agerpena merkatuan

1982an *Pharmacia* izena zuen enpresa bateko zenbait ikertzaile *Linkoping*-eko unibertsitateko fisika eta biokimika ikertzailerekin elkarlanean hasi ziren molekulen arteko interakzioa neurtzen zuen bioanalitika instrumentu berri baten garapenerako. Honela, 1984ean *Pharmacia Biosensor* izeneko enpresa berri bat osatu zuten. 1990. urtean *BIAcore* izenarekin gailu berri bat merkaturatu zuten, biosentsore komunitatean zerresan handia eman zuena (1.3 irudia).

Gailu berri honen prezioa garai horretan merkatuan aurkitzen ziren gailu optiko edota elektrokimikoak baino 100 aldiz garestiagoa zen eta gainazaleko plasmoien erresonantzian oinarritzen zen. Gainera, guztiz automatizatua zegoen eta laginaren interakzio biomolekularrak neurtzen zituen.

Gailu honek ikaragarrizko aurrerapausua ekarri zuen. Izan ere, 192 lagin batera kudeatu zitzakeen inolako erabiltzaileren beharrik gabe, modu honetan, errepikagarritasun

handia bermatzen zuelarik. Horretaz gain, tenperaturaren kontrol hertsia eskaintzen zuen (0.1 ^{o}C-tan finkatua) eta biomolekulen zinetika ikerkuntzak egiteko erabiltzen zen. Dena den, gailu honen aurrerakuntza nagusia baruan zekarren sentsore-txip teknologian zetzan, honek biomolekulen immobilizazioa oso modu sinplean bermatzen baitzuen.

Instrumentu hau enpresa farmazeutikoei saldu zitzaien lehenengoz, medikamentu berrien diseinu-denborak modu esanguratsuan laburtu zituztelarik. Ondoren, erabilera zabaldu zen eta zenbait ikerkuntza laborategik afinitate kimikoak aztertzeko erabili zuten.

1.3 Irudia. BIAcore neurgailuaren irudia.

1.1.2.3 Azido nukleikoan oinarrituriko sentsoreak

Azido nukleikoa (AN) nukleotido katez osaturiko makromolekula bat da. Izaki bizidunetan AN ezagunenak azido desoxirribonukleikoa (DNA) eta azido erribonukleikoa (RNA) dira, edozein zelula zein birusetan aurkitu baitaitezke. Tradizionalki, AN-ak informazio genetikoa transferitzen duten makromolekula moduan ezagutu dira. Hala ere, 90ko hamarkadaz geroztik, AN molekula batzuk molekula ezberdinak hautakortasun handiz atxikitzeko gai direla ikusi da. Molekula mota honi aptamero deritzo. Honela, aptameroek molekula organiko txikietatik hasi eta proteina, zelula zein partikula birikoak ere atxiki ditzakete. 1994an aurkikuntza garrantzitsua egin zen, lehenengo aldiz DNA kateek katalizatzaile gisa ere joka zezaketela erakutsi baitzen. Honela jokatzen duten DNA

kateak eta aptameroak DNA funtzional gisa dira ezagunak eta horien funtzioak asko zabal daitezke.

Honenbestez, AN-ak eta estimulu kimikoei erantzuteko gai diren DNA kateak biosentsoreak osatzeko erabili izan dira. Mota honetako biosentsoreak DNA/RNA zatiak edo espezie biologikoak detektatzeko erabiltzea da ohikoena.

1.1.3 Biosentsore motak

Biosentsore munduan izaniko hiru mugarri hauek aztertu ostean, gaur egun aurki daitezkeen biosentsore moten sailkapen bat azaltzen da [15]. Sailkapen hau biosentsorearen transduktorearen edo osagai biologikoaren eta darabilten elementu biokimikoaren araberakoa izango da [16], [17]. Biosentsore diseinuak egiterako orduan, edozein motako elementu hartzaile, analito edo helburu-molekula konkretu bat atxikitzeko gai diren elementuak transduktore ezberdinekin konbina daitezkeela aipatu behar da. Hala ere, egungo merkatuaren % 80 transduktore elektrokimikoek osatzen dute.

1.1.3.1 Transduktore elektrokimikoak

Transduktore elektrokimikoen artean aukera zabala dagoenez, azterketa zehatzago bat egingo da.

- Transduktore potentziometrikoak: erreferentzia- eta seinale-elektrodoen arteko potentzial diferentzia da sentsore mota hauen seinale analitikoa. Hala ere, normalean bi seinale elektrodo darabiltzate eta bi elektrodoak geruza erdiiragazkor baten bidez banatzen dira. Normalean transduktorea elektrodo ioi-hautakor batez osatzen da, pH elektrodoa izanik hedatuen dagoen mota honetako biosentsorea.
- Transduktore voltametrikoa: espezie aktiboaren erredukzio edo oxidazio korrontea da biosentsore hauetan neurtzen dena. Ez dira oso ohikoak biosentsore gisa erabiltzerako orduan eta are gutxiago entzimak neurtu nahi direnean. Hala ere, afinitate handiko interakzioak neurtzeko erabil daitezke.

- Transdukore inpedimetrikoak: sentsore hauek helburu-molekula atxikitzen den zelula elektrokimikoaren inpedantzia aldaketa neurtzen dute korronte alternoaren maiztasunaren arabera.
- Eremu-efektuko transistoreak: normalean geruza biosentikorra eremu-efektuko transistorearen sarrerateko bat den eta ioei sentikorra den mintz baten gainean ipintzen da. Eraldaketa biologiko hauei esker, peptido txikiak eta proteinak detekta daitezke, baita beraien karga ere. Hala ere, mota honetako sentsoreen desabantaila nagusia ingurumenarekiko duen dependentzia da, honek aplikazio eremuak mugatzen baititu.

1.1.3.2 Transduktore optikoak

Normalean transduktore optikoak fluoreszentzia, xurgapena, lumineszentzia, gainazaleko plasmoien erresonantzia edo argiak jasaten duen dispertsioaren espektroskopian oinarritzen dira. Tesi honetan garatuko diren sentsore plataformak uhin ebaneszentearen xurgapenean eta Raman espektroskopian oinarrituko dira. Bi efektu hauek aurrerago modu sakonagoan azalduko dira.

1.1.3.3 Gailu piezoelektrikoak

Potentzial elektrikoak eragindako deformazio bat pairatzen duten kristalak darabiltzaten sentsoreek osatzen dute talde hau. Maiztasun zehatz bateko potentzial alternoak uhin geldikor bat osatzen du kristalean. Elementu hartzaile biologiko batez estalia dagoen kristal batek analito bat atxikitzean, honen erresonantzia maiztasuna aldatu egingo da, atxikimendua egon dela bermatuz. Antigenoak pikometrozko kontzentrazioetan detektatzeko gai direnez, gaur egun ezagutzen diren inmunosentsore sentikorrenak dira.

1.1.3.4 Transduktore termometrikoak

Nahiz eta oso komunak ez izan, transduktore termometrikoak analito baten kontzentrazioa neurtzeko erabiltzen dira. Mota honetako transduktoreek energia termikoa sortzen dute erreakzio kimiko baten ondorioz, eta tenperatura aldaketa hau neurtuz kontzentrazioa neurtu daiteke.

Transduktore motak aztertu ostean, helburu-molekula edo analitoa atxikitzeko duten elementuaren araberako sailkapena egingo da.

1.1.3.5 Sentsore entzimatikoak

Talde honetan aktibitate biologikoa aurkezten duten entzima-prestatu edo prestatu-biologikoak sartzen dira; bai ehun, bai mikrobio kultiboak ere. Erreakzio elektrokimiko bat sortzen duen entzima bat eta substratu material bat batuz osatzen da sentsore entzimatiko motarik sinpleena. Sentsore entzimatikoen adibide komunenak glukosa eta urea sentsoreak dira.

1.1.3.6 Inmunosentsoreak

Kasu honetan, hartzaile biokimiko gisa immunitate-sistemak jariatzen dituen immunoglobulina izeneko babes-proteinak erabiltzen dira. Immunoglobulina edo antigorputzek lotura indartsuak osatzen dituzte antigenoekin, eta hauen arteko interakzioen monitorizaziorako erabiltzen dira gehienbat. Adibidez, giza-odolean antigorputzen agerpena eta, ondorioz, infekzio ezberdinak detektatzeko erabiltzen dira gehienbat.

1.1.3.7 DNA sentsoreak

DNA sentsoreen osagai biokimikoak NA ezberdinak dira. Normalean, hauek ez dira organo bizidunetatik lortzen, DNA anplifikazio bidez sintetizatzen dira polimerasa kate-erreakzio bitartez. Gainera, osagai hauek modifikatu egin daitezke sentikortasuna handitzeko edo beste efekturen bat lortzeko asmoz. Helburu-molekula bakoitza erakartzeko zein egitura osatu behar den aurresatea ezinezkoa denez gaur egun, hainbat saiakera egin behar dira, horien artean egokiena aukeratuz eta aptamero egokia osatuz.

DNA sentsoreen beste helburu bat DNA kateekin zenbait proteina edo konposatu ez-makromolekularrek duten interakzioa ikustea da. Honela, afiliazioak ikusi, desordena genetikoak detektatu edo modifikazio genetikoa jasan duten produktuen detekzioa egin daiteke.

1.1.3.8 Biosentsore mikrobialak

Mota honetako sentsore gehienetan monitorizazio gailua eta osagai biologikoa bananduta aurkitzen dira. Hori dela eta, biosentsore mikrobial bat helburu-molekula neurtu nahi den disoluzioan aurkitzen den ehun bertikal batez osatua egon daiteke, eta transduktorea disoluzioan murgilduta aurki daiteke gertatzen ari den erreakzioa neurtzen.

Mikroorganismoak helburu anitzekin erabili daitezke, disoluzioan aurkitzen diren organiko oxidatzaileak zenbatzeko, besteak beste. Sentsore mota hauek hautakortasun baxua eskaintzen dute organismo unizelularrek substantzia organiko anitz deskonposa baititzakete antzerako erreakzioa emanik.

1.1.3.9 Zelulen egitura supramolekularrean oinarrituriko biosentsoreak

Sentsore entzimatiko eta DNA sentsoreen artean kokatuko genuke talde hau. Izan ere, biosentsore hauek egitura konplexua duten entitate intramolekularrak atxikitzeko gai dira. Elementu atxikitzailearen konplexutasuna eta hau aurkitzen den ingurune naturaletik ateratzean duen ezegonkortasuna dela eta, oraindik ez dutela merkatu zabalik esan daiteke. Prozesu biokimikoak aztertzeko erabiltzen dira ikerkuntzan, zenbait kutxatzaileren poluzioaren prozesua ikuskatzeko, adibidez.

1.2 PZOak

Zuntz optikoak material dielektrikoz eginiko eta espektro elektromagnetikoaren uhin ikusgai edo infragorriak eroateko gai diren hariak dira. Horretaz gain, ondorengo ezaugarriak izaten dituzte: silizezkoak edo plastikozkoak izan daitezke, eta ohiko kobrezko kableak baino datu-kantitate handiagoa eta abiadura handiagoan transmititzeko gai izaten dira. Gure kasuan, polimerozkoak jorratuko ditugu soilik, tesi-lan hau aurkitzen den testuingurua dela eta.

Aurrez esan den gisa, lehen PZOak argiztatzeko helburuz garatu ziren 60. hamarkadaren inguruan. Honela PZOen aurrekaria poli(metil metakrilato)-zko (PMMA) MI-PZO-ak izan ziren. Polimeroa beirarekin alderatuz, material merkeagoa eta erabilerrazagoa zen eta horrek komunikazio-sareak osatzeko material interesgarria egiten

zuen. Hala ere, beirarekin alderatuz atenuazio askoz ere handiagoa zuen, garaian 500 dB/km-koa 650 nm-ko uhin-luzera erabiliz.

Murrizketa hori, dena den, *Keio* Unibertsitateko *Koike* irakasleak gainditu zuen lehen IG-PZO-ak fabrikatzean [1]–[3]. Horretarako, polimero amorfo PFetaz baliatu zen atenuazioa minimizatzeko [18]. Momentu horretatik aurrera, PZOak oso erakargarriak bilakatu ziren transmisio sistema moduan erabiltzeko[19].

PZOak, komunikazioetan erabiltzeaz gain, beste asmo batzuetarako ere garatu ziren. Hori dela eta, gaur egun hainbat eremu ezberdinetan ikus ditzakegu PZOak, sentsore, laser-, anplifikagailu, eta kommutadore- optiko gisa, adibidez. PZOen garapen eta ikerkuntza, historian zehar izandako mugarri garrantzitsuenekin batera, ondorengo atalean azalduko da.

1.2.1 PZOen bilakaera historikoa

Alexander Graham Bell-i, telefonoaren asmatzaile izendatzeaz gain, fotofonoaren garapena ere esleitu behar zaio. Izan ere, XIX. mendean eraiki zuen gailu honen bitartez eguzki izpiak modulatuz informazioa transmititzeko gai izan zen. Hala ere, fotofonoak ez zuen arrakasta handirik izan, ondo diseinaturiko tresna izanik, telefonoak iada nahikoa aurrerakuntza ekarri baitzuen. Edonola ere, *Bell*-ek fotonikari buruzko hainbat printzipio ezarri zituen, gaur egun oraindik erabilgarriak direnak.

Lehen mugarri hartan gizarteak behar zuen informazioaren transmisio-abiadura hartatik gaur egungora hainbat magnitudetan hazi da eskaria. Gaur egun negozio guneetan edo aisialdiko kontsumitzaileen biztanleriaren artean transmisio-abiadura andanak eskatzen zaizkio sareari. Ia-ia esan liteke bizi dugun informazioaren garai honetan berebiziko garrantzia duela interneteko abiadurak. Eredu honetan PZOetan oinarrituriko komunikazio sistemak dira etorkizunik oparoena eskaintzen dutenak. Batez ere azken 100 metroetarako erabiltzeko dira aproposak, zuntz optikoen abantailak (banda-zabalera altua, atenuazio baxua eta immunitate elektromagnetikoa) eta, beste alde batetik, manipulazio erraztasunak batzen baitira [20], [21].

PZOen komertzializazioa 1975. urtean hasi zen *Mitsubishi Rayon* konpainiaren eskutik. Nahiz eta 1966an *Dupont* konpainiak lehen MI-PZO-ak sortu, patente guztiak *Mitsubishi Rayon*-i saldu zizkioten, eta hauek, *Eska* izenarekin komertzializatu zuten.

Lehen PZO hau PMMA-z egindako nukleo batez eta partzialki PF-riko estaldurarekin osatua zegoen eta 1000 dB/km-ko galerak zituen; oraindik oso altuak. Hurrengo urteetan beste bi konpainia gehitu ziren PZOen merkatura *Asahi Chemical* eta *Toray* izenekoak. Hiru enpresa hauek PZOen merkatua kontrolatu zuten hasiera horretan, baina atenuzaio optiko handiak zirela eta, ez ziren datu-transmisioetarako sareetan zabaldu.

80ko hamarkadan ikerkuntza nabariak egin ziren PZOen inguruan. Besteak beste, 1983an *Kaino* eta besteek deuteraturiko PMMA erabiliz, atenuazio baxuko MI-PZO-ak lor zitezkeela frogatu zuten [22] . Bitartean, *Groh* eta besteek PMMAn oinarrituriko PZOen atenuazioaren limite teorikoa kalkulatu zuten [23]. Argitalpen honek aipaturiko hiru konpainien arteko lehia sortu zuen eta hamarkada horren amaierarako muga honen inguruko atenuazio-optikoak zituzten PZOak komertzializatu ziren. Horren adibide da *Mitsubishi Rayon* enpresak kaleraturiko eta 150 dB/km-ko atenuazioa zuen MI-PZO-a. Zuntz honekin 50 Mb/s-ko banda-zabalera lor zitekeen 650 nm-ko argi-iturriarekin. PZOetan izan den atenuazio optikoaren garapena ikus daiteke 1.4 irudian, bai MI-PZO-entzat, bai IG-PZO-entzat.

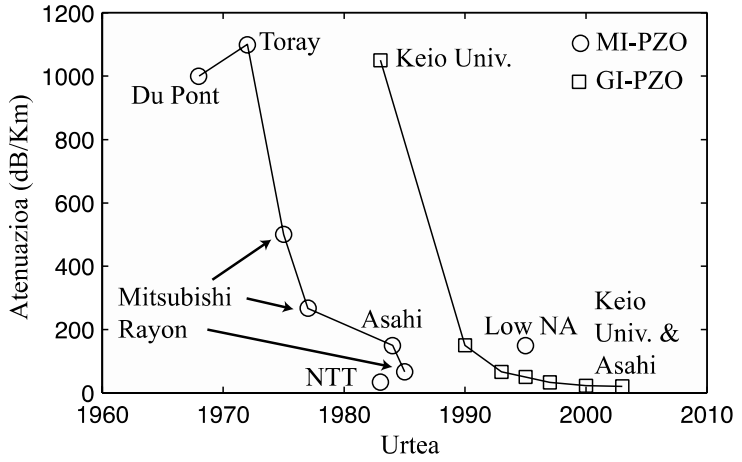

1.4 Irudia. PZOetan izan den atenuazio optikoaren garapena.

IG-PZO-etan zentratuz gero, lehen IG-PZO-ak 1982. urtean sortu ziren. Hain zuzen ere, *Keio* Unibertsitateko *Koike* irakasleak garatu zituen eta lehen IG-PZO-ak 1070 dB/km-ko galerak aurkezten zituen 670 nm-etarako [1]–[3]. Aurrekari honetatik abiatuz, fabrikazio prozesuak doituz eta hidrogeno atomoak fluor atomoekin ordezkatuz,

atenuazio-optikoak modu nabarmenean txikiagotu zituzten 150 dB/km-taraino iritsiz. Hurrengo mugarri garrantzitsua 1996. urtean *Keio* Unibertsitatea eta *Asahi Glass* konpainiaren elkarlanetik sortu zen. Izan ere, lehendabiziko PFzko IG-PZO garatu ziren, ordura arteko PMMAzko PZOen atenuazioa herenera txikiagotuz, hots, 50 dB/km-ko atenuazioa lortuz 650-1300 nm-tako tartean. Material hau CYTOP® izenarekin ezagutzen da. Aurkikuntza honen ondotik *Asahi Glass* enpresak *Lucina* izeneko dibisioa sortu zuen, datu-transmisio gaitasun handiko PZO hauek merkaturatzeko asmoz [24]. 1.1 taulan ageri da PZOek izandako datu-transmisio kapazitatearen bilakaera.

1.1 Taula. PZOen transmisio ahalmenaren eboluzio historikoa.

Bit-Abiadura (Gb/s)	Distantzia (m)	λ (nm)	Afiliazioa
0.531	100	650	Essex Unib.
1	30	670	IBM & Keio Unib.
2.5	100	650	Keio Unib. & NEC
2.5	200	1300	Keio Unib, Asahi G. & Fujitsu
2.5	200	650	Keio Unib., Mitsubishi R., NEC & Eindhoven Unib.
5	140	1300	Keio Unib., Asahi G. & Eindhoven Unib.
2.5	450	1300	Keio Unib., Mitsubishi R., NEC & Eindhoven Unib.
11	100	850	Asahi G., Bell Labs & Lucent Tech.
1	1000	850	Asahi G. & Eindhoven Unib.
4	300	1550	Keio Uninb., JST-ERATO & Asahi G.
40	100	1325	Georgis Inst. Tech.

Azken hamarkadetan hobekuntza nabaria gertatu da PZOen datu-transmisio abiadura, banda-zabalera edota bit-emariari erreparatuz. Horren adibide da 1992an *Koike* eta besteek 10 m-ko distantzian lorturiko 5 GHz-etako banda-zabalera IG-PZO-ak erabiliz [25]. Ondoren, 1994. urtean hain zuzen ere, 100 m-ko distantzian 2.5 Gb/s-ko transmisio-abiadura frogatu zen IG-PZO-ak erabiliz [26]. Hala ere, aurrerapauso handiena 1999. urtean eman zen 11 GB/s-ko abiadura-tasara heldu baitzen PFzko IG-PZO a erabiliz, modu-anitzeko beirazko zuntzaren abiadura-marka hautsiz [27]. Pausoz pauso emaniko aurrerapen txikiei esker, 2000. urtean 1 km-eko distantzian zehar 1 Gb/s-ko transmisio-abiadura lortu zen [28]. Azken mugarri garrantzitsua 2010. urtean gauzatu zen PFzko IG-PZO eta modulazio-teknika aurreratuak erabiliz 100 m-ko distantzian 47.4 Gb/s-

ko marka haustea lortu baitzen [29]. PZO teknologia sare lokaletan edo sarrera sareetan ezartzeko teknologia egokia dela ondoriozta daiteke eboluzio historikoaren azalpen honetan. Azken 40 urteetan izan diren mugarri garrantzitsuenak laburbildu dira 1.2 taulan.

Atal honetan ikusten den moduan, aipaturiko mugarri eta lorpen guztiak PZOak komunikazioetarako darabiltzate, aipatu behar baita ikerkuntza-korronte horrek eraman duela historikoki PZOen garapenaren zama. Izan ere, PZOak sentsore gisa erabiltzea azken urteetan jorratu den ikerketa-lerroa izan da. Horregatik oraindik lan gutxik aurkezten dituzte sentsore gisara lan egiteko diseinatu direnPZOak, eta normalean hasiera batean komunikazioetarako diseinaturikoak moldatu dira. Tesi-lan honetan aitzitik, aurrerago zehaztuko den moduan, zenbait PZO mikroegituraturen (PZOm) geometria zuntz bidez areagoturiko Raman espektroskopia (ZBARE) efektua sortzeko diseinatua izan da.

1.2 Taula. Azken 40 urteetan PZOekin erlazionaturiko mugarri garrantzitsuenen eboluzio historikoa datu-transmisoetarako.

Urtea	Erakundea	Mugarria
1968	Dupont	Lehendabiziko MI-PZO PMMA-zko nukleoarekin.
1972	Toray	Lehenengo MI-PZO poliestirenozko nukleoarekin.
1981	NTT	Atenuazio baxuko PMMA MI-PZO (55 dB/km @ 568 nm)
1982	Keio Unib.	Lehendabiziko IG-PZO (1070 dB/ km @ 670 nm)
	NTT	Lehen MI-PZO deuteraturiko PMMA-zko nukleoarekin (20 dB/km @ 650 nm)
1983	Mitsubishi Rayon	PMMA “Eska” MI-PZO (110 dB/km @ 570 nm)
1990	Keio Unib.	Abiadura altuko lehen transmisioa PMMA-zko IG-PZO-aren bitartez (3 GHz/km)
1992	Keio Unib.	Deuteraturiko PMMA-zko IG-PZO (55 dB/km @ 688 nm)
1993	Essex Unib.	531 Mb/s transmisioa 100 m-tan PMMA-zko MI-PZO-aren bitartez
	Keio Unib.	Lehen PZOzko anplifikagailua Errodamina B-rekin dopaturiko IG-PZO-aren bitartez (27dB @ 591nm)
1994	Keio Unib. & IBM	1 Gb/s transmisioa 30 m-tan IG-PZOren bitartez 670 nm-tan
	Keio Unib. & NEC	2.5 Gb/s transmisioa 100 m-tan IG-PZOren bitartez 650 nm-tan
	Asahi Chemical	Lehen nukleo anitzeko MI-PZO
1995	Mitsubishi Rayon & NEC	156 Mb/s transmisioa 100 m-tan MI PZOren bitartez eta gorri koloreko LED bizkorrarekin.
1996	Keio Unib. & KAST	Lehen IG-PZO PF (50 dB/km a 1300 nm)

		Galeren estimazio teorikoa PZO PF (0.3 dB/km a 1300 nm)
		Transmisio abiaduraren estimazio teorikoa IG-PZOetan (PMMA: 4 Gb/s 100 m-tan; PF: 10 Gb/s 1 km-tan)
1997	POF Consortium of Japan	ATM LAN-aren estandarizazioa (156 Mb/s 50 m-tan MI-PZO) ATM Forum-ean
	Keio Univ., Fujitsu & Asahi Glass	IEEE1394 normaren estandarizazioa (156 Mb/s 50 m-tan MI PZO)
		2.5 Gb/s transmisioa 200 m-tan IG-PZO PF-ren bitartez 1300 nm-tan

Urtea	Erakundea	Mugarria
1998	COBRA, Eindhoven Univ., Keio Univ., Asahi Glass & NEC	2.5 Gb/s transmisioa 300 m-tan IG-PZO PF-ren bitartez 645 nm-tan
	Matsushita	500 Mb/s transmisioa 50 m-tan IG-PZO-ren bitartez eta eta gorri koloreko LED bizkorrarekin.
1999	COBRA, Eindhoven Univ., Keio Univ. & Asahi Glass	2.5 Gb/s transmisioa 550 m-tan IG-PZO PF-ren bitartez 840 eta 1310 nm-tan
	Bell Labs & Asahi Glass	11 Gb/s transmisioa 100 m-tan IG-PZO PF-ren bitartez 830 eta 1310 nm-tan
2000	Asahi Glass	IG-PZO (Lucina) 16 dB/km-ko atenuazioarekin 1300 nm eta 569 MHz·km
2002		IEEE1394 estandarra berretsi eta ibilgailuentzako IDB-1394 osatu
2004	Asahi Glass	Lehen PMMA-zko IG-PZO komertzialki eskuragarri
2005	Chromis Fiberoptic	Lehen IG-PZO PF komertzialki eskuragarri
2010	COBRA & Eindhoven Unib.	47.4 Gb/s transmisioa 100 m-tan IG-PZO PF-ren bitartez 1300 nm-tan

1.2.2 PZO-en egitura

PZO estandarrak edo tradizionalak hiru geruzez osatzen dira, 1.5 irudian erakusten den gisa. Aurrerago ikusiko den moduan, eredu hau ez da beti errespetatzen, baina, hala ere, eredu honek PZOen transmisio ezaugarriak ulertzen laguntzen du. Gainera, PZOak fabrikatzeko erabiltzen diren polimeroak, gehienetan PMMAn oinarriturikoak, material amorfo eta dielektrikoak dira, zilindro itxurako zuntz optiko malguak osatuz. Aipatu diren hiru geruza hauek *nukleoa*, *estaldura* eta *estalkia* izan ohi dira. Argiaren transmisioa berma dadin, nukleoaren EIak estaldurarena baino handiagoa izan behar du, horrela barneko islapen osoa (BIO) gertatuko da. Horretarako materialen osaketa kimikoan aldaketa txikiak egiten dira. Bestalde, estalkiak babes mekanikoa eta isolamendua eskaintzen dio PZOari.

PZO komertzialek 125 eta 980 μm arteko nukleo erradioak (ρ) izaten dituzte, modu honetan zuntz erabilerrazak izanaz. Gainera, nukleoa osatzen duen materialarenEIa uniformea izaten da MI-PZO-etan eta graduala GI-PZO-etan. Estaldurarena aitzitik, uniformea. Erreferentzia gisa, lehenengoetan nukleoaren RI-a 1.492 izaten da eta estaldurarena 1.417. IG-PZO-etan, ordea, nukleoko EIa modu gradualean txikiagotzen da simetria ardatzaren distantziarekiko (r). 1.6. irudian ikus daitezke EI profilak eta zeharkako sekzioak.

1.5 Irudia. PZO baten egitura.

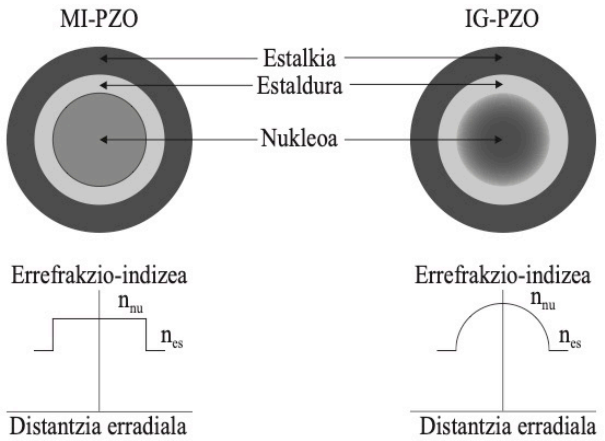

1.6 Irudia. MI-PZO et aIG-PZO-en EI profilak eta zeharkako sekzioak.

1.2.3 Zuntz optikoen sailkapena

PZOak sailkatzeko hainbat irizpide har daitezke kontuan. Lehen kapitulu honetan EI profila izango da irizpidea, modu honetan 3 azpitalde sortuz. Horietaz gain, beste bi gehitu dira duten geometria edo osaketa dela eta. Hala ere, sailkapena transmitituriko modu kopuruaren arabera edo gidapen mekanismoaren arabera egiten bada azpitalde hauek aldatu egingo lirateke. Beraz, EIari erreparatuz, MI-PZO-ak, IG-PZO-ak eta maila anitzeko indizedun PZOak (MAI-PZO) bereizi dira, eta geometria edo osaketa berezia dutela kontsideratuz nukleo anitzeko PZOak (NA-PZO) eta PZO mikroegituratuak (PZOm) gehitu dira.

1.2.3.1 MI-PZO-ak

Mota honetako PZOetan EIaren bi maila bereizten dira, bat uniformea dena, nukleoaren azalera hedatua eta bestea estaldurarena. Honela definitzen da:

$$n(r) = \begin{cases} n_{nu} & r \leq \rho \\ n_{es} & r > \rho \end{cases}, \qquad 1.1)$$

$n_{nu} > n_{es}$ delarik.

Mota honetakoPZOetan modu anitz transmititzen dira aldi berean, eta horrek MI-PZO-en muga handiena sortzen du; izan ere, dispertsio modal altuek transmisio abiadurak mugatzen dituzte. Hala ere, egungo zenbait goi-mailako modulazio erabiliz arazo hau ekidin daitekeela frogatu da [30], [31]. Telekomunikazioetarako erabiltzeaz gain, mota honetakoPZOak beste mota bateko aplikazioetan ere erabili izan ohi dira, produkzio linea industrialetan edo automobil aplikazioetan, besteak beste. MI-PZO estandarren diametroa 980 μm-koa izaten da eta estalduraren lodiera berriz 10 μm-takoa. Argia modu errazean akoplatu daiteke, horren erakusgarri 0.5-eko zenbakizko irekidura izanik.

1.2.3.2 IG-PZO-ak

Aurreko zuntzekin konparatuz, IG-PZO-ek banda-zabalera zabalagoa izaten duteEIaren profilarengatik. Gainera, dispertsio modala minimora murrizten dute [32]–[35]. 1.2. ekuazioan deskribatzen den moduan profil berezi hau gradualki txikiagotzen da simetria ardatzarekiko (r). Horretaz gain, maila-indizedunen gisa diametro handikoak izaten dira.

$$n(r) = \begin{cases} n(0)\sqrt{1 - 2\Delta(r/\rho)^g} & r \leq \rho \\ n(0)\sqrt{1 - 2\Delta} & r > \rho \end{cases} \quad 1.2)$$

Δ ikurrakEIen arteko ezberdintasuna deskribatzen du eta honela definitzen da:

$$\Delta = \frac{n_{nu}^2 - n_{es}^2}{2n_{nu}^2}. \quad 1.3)$$

g parametroak, bestalde, profilaren esponentea adierazten du. g = 2 denean profil parabolikoa izango du PZOak eta g handiagotzen doan heinean MI-PZO-en antza handiagoa izango du, infinituko kasuan berdina izanik. 1.7. irudian ikusi diren bi PZO motetan zehar argia nola hedatzen den azaltzen da, modu-anitzeko zuntzetan beti ere.

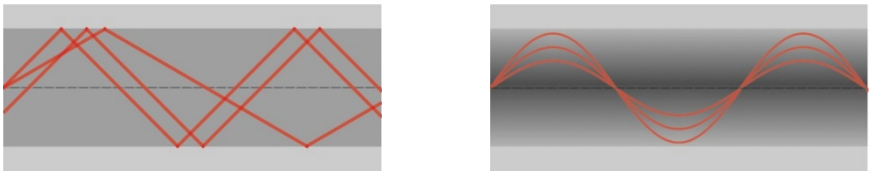

(a) (b)

1.7 Irudia. Argiaren hedapenaPZOetan zehar. (a) MI-PZO-en kasua. (b) IG-PZO-ren kasua.

IG-PZO-en kasuan, gehien erabili izan diren materialak PMMA eta polimero PF-ak izan dira. Hauen ezaugarri nagusienak 1.3 taulan laburbildu dira:

1.3 Taula. PMMA eta Polimero PF-z eginikoPZOen ezaugarri nagusien laburpena.

Ezaugarriak	PMMA IG-PZO	PF IG-PZO
Atenuazioa	150 dB/km @ 650 nm > 1000 dB/km @ 850 nm eta 1310 nm	< 40 dB/km @ 850-1320 nm 10 dB/km @ 1210 nm
Banda-zabalera · distantzia	2 GHz · km @ 650 nm	2 Ghz · km
Lorturiko transmisio distantzia	200 m @ 2.5 GHz	110m @ GHz

1.2.3.3 MAI-PZO-ak

PZO mota hau aurreko bien arteko nahasketa moduan ikus daiteke. Izan ere, ikertzaileek IG-PZO-en EI profila garatzeko zituzten arazo teknikoak zirela eta, soluzio

honekin topo egin zuten [36]–[38]. Kasu honetan, nukleoa EI ezberdineko hainbat geruzez osatua dago, eta denak batzean EI profil paraboliko baten tankerako profila lortzen da. Bere ezaugarrien artean fabrikazio prozesu sinplea eta hezetasuna eta tenperaturaren aldaketekikoEIak duen egonkortasuna aipatu behar dira.

MAI-PZO-ek MI-PZO-en fabrikazio sinplea eta IG-PZO-en banda-zabalera konbinatzen dituzte. Adibide gisa, 0.25 zenbakizko irekidura duen 3 geruzako MMI-PZO-aren banda-zabalera 250 MHz · 100 m-koa da, IEEE 1394/S400 estandarraren eskakizunak betetzen dituelarik [36].

1.2.3.4 NA-PZO-ak

Nukleoaren diametro zabalak dituzten PZOek galera handiagoak izaten dituzte kurbadurengatik. Bestalde, tamaina txikiko PZOak konplexuagoak izaten dira manipulatzeko edo argiaren akoplamendua egiterako orduan. Bi ezaugarri hauek kontuan izanda, NA-PZO-ak asmatu zien [39]. Berauek tamaina txikiko hainbat PZO taldekatzen dituzte gurutze-sekzio handia sortzeko asmoz; normalean 1 mm inguru izaten delarik. Zuntz mota hauek hamaika diseinu ezberdin onartzen dituzte, aplikazioaren arabera alda daitekeelarik. 1.8. irudian ikus daitezke hainbat adibide.

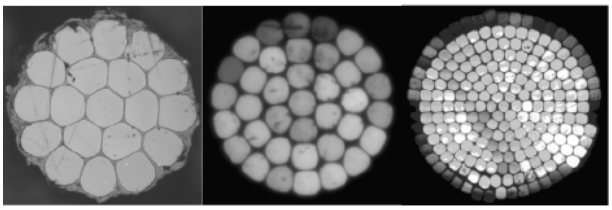

1.8 Irudia. Hainbat NA-PZO diseinuren argazkiak.

1.2.3.5 PZOm-ak

PZOm-en eredua erlatiboki berria dela esan daiteke eta *P. Russell* ikerlariak beirazko zuntz mikroegituratuak kristal fotoniko izenarekin eman zituen ezagutzera [40]. PZOm-etan hainbat gidapen mekanismo eman ahal dira argi-transmisiorako *band-gap* efektua eta aldaturiko barne islapen osoa (ABIO) izanik nagusienak. Bi gidapen mota hauek aurrerago aztertuko dira sakonago, baina esan behar da *band-gap* efektu bidez

argi-transmisioa lortzen bada, argia hutsean transmititu ahal izango dela, dispertsio materiala ekidinez [41], [42]. 1.9 irudian hainbat PZOm-ren diseinu ikus daitezke.

Irudi honetan azaltzen diren PZOm ezberdinak Australian aurkitzen den Sydney-ko unibertsitateko ikerlariek fabrikaturiko PZOm-ak dira. Izan ere, bertan aurkitzen den *Optical Fibre Technology Centre*-ko ikerlariak izan baitira PZOm-en fabrikazioak garatu eta aurrerakuntza garrantzitsuenak egin dituztenak. Beraiek fabrikatu baizituzten lehenengo aldiz modu bakarreko PZOm-a, NA-PZOm-ak eta birrefrigentzia altuko PZOm-ak [43].

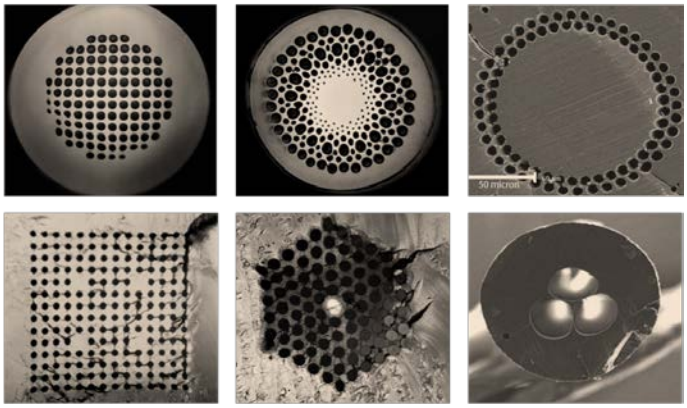

1.9 Irudia. PZOm ezberdinen irudiak (Maryanne Large eta Australian aurkitzen den Sydney-ko unibertsitatearen adeitasunez).

Azken urteetan izan den aurrerakuntzei esker, bai simulazio eta modelizazio aldetik, bai fabrikazio prozesuen aldetik, zuntz mota hauek garrantzi handia hartu dute fotonikaren munduan. Berauekin efektu ezberdinak lor daitezke eta eremu ezberdinetan erabili. Aurrerago ikusiko den moduan, gure kasuan glukosa zenbatzeko Raman espektroskopia neurketa plataforma gisa inplementatu dira gure instalazioetan fabrikaturiko hainbat PZOm.

1.3 Jorratutako neurketa teknikak

Ondoren, tesian zehar jorratutako neurketa teknikak azalduko dira. Lehenik eta behin, uhin ebaneszentearen ezaugarriak eta sentsore moduan uhin honetaz baliatzeak duen interesa azaltzen da. Ondoren, Raman espektroskopia zer den eta laborategian zein motako ekipamendua dagoen deskribatuko da.

1.3.1 Uhin ebaneszentearen xurgapena

Uhin ebaneszentearen xurgapenaren neurketak egin ahal izateko, uhin ebaneszentea zer den eta zein ezaugarri dituen azalduko dira. Ezaugarri hauek ulertu ostean sentsore gisa nola jorratu daitekeen sakonduko da bigarren kapituluan, bertan azaltzen den detekzio sistemaren oinarria baita.

PZO tradizionaletan argia BIO bitartez gidatzen da. Honek esan nahi du angelu kritikoa baino eraso-angelu (θ_e) handiagoarekin erasotzen duten argi-izpiek nukleo-estaldura interfazea, nukleora islatuko direla θ_i angeluarekin eta gidatu egingo direla; beti ere, EI perfila egokia dela suposatuz (1.10 irudia). Hala ere, angelu kritikoa baino eraso-angelu handiagoak gertatzen direnean, ez du esan nahi 2 ingurunera (PZO tradizionalaren kasuan estaldurara) ez dela argi transmisiorik gertatuko, bai ordea θ_t angeluak zentzu fisikoa galduko duela $\theta_t > \pi/2$ izango baita.

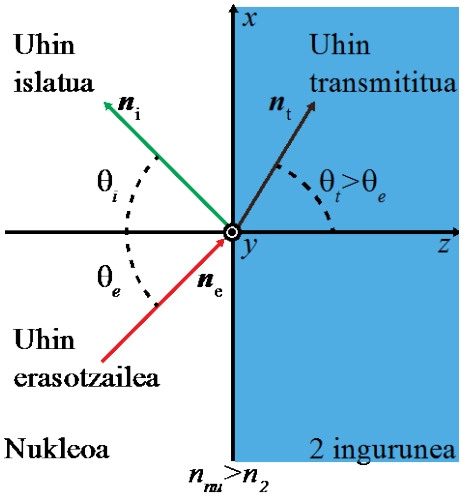

1.10 Irudia. Argi izpi erasotzailea, islatua eta transmititua bi inguruneen arteko erasoan.

Hala ere, posible da ikuspuntu matematiko batetik bi inguruneen arteko interfazean gertatzen dena aztertzea. Horretarako, lehenik eta behin, uhin transmitituaren adierazpena definituko dugu:

$$E_t = E_t^0 \exp[-j\beta_2(\sin\theta_t x + \cos\theta_t z)]. \tag{1.4}$$

Snell-en legea aplikatuz interfazean:

$$\sin\theta_t = \frac{n_{nu}}{n_2}\sin\theta_e,$$

$$\cos\theta_t = \pm(1-\sin^2\theta_t)^{1/2} = \pm\left[1-(\frac{n_{nu}}{n_2}\sin\theta_e)^2\right]^{1/2}, \tag{1.5}$$

eta $\sin\theta_e > n_2/n_{nu}$ kasua konsideratzen ari garenez,

$$\cos\theta_t = j\left[(\frac{n_{nu}}{n_2}\sin\theta_e)^2 - 1\right]^{1/2}. \tag{1.6}$$

Ordezkatuz:

$$E_t = E_t^0 \exp\left(-j\beta_2\frac{n_{nu}}{n_2}\sin\theta_e\, x\right)\exp\left\{\mp\left[\left(\frac{n_{nu}}{n_2}\sin\theta_e\right)^2 - 1\right]^{1/2} z\right\}. \tag{1.7}$$

Azken adierazpen honetan esponentzial positiboa arbuiatuko dugu, fisikoki ez delako posible. Honela nukleoa inguratzen duen ingurune arinagoan sartu ahala (*z* noranzkoan), anplitudea esponentzialki txikitzen zaion uhin baten adierazpena daukagu. Uhin ebaneszente hori *x* norabidean zehar hedatzen da bi inguruneak banatzen dituen

gainazalean eta, arrazoi horregatik, gainazal-uhin ere deitzen zaio. Uhin ebaneszente honen anplitudea ez da konstantea uhin-frontean zehar, eta, beraz, ezin daiteke homogeneotzat jo. Bere anplitudea oso azkar ahultzen da *z* norabidean zehar, honi aurrerago irismen sakonera, edo *penetration depth* deritzo. Beraz, uhin ebaneszentea komunikazioetarako egoki ez izan arren, sentsoreak diseinatzerako orduan garrantzi handia izango du ingurumenarekin hartu-eman handia duelako.

1.3.2 Raman espektroskopia

Raman espektroskopiak laginaren bibrazio molekularrak deskribatzen ditu argi erasotzailearen dispertsio inelastikoaren bitartez [44]. Hori dela eta, laginaren bibrazio molekularrak aztertuz, laginaren hatz-marka lortzen da eta bertan agertzen diren bibrazioak egitura molekular zehatz batzuri eslei dakizkieke inolako zalantzarik gabe. Laginaren informazioa lortzeko eskaintzen duen bereizmen altu honek Raman espektroskopia oso teknika erabilia bilakatu du gaur egun hainbat helburutarako. *C.V. Raman* eta *K. S. Krishnan* ikerlariek frogatu zuten dispertsio inelastikoa lehenengo aldiz 1928. urtean [45]. Aurkikuntza honek 1929-ko fisika Nobel saria irabazteko balio izan zien gainera. Teknika hau argia eta materiaren arteko interakzioan oinarritzen da eta nahiz eta aurrerago ideia honetan sakondu, oso efizientzia baxua du, hau izanik teknikaren desabantaila handiena.

Argiak materiarekin interakzionatzean lau gertaera ezberdin gertatuko dira: transmisioa, islapena, xurgapena eta dispertsioa. Gure kasuan dispertsioa izango dugu aztergai, Raman espektroskopia prozesu horretan oinarritzen baita. Argia eta materiaren arteko elkarrekintzan argia bi modutan dispertsa daiteke, modu elastikoan zein inelastikoan. Lehenengoan (*Rayleigh* dispertsio moduan ezagutzen da), argia uhin-luzera baino txikiagoak diren partikulengatik dispertsatzen da. Elkarrekintza honetan argiak ez du uhin-luzeran aldaketarik jasango dispertsaturiko argiaren energia hasierakoaren berdina baita.

Bestalde, modu inelastikoan dispertsaturiko argiak uhin-luzeran aldaketa izango du, materiaren bibrazioekin interakzionatzean argi erasotzaileak bibrazio horien naturaren arabera energia irabazi ala galdu egin duelako. Hori gertatzen denean energia trukea gertatzen dela esaten da eta efektu hau Raman dispertsio gisa ezagutzen da, hain zuzen ere.

Hala ere, hurrengo ataletan dispertsio honen inguruan sakonduko dugu bi ikuspuntu ezberdin azalduz.

1.3.2.1 Raman espektroskopiaren ikuspuntu klasikoa

Maila makroskopikoan Raman dispertsioa honela ikus daiteke: eremu elektromagnetiko baten eraginez, dipolo oszilatzaile batek igorritako energia litzateke. Fisika klasikoa erabiliz, fenomeno hau ondoren azalduko den moduan ikus daiteke [46], [47]: *z* ardatzean zehar hedatzen den argi monokromatiko batek *x* ardatzean oszilatzen duen eremu elektriko bat du. Eremu elektrikoaren balioa (E_x), edozein denboran (t) honela espresatu daiteke:

$$E_x = E_x^0 \cos(2\pi\nu_0 t), \tag{1.8}$$

non E_x^0eremu elektrikoaren anplitude maximoa den eta ν_0 argi monokromatikoaren maiztasuna. Argi honek materiarekin elkarreragina duenean, honen eremu elektrikoak materia inguratzen duen elektroi lainoa polarizatuko du eta elektroi hauek oreka posiziotik atera. Elektroien desplazamendu honek eremu elektrikoarekin batera oszilatuko du eta dipolo elektriko oszilatzaile baten gisa jokatuko du. Egoera honetan, berriki sortu den dipoloak argia igorriko du (argi dispertsatua) oszilatzen ari den korronte elektrikoaren ondorioz. Beraz, argi dispertsatua dipolo elektrikoaren oszilazioaren menpekoa bada, dipoloaren polarizazioaren aldaketek dipoloaren argi-emisioaren maiztasunean eragina izango dute. Dipoloaren polaritatea bere dipoloaren momentuak determinatzen du (μ):

$$\mu = \alpha E_x = \alpha E_x^0 \cos(2\pi\nu_0 t), \tag{1.9}$$

non α polaritate tentsorea den eta kanpoko eremu elektriko baten aurrean elektroi lainoaren distortsioaren joera deskribatzen duen. Molekula bat bere maiztasun naturalean oszilatzen ari bada (ν_m), molekularen nukleoaren desplazamendua (q) honela deskriba daiteke:

$$q = q_0 \cos(2\pi\nu_m t), \tag{1.10}$$

non q_0 bibrazioaren anplitudea den. Bibrazio anplitude txikientzako α-ren balioa q-ren funtzio linear gisa espresa daiteke Taylor-en seriea erabiliz:

$$\alpha = \alpha_0 + \left(\frac{\partial \alpha}{\partial q}\right)_0 q + \cdots . \qquad 1.11)$$

1.9 eta 1.11-ko lehen bi osagaiak konbinatuz gero, dipolo momentua honela azaldu daiteke:

$$\begin{aligned} \mu &= \alpha E_x^0 \cos(2\pi \nu_0 t) \\ &= \alpha_0 E_x^0 \cos(2\pi \nu_0 t) + \left(\frac{\partial \alpha}{\partial q}\right)_0 q E_x^0 \cos(2\pi \nu_0 t) \\ &= \alpha_0 E_x^0 \cos(2\pi \nu_0 t) + \left(\frac{\partial \alpha}{\partial q}\right)_0 q_0 \cos(2\pi \nu_m t)\, E_x^0 \cos(2\pi \nu_0 t) \\ &= \alpha_0 E_x^0 \cos(2\pi \nu_0 t) + \tfrac{1}{2}\left(\frac{\partial \alpha}{\partial q}\right)_0 q_0 E_x^0 \{\cos[2\pi(\nu_0 + \nu_m)t] + \\ &\qquad \cos 2\pi\nu 0 - \nu m t. \end{aligned} \qquad 1.12)$$

Azken adierazpen honetatik elkarrekintzan parte hartzen duen eremu elektromagnetikoaren maiztasun beran igortzen duen dipoloa adierazten du lehen osagaiak. $\nu_0$maiztasunean erradiatzen duenez, *Rayleigh* dispertsioari dagokio. Bestetik, bigarren eta hirugarren osagaiek $\nu_0 + \nu_m$ eta $\nu_0 - \nu_m$ maiztasunetan igortzen dute. Maiztasun hauek argi erasotzailearekiko ezberdinak direnez, dispertsio inelastikoa edo Raman dispertsioa gertatu dela esan daiteke. Igorpen hauen inguruan aipatu behar da maiztasun altuagoan igortzen den argiak ($\nu_0 + \nu_m$ osagaiak) *anti-Stokes* dispertsioa jasan dutela esaten dela eta maiztasun baxuagokoak berriz *Stokes* dispertsioa.

Garrantzitsua da aipatzea Raman dispertsioaren bi osagaiek ez dutela zertan aktiboak izan. $\left(\frac{\partial \alpha}{\partial q}\right)_0$ osagaia zero izaten bada zenbait bibraziorentzat, bibrazio hauek Raman ez-aktiboak direla esaten da. Beraz Raman aktiboak diren bibrazioek polaritate aldaketa jasan behar dute. Bestalde, $\left(\frac{\partial \alpha}{\partial q}\right)_0$ osagaiak Raman maiztasun horren anplitudea ezarriko du eta 1.12 ekuaziotik begi bistako ez izan arren, *Rayleigh* dispertsioa baino magnitude-ordena batzuk ahulagoa izan ohi da.

1.3.2.2 Raman espektroskopiaren mekanika kuantiko ikuspuntua

Ikuspuntu klasikoan maila makroskopikoa aztertu da, baina kasu honetan maila mikroskopikoan aztertuko da efektua. Ikuspuntu honetan Raman dispertsioa energia transferentzia ereduarekin aztertu daiteke [46]–[48]. Eredu honetan argiaren materia izaera jorratzen da fotoiak aztertuz. Fotoiaren energia (*E*) argiaren maiztasunarekiko proportzionala da:

$$E = h\nu,$$

1.13)

non h Plancken konstantea den. Argiarekin interakzioa duten materiaren molekulak hainbat energia-maila daituzten sistema modukoak direla jo dezakegu. Energia-mailarik baxuena oinarrizko egoera moduan ezagutzen da eta maila altuagoak egoera kitzikatuak. Fotoi talde batek materia erasotzean eta dispertsioa jasatean materia osatzen duten molekulak kitzikatu egiten dira egoera birtual izeneko energia altuagoko egoera batetara. Kitzikapen honen energia kopurua fotoi erasotzaileek dutenaren berdina da. Molekula hauek kitzikapen aurreko egoerara itzuliko dira berehala, baina prozesuan fotoi bat igorriko dute. 1.11 irudian modu eskematikoan agertzen da prozesua, kitzikapen aurreko egoera oinarrizkoa dela suposatuz (*anti-Stokes* prozesuaren azalpenerako hasieran egoera kitzikatuan dagoela suposatuko da).

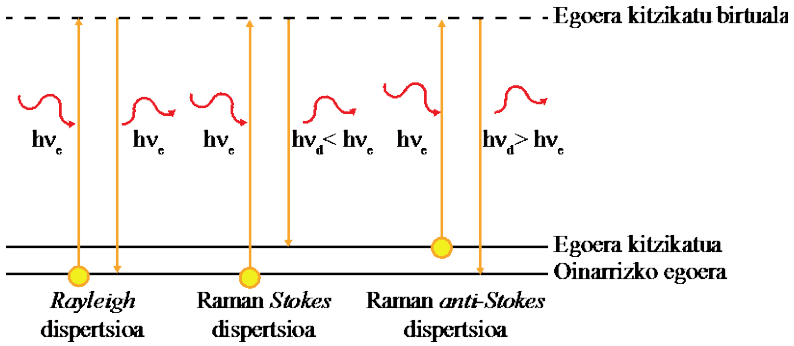

1.11 Irudia. *Rayleigh*, *Stokes* eta *anti-Stokes* dispertsioaren energia egoeren ereduaren azalpena.

Prozesuan zehar molekula egoera birtual horretara kitzikatzen dela esaten da, ez delako elektroien energia maila ezagun bat, bi maila ezberdinen arteko aldiuneko egoera delako. Kitzikapen egoeratik aurrez zegoen egoerara itzultzean, bi energia egoeren energiaren diferentzia duen fotoi bat igorriko du. Prozesuaren amaierako egoera hasierakoaren berdina bada, igorri den fotoiak erasotzailearen energia bera izango du eta ondorioz maiztasun bera. Efektu hau gertatzean *Rayleigh* dispertsioa eman dela esaten da. Gerta daiteke ordea, molekula aurreko egoerara itzuli beharrean, maila bereko azpiegoera batera itzultzea. Hau gertatzean, igorritako fotoiak energia gehiago edo gutxiago izango du erasotzailearekin alderatuz, eta ondorioz, maiztasun ezberdina. Beraz, hasierako egoerarekin alderatuz molekula prozesu amaieran energia maila altuagoan geratu bada,

igorritako fotoiak energia gutxiago izango du eta maiztasun baxuagoa, *Stokes* dispertsioa gertatuz. Amaierako egoera energia gutxiagoko egoera bada, igorritako fotoiek energia gehiago eta maiztasun altuagoa izango dute eta *anti-Stokes* dispertsioari sorrera emango diote.

Hala ere, ikuspuntu honetan hainbat ezaugarri izan behar dira kontuan. Lehenengo ezaugarria Raman dispertsioa jasan duen argiaren maiztasuna materiaren molekulen egoeren menpekoa dela da. Beraz, materiaren egoera alda dezakeen edozein fenomenoren aurrean, tentsioa, tenperatura edo potentzial kimikoen aurrean, Raman maiztasunaren aldaketa eman daiteke, beraz kontu handia izan behar da honekin.

Bigarren ezaugarria *Stokes* eta *anti-Stikoes* fotoien kopuruari buruzkoa da. Izan ere, fotoi hauen kopurua molekula hasieran dagoen egoeraren araberakoa izango da. Boltzmannen banaketaren arabera, litekeena da molekula gehienak oinarrizko egoeran egotea, kitzikapena giro tenperaturan egiten bada. Egoera kitzikatuagoetan badago materia edo molekula, maila hauetan dauden elektroi kopurua modu esponentzialean jaitsiko da mailaz-maila. Hori dela eta, fotoi gehienak *Stokes* motakoak izango dira eta ondorioz argi erasotzailea baino maiztasun baxuagoa eta energia gutxiago izango dute fotoi dispertsatuek.

1.3.2.3 Raman espektroskopiaren efizientzia

Aurrez esan den moduan, argi batek materia bat erasotzean hainbat efektu ematen dira aldi berean. Gerta liteke argi erasotzailea osatzen duen potentziaren zati bat xurgatua izatea, beste zati batek *Rayleigh* dispertsioa jasatea edota beste batek fluoreszentzia sortzea. Eman daitezkeen efektu guztiekin alderatuz Raman dispertsioa jasango duen argiaren potentziaren kopurua oso txikia izaten da. Hori dela eta, helburu-molekula baten Raman edo beste edozein efekturen efizientzia neurtzerako orduan sekzio efikaza (σ) edo sekzio efikaz diferentziala ($\frac{d\sigma}{d\Omega}$) definitzen dira [48], [49]. Sekzio efikaza prozesuan zehar norantza guztietan igortzen den fotoi kopurua eta helburu-molekula jotzen duten fotoi kopuruaren arteko erlazioa da. Horretarako m^2 edo cm^2 unitateak erabiltzen dira eta prozesu optiko konkretu batean parte hartu duen molekularen azalera moduan interpretatu daiteke. Raman dispertsioa kasu, honela egokitu genezake sekzio efikaza (σ_{RD}):

$$\sigma_{RD} = \frac{I_{RD}}{I_0} = \frac{P_{RD}}{E_o},$$

1.14)

non I_{RD} Raman dispertsioa jasan duten batezbesteko fotoi kopurua segundoko den edozein norantza kontuan hartuz eta fotoi/s-tan neurtzen den. P_{RD} antzerakoa litzateke baina potentzia gisa neurtuta, beraz unitateak W-ak lirateke. Bestalde, I_0 fotoi fluxua litzateke fotoi/s/m^2-tan neurtuta eta E_o berriz, irradiantzia W/m^2-tan neurtuta. Molekula baten sekzio efikaza honela ulertu daiteke: I_0 fluxupean Raman dispertsioa sortzen duen helburu-molekularen azalera. Halaber, Raman sekzio eragile diferentziala Raman sekzio eragileak angelu solidoarekiko duen aldaketa moduan ulertuko da.

Raman sekzio efikaza gainera, honako bi parametroen proportzionala da teorikoki: *m* egoeratik *n* egoerara trantsizio bibrazionala egiteko duen polarizazioaren deribatua eta dispertsio maiztasuna. Ondoren ikus daiteke erlazio hau:

$$\sigma_{RD} = C\nu_D|\alpha'_{mn}|\,,$$

1.15)

non *C* zenbakizko konstante bat , ν_D argi dispertsatuaren maiztasuna eta α'_{mn} parametroa 1.3.2.1 atalean azaldutako polaritate deribatua ($\alpha'_{mn} = \left(\frac{\partial\alpha}{\partial q}\right)_0$) den.

1.4 taulan hainbat prozesu optikoren sekzio eragilearen magnitude-orden orientatiboa azaltzen da molekulako. Konparatzen diren prozesu guztien artean Raman dispertsioa da sekzio eragile txikiena duena, hau izanik Raman espektroskopiaren desabantaila handiena. Hori dela eta, aurrerago Raman dispertsioaren efizientzia hobetzeko plataforma bat garatuko da. Horretaz gain, fluoreszentzia eta Raman dispertsioaren arteko alderaketa egiten bada, fluoreszentzia 10 magnitude-orden efizienteagoa dela ikusten da. Honek garrantzi handiko beste ideia bat azaleratzen du. Izan ere, fluoreszentziaren efizientzia dela eta, gerta liteke zenbait helburu-molekularen Raman espektroa ezin neurtu izatea molekularen fluoreszentzia dela eta. Horretarako kitzikapen maiztasuna ondo pentsatu beharreko parametroa da.

1.4 Taula. Hainbat prozesu optikoren sekzio eragilearen magnitude-orden orientatiboa molekulako [49].

Prozesua	Sekzio eragilea non gertatzen den	$\sigma(cm^2)$
Xurgapena	Ultramorea	10^{-18}
Xurgapena	Infragorria	10^{-21}
Igorpena	Fluoreszentzia	10^{-19}
Dispertsioa	Rayleigh dispertsioa	10^{-26}
Dispertsioa	Raman dispertsioa	10^{-29}
Dispertsioa	Erresonantzia Raman dispertsioa	10^{-24}
Dispertsioa	Gainazal bidez areagoturiko Raman dispertsioa	10^{-16}

1.3.2.4 Ekipamendua

Tesi hau aurrera eraman den instalazioetan *Renishaw* markako mikroskopio konfokal bat erabili da, *InVia* modeloa hain zuzen ere; 1.12 irudian ikusten denaren modukoa. Neurketa sistemaren arkitekturagatik, mikroskoioak *backscattering* edo atzerakako dispertsio moduan jasotzen du argi dispertsatua.

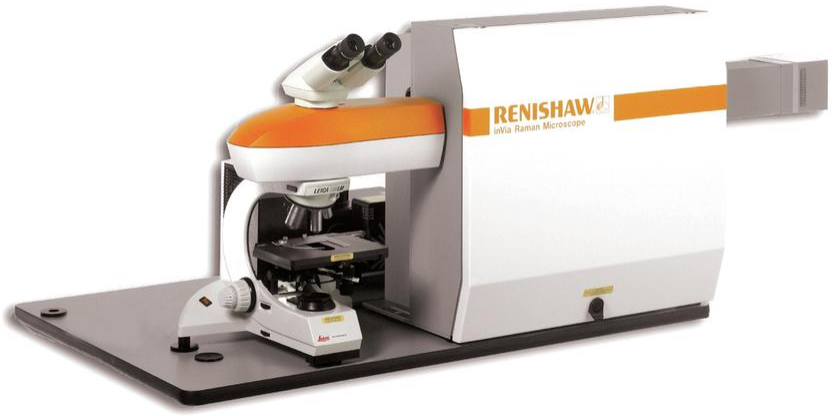

1.12 Irudia. Renishaw Invia Raman mikroskopioaren argazkia.

Kitzikapen iturriei dagokienez, bi laser ditugu aukeran. Lehenengoak 532 nm-ko uhin-luzeran igortzen du eta laginera 55 mW-eko potentzia optikoa helarazteko gai da.

Bigarrenak, 785 nm-tako argi-iturriak, 170 mW-eko potentzia igortzen du laginera. Hala ere, bigarren laser honek *spot* lineal batez erasotzen duenez lagina, posible da *spot* zirkular bat sortzea *pin-hole* bat gehituz laserraren bidean. Kasu honetan ordea, 7.64 mW-etako potentzia bakarrik lortzen da laginean. Azaldu diren kasuak laserren potentzia maximoarenak dira. Hala ere, potentzia hauek txikiagotu daitezke sistemak hiru iragazki (*optical density* motakoak) baititu sisteman integratuta. Honi lotuta, mikroskopioak bi difrakzio sareta ditu, bakoitza laser bati doituta. 532 nm-tako laserrarekin 1800 lerro/mm-koa erabiltzen da eta 785 nm-koarekin, berriz, 1200 lerro/mm-koa.

Erabiltzen diren objektiboei dagokienez, mikroskopioak lau objektibo ditu muntatuta objektiboen erriflean. Laurak ere Leica markakoak dira eta 5X, 20X, 50X eta 100X-ko magnifikazioak dituzte eta 0.12, 0.4, 0.75 eta 0.85-eko zenbakizko irekidurak hurrenez hurren.

Gainera, laginaren leku egokian erasotzeko helburuz, lagina XYZ platforma motorizatu batean jartzen da. Honek mapeoak egitea ahalbidetzeaz gain, 0.1 μm-tako erresoluzio espaziala eskaintzen digu.

Sistemaren parte diren beste zenbait osagarri 1.13 irudiko eskeman ageri dira. Bertan, gainera, laser izpiak egiten duen ibilbidea ageri da. Bertan ikusten da kitzikapen laserra ispilu dikroiko bat pasatuz objektibora eta ondorioz lagina erasotzera iristen dela. *Backscattering* arkitektura dela eta, lagina eraso duen argi-izpia aurkako noranzkoan zehar ispilu dikroikora bideratzen da. Ondoren *notch* iragazkira zuzentzen da atzera dispertsatu den argia. Aipatu behar da *notch* iragazkira dispertsaturiko uhin-luzerak iristeaz gain, atzera islatu den argia ere iristen dela, eta, beraz, azken osagai hau iragazi egiten dela bertan. Ondoren, iragazitako argia irekidura batetik pasatzen da konfokaltasuna handitzeko. Irekidura honen zabalera software bidez kontrola daiteke eta foku-planotik at dagoen dispertsio oro ezabatzea da helburua. Azkenik, ispilu sistema baten bitartez, dispertsaturiko argia saretara bidaltzen da eta bertan argia errefraktatu eta CCD-ra bideratzen da Raman espektroaren irakurketa egiteko.

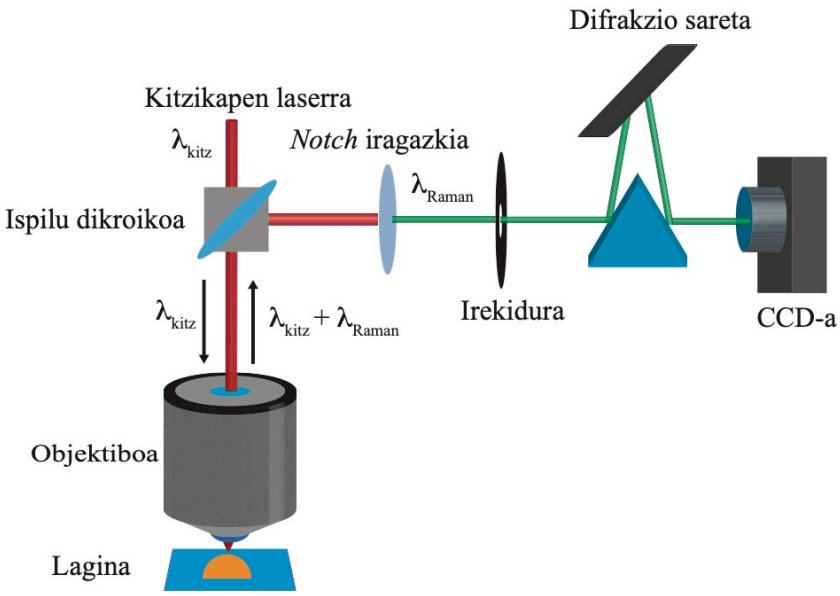

1.13 Irudia. Raman ekipamenduaren eskema.

Raman espektroskopiak baditu beste ezaugarri aipagarri batzuk. Batetik, Raman tontorren naturak banaketa *Lorentziarra* jarraitzen du. Hala ere, neurketa egiterako orduan, argi-izpiek igaro behar dituen osagai optikoak eta CCD-aren distortsioa direla eta, tontor hauek *Gaussiar* moduan tratatzea da egokiena. Bestetik, Raman espektroen zaratak *Poisonen* banaketa jarraitzen du. Bi ezaugarri hauek kontuan izan behar dira datuak tratatzerako orduan.

1.4 Tesiaren testuingurua eta helburuak

Tesi honek PZOetan oinarrituriko biosentsore plataformak garatzea du helburu nagusi. Asmo horrekin, biosentsoreei produkzio-kostu baxukoak, hautakortasun handikoak eta sentikortasun itzelezkoak izatea eskatuko zaie, beti ere, glukosa finkatuz helburu-molekula gisa. Beraz, tesi-lan honen amaierako helburua sentikortasun eta hautakortasun handia duten sentsore plataformak eraikitzea izango da; betiere guk geuk fabrikatutakoPZOak erabiliaz. Sentsore plataformari eskatuko zaion sentikortasuna milimol gutxi batzurena izango da, hor baitago medikuntzarentzat erakargarritasuna.

Tesia honela antolaturik dago:

- Bigarren kapituluan uhin ebaneszentearen xurgapenean oinarrituta, funtzionalizaturiko gainazala duen polimerozko zuntz optikozko zunda bat aurkezten da glukosa detektatzeko. U formako zundaren gainazala fenilboroniko taldeekin funtzionalizatuz, glukosa detekta daiteke; prozesu horretan, gainera, ez du inolako eraginik glukosa disolbatuta daukan inguruneak. Gainera, U formak detekzio sistemaren sentikortasuna areagotzen du.
- Hirugarren kapituluak glukosa disoluzio hurtsuetan zenbatzeko plataforma berri bat aurkezten du likidoz beteriko nukleodun PZOm-etan (LBN-PZOm) eta Raman espektroskopian oinarritua. Modu honetan, ZBARE neurketak egin dira gure fabrikazio dorrean fabrikaturiko NH-PZOm-en geometria bi eta geometria konkretu baten dimentsio bi erabiliz. Asmoa bigarren kapituluan aurkezturiko detekzio sistemaren puntu ahulak ekidin eta medikuntzarako interesgarriak diren kontzentrazioetan (SGLT2 inhibitore terapian) glukosa zenbatzeko gai izatea da.
- Laugarren kapituluan aurreko bi kapitulutan garaturiko plataformen ondorioak zerrendatu eta hobekuntza posibleak azaltzen dira. Horretarako lehenik uhin ebaneszentearen xurgapenean oinarrituriko detekzio sistemaren ondorioak, eta hobekuntza eta aldakuntza posibleak zerrendatzen dira aplikazio errealetan erabiltzeko asmoz. Ondoren, berdintsu egiten da hirugarren kapituluan deskribaturiko NH-PZOm-etan oinarrituriko plataformarentzat. Bi kasuetan, aplikazio errealetan eginiko lehen emaitzak azaltzen dira. Azkenik, PZOetan oinarrituriko biosentsoreen munduak izango dituen etorkizuneko eskaerak eta ikerketa norabideak agertzen dira.
- Azkenik, bostgarren kapituluak tesi-lan honetan zehar eginiko ikerkuntzen ondorioz izan diren ekarpenak zerrendatzen ditu.

Chapter 2 / 2. Kapitulua

U-shaped Surface Functionalized Polymer Optical Fiber probe based on Evanescent Wave Absorption for Glucose detection

Glukosa detektatzeko zunda, U forma eta funtzionalizaturiko gainazala duten polimerozko zuntz optikoan eta uhin ebaneszentearen xurgapenean oinarrituta

Abstract—In this chapter, we present a surface functionalized polymer optical fiber probe based on evanescent wave absorption for glucose detection. The surface functionalization of the U-shaped probes with phenylboronic groups allows the glucose detection regardless the medium where it is solved. Besides, the U-shape of the probe enhances the sensitivity of the measuring system, which only consists of a supercontinuum light source, the probe itself and a high resolution spectrometer. Within this chapter, all the fabrication process from the very beginning is described, and afterwards, the performed glucose detection measurements in different media are shown and discussed widely.

Laburpena—Kapitulu honetan, uhin ebaneszentearen xurgapenean oinarrituta, funtzionalizaturiko gainazala duen polimerozko zuntz optikozko zunda bat aurkezten da glukosa detektatzeko. U formako zundaren gainazala fenilboroniko taldeekin funtzionalizatuz, glukosa detekta daiteke; prozesu horretan, gainera, ez du inolako eraginik glukosa disolbatuta daukan ingurumenak. Gainera, U formak detekzio sistemaren

sentikortasuna areagotzen du. Neurketa sistema honako hiru osagai hauek osatzen dute: supercontinuum argi-iturri batek, aurkezturiko zundak eta erresoluzio altuko espektroskopio soil batek. Kapitulu honetan zehar, zundaren fabrikazio prozesua hasieratik amaierara azaltzen da, eta, ondoren, glukosa ingurumen ezberdinetan detektatzeko asmotan, hainbat neurketa egin eta erakusten dira.

As first approach to biosensors, we decided to develop a fiber optic evanescent wave (FOEW) absorption glucose detector. For that purpose, a polymer optical fiber (POF) probe in U-shape geometry was implemented. FOEW systems are widely used [50]–[57] in biosensing, and they rely on detecting a change on the transmitted light intensity due to the coupling of the light to the surrounding medium. In addition, with the aim of providing the system with high selectivity for glucose, the probes were functionalized with phenylboronic groups. Hence, we were able to design and fabricate a glucose detector by joining diverse research-areas, such as POF fabrication and chemical surface functionalization.

FOEW sensing systems, which are composed of silica fibers or POFs, are widely applied in chemistry, biochemistry, and environmental research because they provide fast and reliable results in terms of measuring solution concentrations, analyzing chemical components, and obtaining the absorption spectra of chemicals of interest during real-time monitoring [53], [58]. Regarding currently available FOEW sensors, those based on POFs have attracted intense interest because of their several potential advantages, including low cost, large-diameter core, large numerical aperture and high degree of shape diversity (i. e. U-, D-, taper-, and spiral-shaped fibers). The large diameter and numerical aperture of the POFs increase the optical transmission capacity of the fiber, and, therefore, the performance of such sensors in terms of improved sensitivity and measurement range. Although wave-optics theory for single-mode fibers has been developed to give an accurate description of the ray transmission, this is not the case for multimode optical fibers. The entire geometrical development of the basic measuring principle is described within this chapter.

Additionally, from the mechanical point of view, sensors employing POFs have gained popularity over their silica counterparts. A POF based probe offers much better behavior for strain than a traditional glass fibers: a silica based probe will break when a 5%

of the length strain is applied to it, whereas a POF based probe will break with a 50% [59]. Besides, a smaller bending radius can be obtained. The simplicity of the system, according to the probe itself, its set-up and, absence of expensive components, make POF based sensors an excellent replacement for traditional glass fiber based sensors.

A guided ray through a conventional fiber hardly interacts with the surrounding media if the fiber is straight and uniform in diameter, making it impossible to use it as a FOEW absorption sensor [60]. Typically, in order to create FOEW sensing platforms, the interaction with the surrounding media, and, therefore, absorption spectra, is enhanced either by tapering the fiber or by bending it in a certain shape [50]. On the one hand, tapered probes are built by removing the cladding of the fiber and reducing the core-diameter of the probe [59], and this tapered region is usually obtained by chemical treatment or mechanical strain, also known as the heat-and-pull technique. In the chemical treatment, many irregularities may appear in the outer surface of the sensing region. In the heat-and-pull technique, the mechanical modification could also modify the light transmission properties, resulting in non-desired effects. Nevertheless, uncladded glass fiber tapers have been used for evanescent absorption measurements and fluorescence excitation/collection due to their strong evanescent field. On the other hand, the fiber bending increases the interaction with the surrounding media by forcing the transmitted light-rays to pass through the U-shaped curved region, and, therefore, increment the interaction with the surrounding media. Besides, this approach simplifies the fabrication process.

In most cases, these FOEW sensors depend on indirect measurements to obtain the glucose concentration in a specific media, such as measuring the change in the refractive index of the solution induced by the presence of glucose [61]. In contrast, the detector described in this chapter attaches selectively the glucose and thus, disaggregates a reporter, making the sensor solvent-independent and straightforward. This way, problems with stability and optical power transmission, which are significantly affected by temperature and humidity [53], have been overcome.

In order to create a sensor with high selectivity capable of attaching a specific target separated from other undesired substances, the outer surface of the POF must be chemically functionalized. For that purpose, the PMMA POF probe surface was

functionalized with phenylboronic acid (PBA) groups. The glucose sensing behavior of these functional groups is based on the interaction between boronic acid and glucose, forming a cyclic boronate ester. The measurement principle relies on the disaggregation of an optical reporter called Alizarin Red S (ARS), which causes a high absorption near the red wavelength. The sensing system is composed by a 500 μm diameter uncladded POF bent in a U-shape of 2.5 mm diameter. By immersing the sensitive area of the probe in a glucose containing solution, the ARS is disaggregated, and, therefore, a change in the absorption spectra is observed. Employing an ad-hoc designed experimental set-up, these absorption spectra were measured and recorded.

Within this chapter, in first instance the theory regarding the FOEW sensing is deeply explained. Afterwards, the chemical explanation for the chosen surface functionalization and the interaction between the target sample and boronic acid is described. Next, the fabrication of the probe is revealed and the experimental set-up is shown. Finally, the experimental measurements are depicted and analyzed, along with their respective conclusions.

2.1 U-shape Evanescent Wave Absorption

When light is transmitted along an optical fiber, the evanescent wave decays exponentially with the distance from the core-cladding interface until its intensity is negligibly small [62], being this parameter defined as the penetration depth (d_P). This depth defines the distance in which the molecules may have a discernible effect in the evanescent wave [63]:

$$d_P = \frac{\lambda}{2\pi n_1 (cos^2\theta_c - cos^2\theta sin^2\theta_\phi)^{1/2}}, \tag{2.1}$$

where λ is the vacuum wavelength of the light launched to the fiber, n_1 the refractive index of the core, θ_c the critical angle in the sensing region with respect to the normal to the core-cladding interface, θ is the angle of the wave with the normal to the core-cladding interface and θ_ϕ is the skewness angle [63] (which is $\pi/2$ for a meridional transmission mode).

The d_P of an evanescent wave is very small in a straight fiber, but it can be notably increased by bending the fiber. Thus, using a U-shaped bending enhances the sensitivity of the fiber probe. Furthermore, the analysis of the skewness can be split depending on whether the light interacts with the outer or the inner surface. In the former case, the skewness angle changes from

$$\phi_1 = sin^{-1}\left[\left(\frac{R+h}{R+2\rho}\right)\frac{n_{cl}}{n_1}\right] \tag{2.2}$$

to

$$\phi_2 = sin^{-1}\left[\frac{R+h}{R+2\rho}\right], \tag{2.3}$$

where R is the bending radius of the probe, ρ the radius of the fiber core, and h the height at the entrance of the bent region from the inner core-cladding interface. At the inner surface, the angle goes from

$$\delta_1 = sin^{-1}\left[\left(\frac{R+h}{R+2\rho}\right)\frac{n_{cl}}{n_1}\right] \tag{2.4}$$

to

$$\delta_2 = \pi/2. \tag{2.3}$$

Using these equations it can be proved that d_P is much higher for U-shaped bent fibers than for straight fibers (R=∞) [64]. Moreover, the absorbance is higher for smaller diameters and for lower numerical apertures [55]. The graphical explanation of the described parameters is shown in Figure 2.1.

Figure 2.1. Geometry of the U-shaped sensing region and the representation of a meridional transmission mode, and an illustration of the penetration depth.

2.2 Phenylboronic acid diol interaction

The POF probe described in this chapter is functionalized with phenylboronic groups in the surface of the sensing region in order to provide the detector with high selectivity for glucose, which has the diol moieties. Boronic acids bind compounds containing diol moieties with high affinity forming, reversible boronate esters [65]. Consequently, boronic acid compounds have widely been used for the synthesis of artificial receptors for sugars with great success [66]. The scheme in Figure 2.2 depicts a substrate containing 3-aminophenylboronic acid (APBA), which is a synthetic molecule capable of forming reversibly boronates with 1, 2-diol, 1,3-diol or multi-hydroxyl groups including glucose [67]. Boronic acid-diol binding reactions are highly pH-dependent [68], and pH values above the acid dissociation constant of the boronic acid are required, so that this study makes use of buffers usually employed for biological applications (PBS and TRIS) to control the pH of the media. [69]. However, it can be difficult to monitor the binding without using any fluophore.

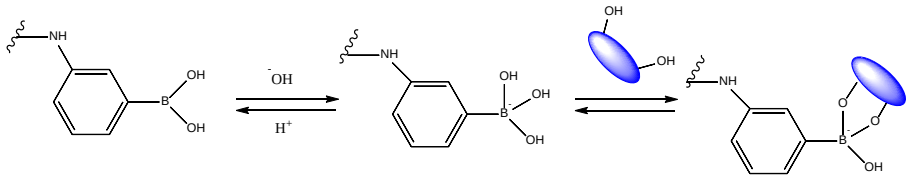

Figure 2.2. Simplified APBA equilibrium in the presence of glucose.

ARS has been used as a reagent for the fluorimetric determination of boronic acid concentrations. Free ARS is an organic dye with a very poor fluorescence. However, when ARS interacts with boronic acid groups, the active protons responsible for the fluorescence quenching are removed (Figure 2.3), leading to a dramatic increase in the fluorescence intensity of ARS [70], [71]. In this work, the ARS has been used as an optical reporter. In the presence of glucose the ARS is displaced from the boronic acid complex so the change in the absorption of the reporter allows the glucose detection by UV-Vis spectroscopy.

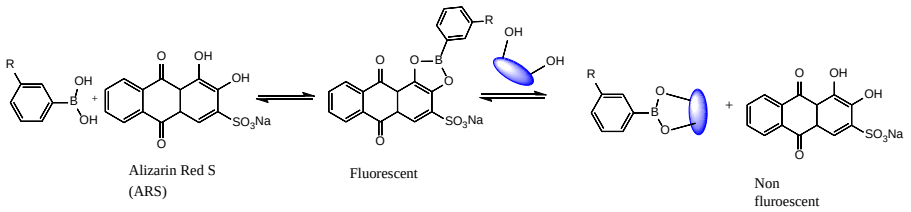

Figure 2.3 Competitive binding of PBA with ARS and glucose.

In summary, a PMMA fiber probe containing PBA groups in the outer surface has been developed [67]. Firstly, the fiber surface has been functionalized with PBA groups and binded with ARS. And, secondly, the fiber has been immersed in a solution containing 1,2-diol analytes. The competitive nature of boronic acid/diols complexes will favor the ARS-PBA bound breaking and glucose-boronic acid bond formation. The careful design of the experiment ensures that only glucose and boronic acid interaction can cause the ARS-boronic acid disruption.

2.3 Probe fabrication and surface functionalization

In this section, we explain how the U-shape POF probes were fabricated, and how we functionalized them with phenylboronic groups in order to obtain the disaggregation and, therefore, the glucose detection.

2.3.1 Probe fabrication

We firstly annealed a Plexiglass® extrusion rod of two centimeters of diameter for 7 days in an oven with low humidity (20 %) and high temperature (80 ^{o}C) conditions in order to remove all humidity from the preform, and, hence, do not compromise the quality of the POF. Afterwards, we drawn it directly to a 500 μm diameter bare fiber using our POF drawing tower [72]. This fabrication method allowed us to fabricate only-core POFs in one step. This way, we had a complete control on the fiber diameter as it is depicted in Figure 2.4, showing a diameter mean value of 499 μm and a standard deviation of less than 1 % in one hour of drawing. In addition, the core surface roughness was much lower

compared to the results obtained with other methods, such as the striping of a commercial fiber.

After fabricating the POF, we bent it taking the following procedure: in first place, a sample of 30 cm of fiber was cut. Then, using a 2.5 mm diameter glass tube as a guide, a hot-air gun set at 120 ^{o}C was directed to the section of the fiber selected to be bent and the U-shape was done carefully. After that, the fiber probes were washed in isopropyl alcohol for one hour and dried in a vacuum chamber at 60 ^{o}C overnight, in order to remove any internal stress. Finally, both ends of the fiber were carefully polished. The resultant sensor-probe is shown in Figure 2.5.

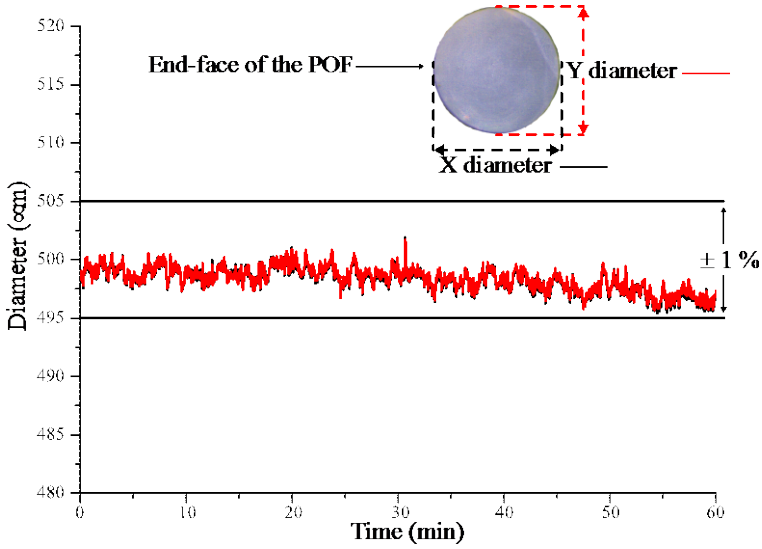

Figure 2.4 .Diameter measured during the fiber drawing of the 500 μm only-core POF.

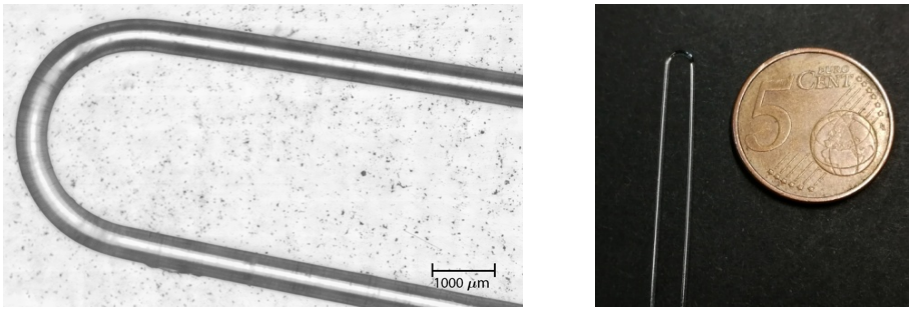

(a) (b)

Figure 2.5 The U-shaped probe. (a) Microscope image. (b) Comparisson with a 5 cent Euro coin.

2.3.2 Surface functionalization

In order to functionalize the outer surface of the sensing region, the following chemicals were purchased from Sigma Aldrich (Europe): APBA, ARS, *N*-(3-Dimethylaminopropyl)-*N′*-ethylcarbodiimide hydrochloride (EDC), *N*-Hydroxysuccinimide (NHS), glucose, Phosphate Buffered Saline System (PBS), and Tris Base (TRIS). Sulfuric Acid (96 % purity) and Hydrochloric Acid (HCl), ethanol and isopropanol were purchased from Panreac (Spain), and were used without further purification.

The functionalization of the PMMA fiber surface was carried out by modifying slightly the method described by *Fortin and Klok* [73]. Briefly, starting with an unmodified U-shaped probe (Figure 2.6(a)), 2 cm of the probe were hydrolyzed by immersing them in a 3 M sulfuric acid solution in deionized water at 60 ^{o}C for 15 minutes, then they were washed in deionized water and were left on a vacuum chamber overnight (Figure 2.6(b)). Afterwards, an activation process of the carboxylic groups was started by immersing the hydrolyzed probes in a 0.1 M EDC and 0.2 M NHS in deionized water for 4 hours at room temperature. Subsequently, they were rinsed in ethanol, and later, they were left overnight in a solution of 16 mg·mL^{-1} APBA in a PBS buffer (pH 7.2). After 12 hours, the probes were washed by rinsing in deionized water (20 min, 3 times) and, finally, they were dried in a vacuum chamber (Figure 2.6(c)).

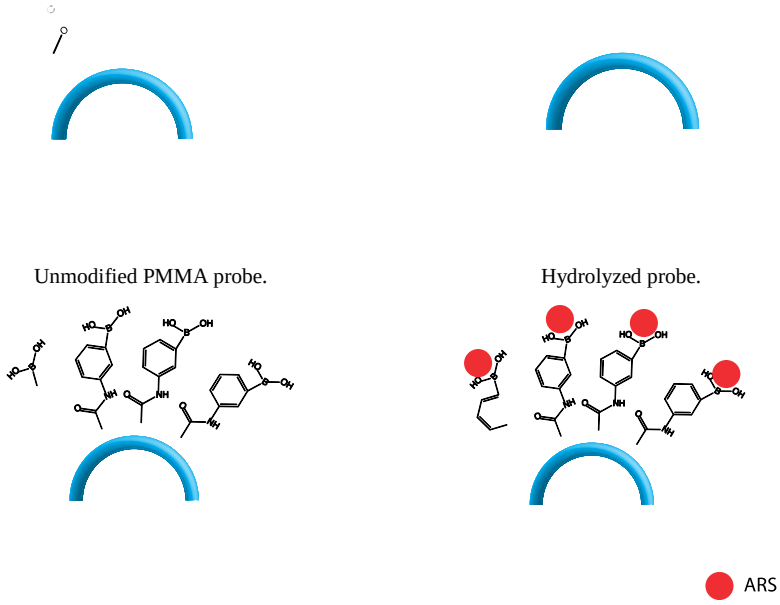

Figure 2.6 Functionalization process of the probe.

Once the fibers were functionalized with PBA groups, they were charged with ARS following the procedure described by *Chen et al.* [74]. Firstly, the tips were immersed for 3 hours at room temperature in 0.1 $mg \cdot mL^{-1}$ ARS solution prepared in a buffer of pH 7.4 with 50 mM TRIS and 44.7 mM HCl in deionized water. Secondly, they were washed with the buffer solution and dried in a vacuum chamber (Figure 2.6(d)).

2.4 Experimental set-up

The experimental set-up employed on the measurements is shown in Figure 2.7, along with the illustration of the chemical disaggregation of the ARS produced by the glucose. The supercontinuum light source (EQ-99-FC LDLSTM, ENERGETIQ) was used to illuminate the fiber probes using the minimum amount of components. The light emitted from the source was collimated with a collimating lens and then filtered with a band-pass

filter (390-750 nm) to remove the UV emission. Afterwards, the launched light was attenuated by an OD3 attenuator to avoid saturation in the detector. In order to cancel power fluctuations of the light source, light power was monitored using a beam splitter and a photodiode connected to a power meter. The pump light was focused on the end face of the fiber-probe using an objective (40x, 0.65 NA). The output light from the other end face was captured and focused through another collimator to the UV-Vis spectrometer (USB Flame 390-750 nm, Ocean Optics® Inc, USA).

The detected light in the spectrometer was recorded by a custom-made LabView program capable of recording and averaging 100 consecutive measurements. The spectrometer integration time was tuned automatically during the measurements to avoid saturation effects in the original spectra. A picture of the probe during measurements is shown in Figure 2.8.

During the measurements, we realized that the transmitted power decreased in the first minutes for the only-core fiber probes that were dried in a vacuum chamber and measured immediately after. This effect can be attributed to the environmental humidity attached to the probe surface. This undesired effect could be overcome either by adding a cladding or by letting the probes settle until they completely adapt to the environment. We chose the second strategy for simplicity, so all the probes were left for 2 hours before using them for measurements. In Figure 2.9, is shown a real example of the transmitted power of the probe and the measured environmental humidity using a humidity sensor.

According to the example, during the first sixty minutes, while the humidity remains constant at around 42 %, the transmitted power decreases due to the aforementioned lack of adaptation. Then, between minutes sixty and seventy, the transmitted power is stable, so we could say that the probe is already adapted to the environment.

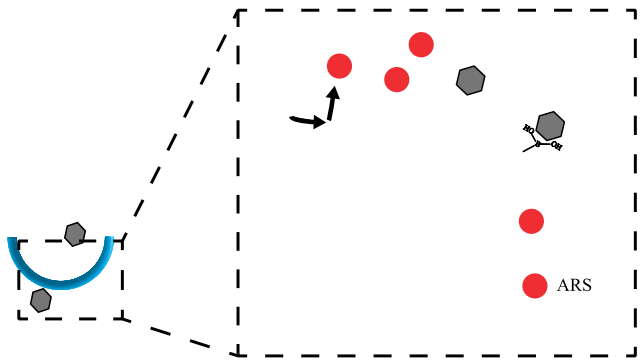

Figure 2.7 Experimental set-up employed to carry out the measurements. Legend: Col1/Col2: collimators, Fil: band-pass filter (390-750nm), Att: optical attenuator of optical density 3, BS: beam-splitter, Obj: objective, and PD: photo detector; next to the cuvette an illustration of the chemical disaggregation of the ARS is also shown.

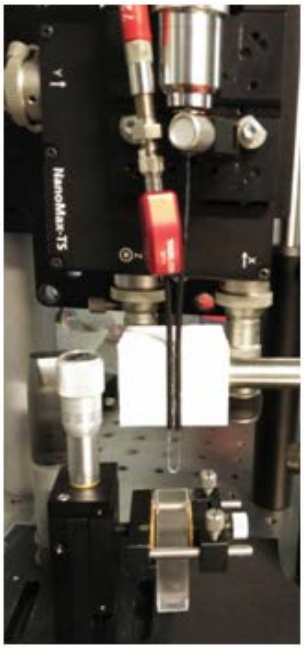

Figure 2.8 Photograph of the set-up.

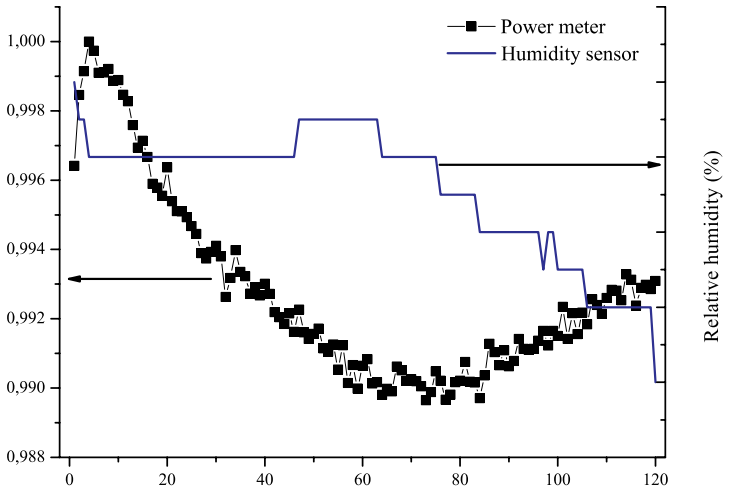

Figure 2.9 Transmitted power in an unmodified 500 mm only-core probe in time and the environmental relative humidity.

From that point on, we made the humidity to decrease from the 42 % to the 39%, and, then, the transmitted power increased as it was expected. In order to overcome this drawback, the probes were firstly adapted leaving them two hours before measurements. Anyway, our detection system did not relay on the transmitted power, as many others in literature did. In our case, every recorded spectra was normalized and its spectral shape was processed in order to see the disaggregation of the ARS produced by the glucose. This method differs completely from the approach taken by many other FOEW sensors.

2.5 Results and discussion

The main idea behind these FOEW absorption detector measurements was to join two different research fields in a glucose detector. On one hand, prior to the functionalized POF probe stage, many attempts were made in plain PMMA layers until the correct functionalization recipe was optimized. These measurements are shown in first instance. On the other hand, once this recipe was optimized for PMMA substrates, we monitored the functionalization process and the ARS aggregation in POF probes with the FOEW absorption set-up in order to verify this process, and therefore, obtain the POF probes ready for the detection; all these measurements are shown afterwards. Lastly, measurements of glucose detection in different media were performed with the ARS charged probes. The results are shown at the end of the section.

2.5.1 Functionalization process in plain samples

The functionalization process carried out in this work required an exhaustive control of the surface modification at each step. This was achieved by making an X-ray photoelectron spectroscopy (XPS) study in plain samples of PMMA sheets; measurements were done using a SPECS system equipped with a Phoibos 150 1D-DLD analyzer and a monochromatic radiation source Focus 500 with dual anode Al/Ag.

The XPS spectra of Figure 2.10 shows the general spectra of unmodified PMMA and a PBA functionalized PMMA plain sheets. Regarding the specified binding energy of the boron atom (187.2 eV binding energy), a prominent peak can be observed in

functionalized samples. The surface functionalization with PBA groups was confirmed by high resolution spectra of the boron binding energy (Figure 2.11), being 0.67 % of the surface covered by boron atoms (table Table 2.1). Although this figure may seem small, it is completely expectable as boron atoms do not show a strong XPS signal. However, as it will be shown in next sections, such a figure was more than enough to detect glucose.

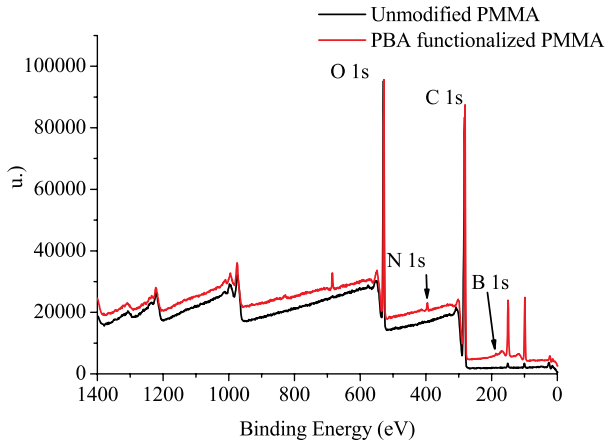

Figure 2.10 XPS general spectra of PMMA plain sample unmodified.

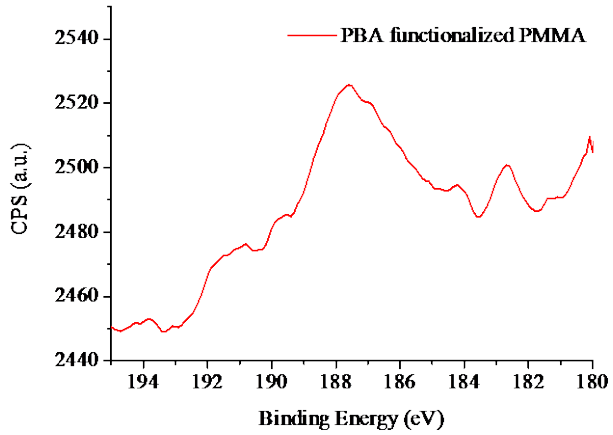

Figure 2.11 High resolution spectrum of the PBA functionalized sample for boron 1s.

Table 2.1 Elemental composition of PMMA and PBA functionalized surface from XPS analysis.

Sample	C %	O %	N %	B %
PMMA	75.09	24.91	--	--
PBA functionalized surface	72.07	25.95	1.30	0.67

Functionalization of PMMA with PBA groups was then confirmed in plain samples. At this point, we continued with the U-shaped probes functionalization and glucose detection measurements.

2.5.2 Functionalization process in the U-shaped probe

U-shaped probe spectra were recorded in each step of the above detailed functionalization process. As the transmitted signal power varied in different steps, all the obtained spectra were normalized with the minimum absorption value of each measurement.

Regarding the absorption spectra shown in Figure 2.12, we can observe that there is a significant difference between the unmodified fiber (black line) and the PBA modified fiber (red line). For the case of the functionalized probe, the light entering the fiber suffered from absorption caused by the PBA groups in the surface, so comparing it with the unmodified probe, a strong absorption curve appears on the low wavelength region (450-500 nm). In order to highlight the absorption caused by the functionalization process, the spectra were normalized with the unmodified probe, Figure 2.13 (red line). The maximum of the absorption at 440 nm indicates the presence of PBA groups.

Afterwards, these probes were charged with the ARS reporter. This step changed drastically the absorption spectra of the fiber for shorter wavelengths, as it is shown in Figure 2.12 (blue line). Normalizing it with the unmodified probe absorption spectra, Figure 2.13 (blue line), we can observe a much wider maximum of absorption due to the PBA groups and the recently added ARS. In the Figure 2.13 an absorption curve of ARS in solution is added (dotted line) in order to demonstrate that the ARS charged probe has attached successfully the reporter.

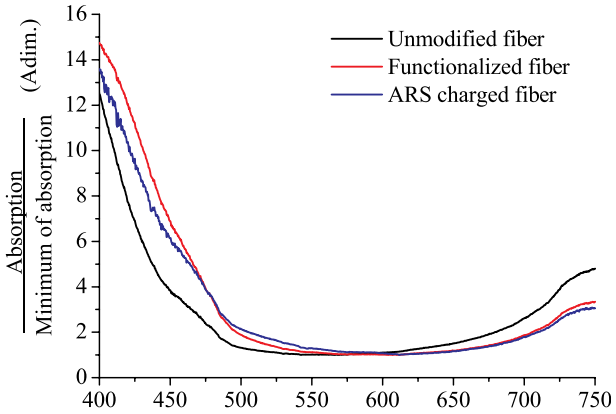

Figure 2.12 Normalized absorption curves of different probes: unmodified, functionalized, and ARS charged fibers.

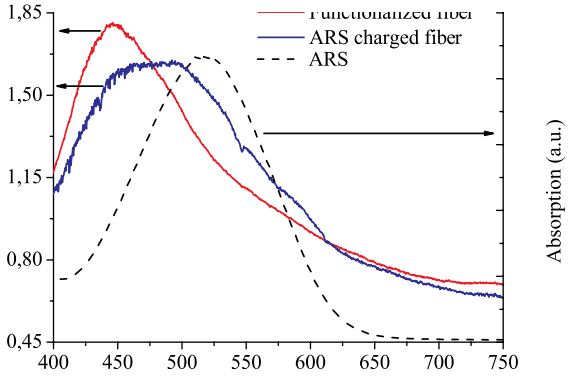

Figure 2.13 Absorption curve of functionalized and ARS charged probe normalized with the unmodified probe and absorption curve of ARS.

2.5.3 Glucose detection in different media

Regarding glucose detection measurements, we recorded and compared the absorption spectra of different fiber probes before and after their immersion in different glucose solutions for ten minutes. 1.5 cm of the U-shaped active region of the probes was immersed in a polycarbonate cuvette which contained 6 ml of solution. Then, the probes were left in air until the transmission signal was stable enough before recording its

transmitted spectra and, afterwards, they were compared to the initial spectra. The measurements were made using the same glucose concentration (0.1 mol/l) and in three different media, being two of them physiological, i.e. with a pH similar to that of human body, 7.2-7.4. More specifically, these three media were deionized water (H_2O), PBS buffer, and TRIS buffer. Notice that these media have pH values well above the pKa of the boronic acid, being these buffers also used for a physiological media, making it possible the interaction with glucose. By testing the method in different media, we intended to prove the suitability of the fiber probe regardless of the selected medium and its hypothetical application to a biological medium.

For the H_2O solvent, results are shown in Figure 2.14 and Figure 2.15. From the absorption spectra (Figure 2.14), it can be noticed that the absorbance of the ARS charged fiber probe (blue line) is higher than in subsequent steps for shorter wavelengths, i.e. when the same probe has been immersed in the solution with glucose and has released ARS (green line). (Ideally, if the glucose was able to disrupt all the ARS-boronic bonds, we would achieve the original absorption curve corresponding to the functionalized fiber (Figure 2.14, red line)). In order to see the effect clearly, the right-hand side graph (Figure 2.15) plots the normalization of the immersed absorption with the ARS charged state, showing a dramatic decrease of the absorbance around the ARS absorption wavelength.

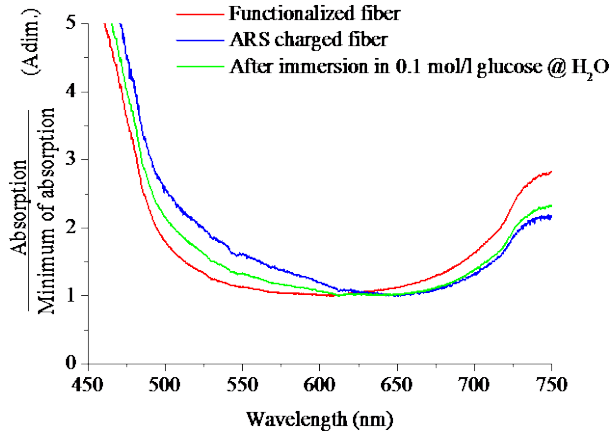

Figure 2.14 Normalized absorption curves of the probe before and after 10 minutes of immersion in 0.1 mol/l glucose solution in H_2O.

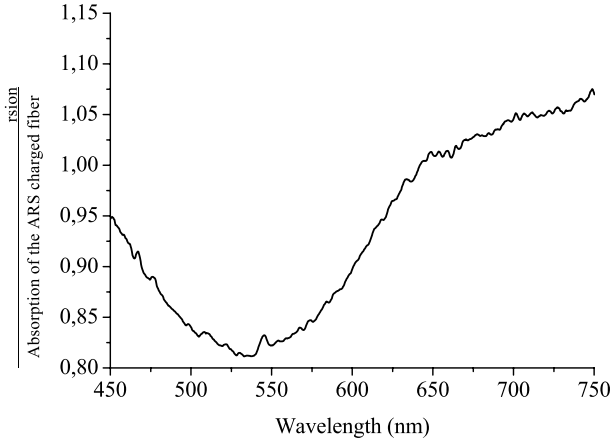

Figure 2.15 Division of ARS charged absorption and post-immersion absorption curves.

Regarding the physiological media, PBS and TRIS, their results are shown in Figure 2.16, Figure 2.17, Figure 2.18 and Figure 2.19.

For both physiological media, the charged probe released the ARS due to the bonding of glucose on the boronic acid functionalized surface of the probe. For the case of PBS (Figure 2.16), we can also observe a valley in the absorption spectrum around 533 nm, as it can be observed in Figure 2.17. In the case of TRIS (Figure 2.18), the probe behaved qualitatively in the same way as in the other media. In fact, it has been ensured

that in the reaction no other effect might influence the absorption of the fiber probe. All in all, we can conclude that, irrespective of the media, the performance of the sensor is similar, even though the experimental results suggest a larger amount of ARS released in H_2O.

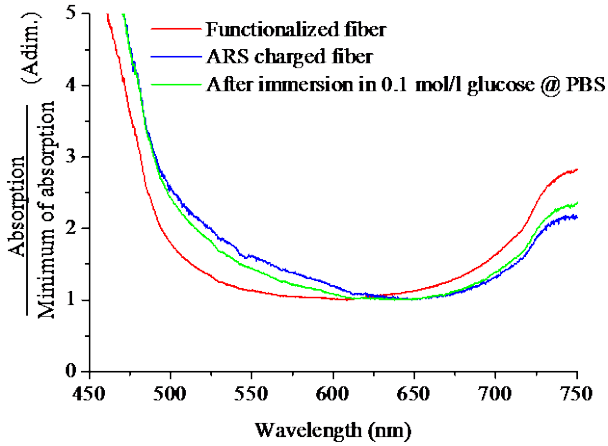

Figure 2.16 Normalized absorption curves in 0.1 mol/l in PBS detection.

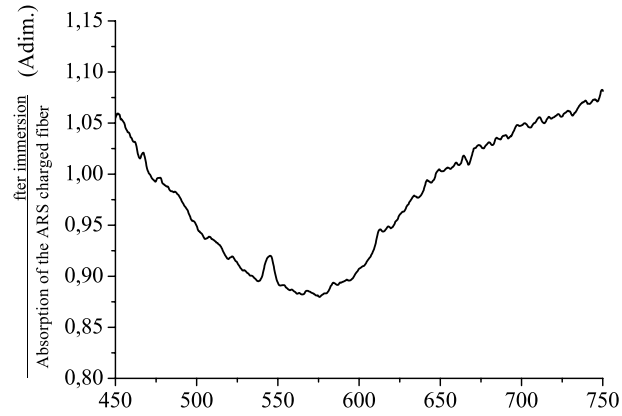

Figure 2.17 Division of ARS charged absorption and post-immersion absorption curves.

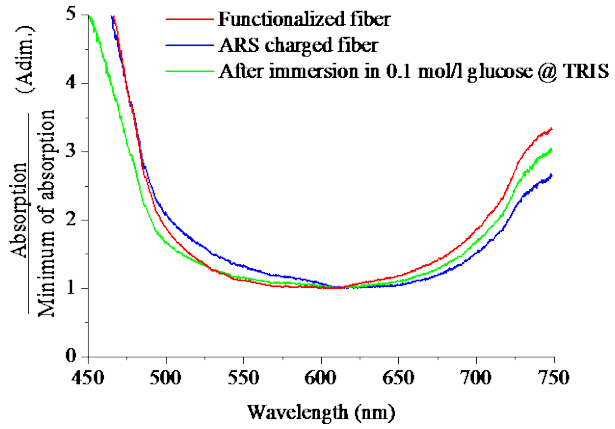

Figure 2.18 Normalized absorption curves in 0.1 mol/l in TRIS detection.

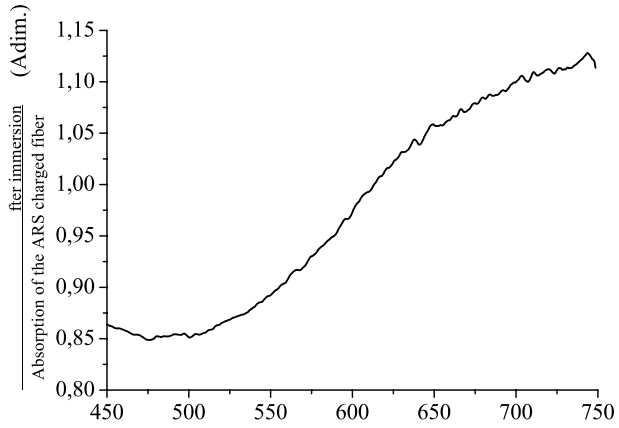

Figure 2.19 Division of ARS charged absorption and post-immersion absorption curves.

2.6 Conclusions

The main conclusion that we obtain from the presented glucose detection system is that we have been able to join two research areas, such as the POF sensing and surface functionalization techniques, resulting in a reliable low-cost and highly selective glucose detector. The functionalized U-shaped probes for FOEW absorption measurements are able to detect glucose in three different media, being the three of them of great interest in the

biosensing field. It has been the first time that such type of detector has been developed so far, and we have successfully adapted a functionalization process to our POF probes, in order to provide them with a bigger selectivity. Additionally, we have fabricated our own POF, which suits the requirements of the detector. Besides, by the described experimental set-up we are able to monitor the spectra during all the functionalization steps, and hence confirm that the probes have been successfully functionalized.

Nevertheless, even if the U-shaped POF probes have been a successful research up to this point, there are many of its biosensing characteristics that have to be improved due to the sensing limitation that arose during its development. The main lack of the detector is that they are not able to measure the concentration of the solution in which the sensor is immersed. For that reason, we decided to change completely the sensing approach as it is described in the forthcoming chapter.

Chapter 3 / 3. Kapitulua

Glucose sensing by Raman spectroscopy using Liquid-Core microstructured Polymer Optical Fibers

Raman espektroskopia bidezko Glukosa-neurketak Likidoz betetako nukleodun Polimerozko Zuntz Optiko mikroegituratuak erabiliz

Abstract—This chapter describes a new approach to measure the Raman spectra of glucose in low concentration solutions using Liquid-Core microstructured Polymer Optical Fibers. The Modified Total Internal Reflection enables the transmission of the pumped light through the core, which is filled by the solution containing the target sample, and, therefore, it produces large interaction distances between the light and sample, as well as the guidance of the scattered light. With this approach, the fiber-probe enhances the Raman spectra of the glucose. Herein, low concentrations of glucose are measured and quantified in three different fibers; all the measured concentrations are in the range of interest by medicine.

Laburpena—Kapitulu honetan, kontzentrazio baxuko glukosa-disoluzioen Raman espektroa neurtzeko metodo berri bat azaltzen da Likidoz Betetako Nukleodun Polimerozko Zuntz Optiko Mikroegituratuak erabiliz. Aldatutako Barneko Islapen Osoari esker, neurtu nahi den disoluzioz beteta dagoen nukleoan zehar hedatzen da ponpatutako argia, eta, ondorioz, interakzio-distantzia luzeak lor daitezke eta dispertsatutako argiaren gidapena ziurta daiteke. Neurketa-modu horrekin, zundak glukosaren Raman espektroa areagotzen du. Kapitulu honetan, kontzentrazio baxuko glukosa-disoluzioak neurtu eta

kuantifikatu dira hiru zuntz ezberdin erabiliz, beti ere medikuntza-eremuak interesgarri deritzon kontzentrazioetan.

Microstructured Optical Fibers (MOF), also known as photonic crystal fibers, owing due to their unique geometry structure and light guiding properties, show an outstanding potential for microliter –or even nanoliter- volume biosensing purposes. This field has recently invoked much attention due the gradually maturing fabrication techniques of fiber microstructures, as well as the development of surface processing techniques that enable the activation of fiber microstructures with functional materials [75]. Many approaches have been taken in order to exploit the potential of MOFs in biosensing applications, such as those that rely on light absorption from aqueous biosample in the holes of the structure [76], or those that use the surface plasmon resonance in order to detect the target sample [77]. Even though, the approach that will deeply be studied herein is the implementation of the MOFs as part of a Raman spectroscopy sensing platform, in order to enhance the scattered signal.

The Raman spectroscopy is a chemical selective and noninvasive technique that has evolved as an extremely powerful analytical tool in many biosensing applications [45]. The Raman spectrum of the sample gives vast information which is either qualitative or quantitative. The unique fingerprint of each target sample also provides a huge selectivity. However, this tool has its own challenges that have to be overcome such as the low efficiency, i.e. only one of 10^7 photons suffers from inelastic scattering and, therefore, it needs elaborated enhancement techniques[78]–[80].

One of the most promising method to overcome the low efficiency of the Raman scattered signal for liquid samples or solutions is to use hollow-core MOFs [81], [82]. These kinds of fibers have a central hollow-core surrounded by a holey structure and have the ability to guide the light within their central core. By this way, it is possible to guide the launched and the scattered light through a solution containing the target sample, which is contained in the central hole, and obtain large interaction distances and an enhancement of the Raman signal [83]. As the enhancement of the Raman spectra resides in the light guiding through the fiber, this enhancement phenomenon is called Fiber Enhanced Raman Spectroscopy (FERS).

The predecessors of MOFs for biological solution analysis were the Liquid Core Waveguides or Liquid Core Optical Fibers [84]–[91], which took advantage of the lower Refractive Index (RI) in the waveguide compared with the RI in the core, in this case the RI of the solution containing the sample. By this way, we could ensure the light transmission through the core by total internal reflection. These waveguides were mainly made of low-RI Teflon-AF or fused silica. The former shows a RI of 1.29, which is well-below to the aqueous solutions, close to 1.33, and important enhancements were reported for organic solvents or aqueous solutions. The latter, on the contrary, has a RI of 1.45, even though, the layer was thin enough to ensure the total internal reflection in the silica-air interface. This set-up showed many disadvantages as the light guiding was sensible to any stain on the outer surface, or the strong background signal of the silica as the light was also propagating through the waveguide.

Current researches show that FERS is a chemical selective, ultrasensitive technique, with extremely low sample demand and has remarkable potential for wide range of life-science applications using Liquid-Core microstructured Polymer Optical Fibers (LC-mPOF) filled by the solution containing the target sample. Yan et al. [92] reported in many published works, different type of fibers, apart from MOFs, in order to obtain the Limit of Detection (LOD) and the Limit of Quantification (LOQ) values required for the diagnosis in the early stage of many diseases, such as those related to hyperbilirubinemia and hyperbiliverdinemia.

Besides, in many other works, researchers modified slightly the FERS approach in order to design and implement an ideal platform for Surface Enhanced Raman Spectroscopy (SERS) [93], as the inclusion of metallic nanoparticles enhances the Raman spectra of the target samples in many orders of magnitude. By confining the light in the core filled with the target sample and nanoparticles (either adding them to the solution or attaching them to the inner walls of the hollow-core), a much better excitation of the plasmons is obtained and, therefore, a much better Raman spectrum. Nevertheless, SERS measurements can increase the budget of the platform and need deeper studies in order to optimize the platform for each target sample.

Another important feature about MOFs is the base material. Typically, the market and research has entirely been dominated by glass fibers; however, Hollow-Core

microstructured Polymer Optical Fibers (HC-mPOF) are actually emerging thanks to their useful properties. Fabrication of HC-mPOFs with polymers such as Poly(methylmethacrylate) (PMMA) or polycarbonate (PC) decreases the production costs considerably due to the low cost of the materials. Besides, the melting temperature in the fabrication process is much lower; it decreases from nearly 1900 ^{o}C down to 240 ^{o}C for the polymer of choice. By this property, the inner walls of the probe can be easily functionalized in different fabrication steps. Extra advantages over their silica counterparts are their flexibility or biocompatibility, among many others. Contrarily, the main challenge that arises with HC-mPOFs for Raman sensing, is the strong background signal, which apparently, constraints the use polymeric materials for sensing. Nevertheless, if a correct target sample is chosen, and with adequate signal processing, this drawback could easily be overcome. From now on, although the explained basics can be applied to either silica or polymer fiber, we will only focus on the latter.

Herein, the advantages and principles of the FERS enhancement are firstly discussed and, afterwards, the fabrication process of the HC-mPOFs is described. Finally, the performed measurements are shown in order to define the enhancement that the platform could offer. For the applications that we had on mind, the SGLT-2 inhibitor therapy monitoring explained in chapter one, we set the goal of the platform in the LOD value under 5 mmol/l of glucos

3.1 Fiber Enhanced Raman Spectroscopy (FERS)

In a traditional measuring method like the droplet, the collected Raman signal comes from a small scattering volume, which is limited by the substance in the focus spot of the optical setup (Figure 3.1(a)). With this setup, the low efficiency of the Raman scattering is evidenced. One widespread method to overcome this limitation is to use HC-mPOFs. By enabling the target solution to fill the holes where the light will be transmitted through, the Raman spectrum of the solution is enhanced. One approach in order to understand the HC-mPOF contribution is to see the fiber as an improved container for the measurement of solutions optimizing the sensitivity (Figure 3.1(b)).

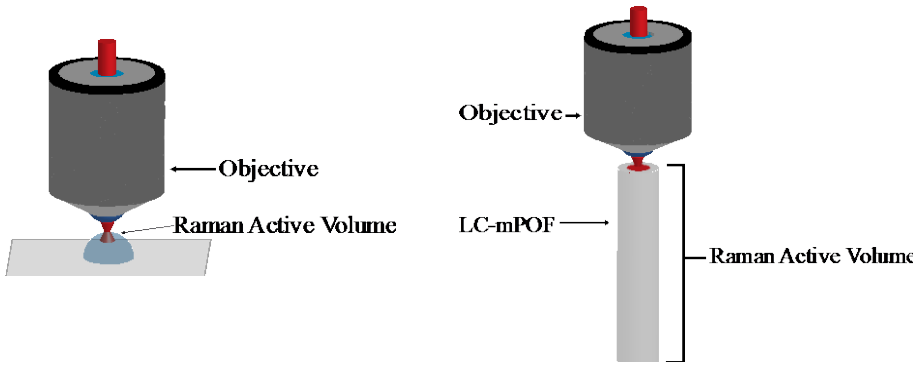

(a) (b)

Figure 3.1 Illustration of different measurement set-ups. (a) A droplet measurement. (b) FERS measurement.

This improved container could also be modelized, considering that the intensity of the Raman peak for a solution containing the target sample can be defined as follows [94]:

$$I_{Raman} \propto N\, I_o\, (w_o - w_r)^2\, |\alpha|^4, \tag{3.1}$$

where I_{Raman} is the obtained scattering intensity of a Raman peak, I_0 the excitation intensity, N the number of target molecules, w_0 the excitation wavelength, w_r the excited vibrational frequency, and α the polarizability of the molecules. None-the-less, for the FERS approach, it can be said that a specific Raman peak of the analyte (I_{Raman}) is proportional to the effective fiber length (L_{eff}), the laser intensity (I_0), the cross-section of the analyte (σ), and the concentration (c).

$$I_{Raman}(\sigma, c) = A'\, I_0\, \sigma\, L_{eff}(c)\, c. \tag{3.2}$$

The coefficient A' gathers the attenuations produced by all the optical components that the launched laser beam has to pass through, and the optical coupling. This coefficient is assumed to be constant in a series of measurements using the same fiber geometry and diameter.

L_{eff} can be deduced by integrating the transmission functions all along the fiber path (L_p). Therefore, the effective length can be defined as follows:

$$L_{eff} = \int_0^{L_p} T_l(z)\, T_r(z) dz, \tag{3.3}$$

where $T_l(z)$ is the ratio of the laser intensity coupled on the fiber at a certain point z. In the same way, $T_r(z)$ describes the ratio of the Raman intensity at the end-face of the fiber to the Raman intensity at scattering point *z*. These transmission equations decay exponentially following the next equations:

$$T_l(z) = e^{-(\mu_{sl}+\varepsilon_l c)\, z}$$
$$T_r(z) = e^{-(\mu_{sr}+\varepsilon_r c)\, z}. \quad (3.4)$$

The $\mu_{sl}(\lambda)$ and $\mu_{sl}(\lambda)$ parameters represent the effective scattering loss coefficients that account for the fiber imperfections at the laser and Raman wavelengths, respectively. $\varepsilon_l(\lambda)$ *and* $\varepsilon_r(\lambda)$ account for the analyte extinction coefficients at the wavelengths of the laser and Raman scattered radiation, and c is the analyte concentration. Calculating (3.3), next expression is achieved:

$$L_{eff}(c) = \frac{1-e^{-(\mu_{sl}+\mu_{sr}+\varepsilon_l C+\varepsilon_r C)L_p}}{\mu_{sl}+\mu_{sr}+\varepsilon_l C+\varepsilon_r C}. \quad (3.5)$$

Replacing the expression obtained in (3.5) in (3.2), the next expression is obtained:

$$I_{Raman}(\sigma, c) = A'\, I_0\, \sigma\, \frac{1-e^{-(\mu_{sl}+\mu_{sr}+\varepsilon_l C+\varepsilon_r C)L_p}}{\mu_{sl}+\mu_{sr}+\varepsilon_l C+\varepsilon_r C}\, c. \quad (3.6)$$

It is convenient to simplify (3.6) to the function expressed in (3.7) for the sake of better understanding:

$$y = A\, \frac{1-e^{-(D+Bx)L_p}}{D+Bx}\, x\,;$$
$$x = c\,;$$
$$y = I_{Raman}(\sigma, c);$$
$$A = A' I_0 \sigma;$$
$$B = \varepsilon_l + \varepsilon_r\,;$$
$$D = \mu_{sl} + \mu_{sr}\,. \quad ((3.7)$$

The main idea of a FERS platform is to adequate the A parameter as much as possible with the Raman microscope equipment available in the laboratory. However, the *D* parameter can be considered to be a key parameter to improve from the point of view of the design of a FERS platform. *D* summarizes the light guiding properties of the fiber in

both wavelengths, the launched and scattered wavelengths, and, by minimizing both, a much better enhancement would be achieved.

In practice, there are two types of fiber guiding mechanisms to obtain this enhancement, the first one is by using band-gap effect fibers and the second one is to use modified total internal reflection fibers by filling selectively the core of the fiber. The advantages and constraints of each of the approaches are explained in the next sections.

3.1.1 FERS by band-gap effect

Unlike conventional optical fibers, HC-mPOFs relying on the band-gap effect enable the light to be guided in an air-filled space (hollow-core), allowing minimal attenuation over extended lengths. Guidance is possible due to coherent Bragg scattering, where specific bandwidths of light are prevented from escaping into the cladding and are confined within the hollow-core [75]. In Figure 3.2 (a) a band-gap HC-mPOF with a lattice called Kagome is shown. Figure 3.2 (b) shows the same fiber, but when light is confined in the hollow-core.

(a) (b)

Figure 3.2 Photograph of the Kagome HC-mPOF. (a) Structure. (b) Structure when light is confined.

However, these band-gaps are closely related to the refractive indices of the material of which is made the HC-mPOF and the RI of the substance filling the holes. This means that the guided bands shift if the holes are filled with water as it can be seen in Figure 3.3.

With the aforementioned band-gaps, FERS enhancement is obtained, but strong limitations have to be taken into account. Firstly, the rather narrow transmission window

constraints its use. This means that some target samples could not be feasible for the platform as the Raman peaks fell out of the transmitted frequencies.

Secondly, the transmitted band-gaps are also very sensitive to the microstructure geometry, so any undesired modification along the fiber, like a fabrication error or end-face meniscus produced by non-correct filling methods, decrease dramatically the provided enhancement.

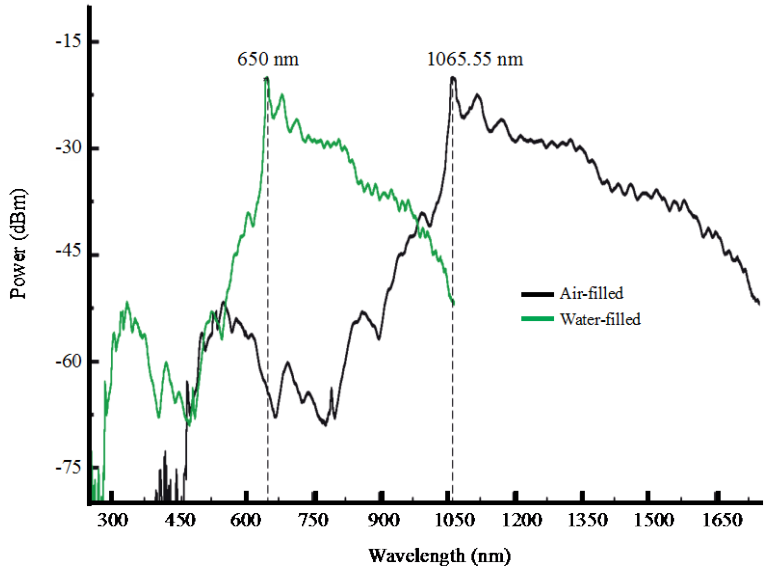

Figure 3.3 Transmission spectra of the Kagome lattice HC-mPOF when it is filled by air and water

3.1.2 FERS by Modified Total Internal Reflection (MTIR)

Conceptually, the Modified Total Internal Reflection (MTIR) is similar to the total internal reflection, which is the guiding mechanism of traditional optical fibers. Essentially, the RI in the core is higher than the RI of the cladding. By this way, the transmitted light will bounce and, therefore, be trapped in the core, enabling the correct light transmission, as it can be seen in Figure 3.4 (a). In order to obtain such a RI layout,

either the core or the cladding material is doped with different substances in order to modify it [20].

In the field of microstructured fibers, and with the aim of measuring aqueous solutions, this RI profile is obtained by accomplishing two goals (Figure 3.4 (b)). On the one hand, the hollow-core of the fiber is filled selectively with the solution containing the sample, obtaining a Liquid-Core mPOF (LC-mPOF) probe with a RI in the core close to 1.33. On the other hand, the effective RI of the cladding region has to be below the solution`s RI in order to get the desired RI profile. The last specification is obtained by increasing the air fraction in the structure. When these two features are achieved by means of MTIR, Raman spectrum is enhanced by FERS.

In comparison with the FERS obtained by band-gap effect, this method needs a slight modification in the probe in order to fill the core selectively, by fusing or collapsing the cladding holes. Nevertheless, the transmission bands are wider, making the same geometry feasible for many target samples. The herein presented and analyzed fiber geometries rely on the MTIR to produce the FERS.

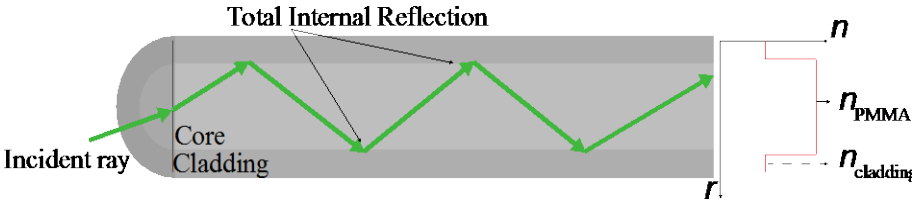

A light ray transmission in a traditional optical fiber through total internal reflection.

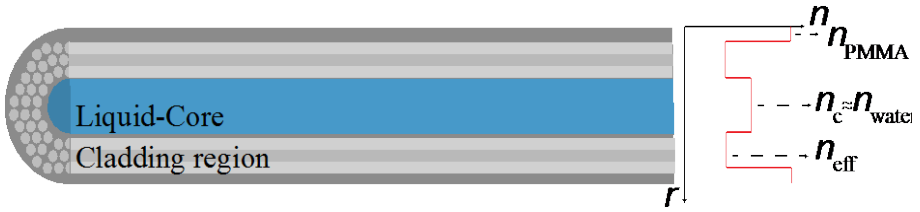

The LC-mPOF case.

Figure 3.4 Illustrations of light guidance in different cases.

3.2 LC-mPOF fabrication

In order to fulfill the aforementioned requirements, two different microstructure geometries were fabricated. The first one was a three-ring flower-shape HC-mPOF (3R HC-mPOF), while the second one was the six-ring HC-mPOF (6R HC-mPOF). Moreover, the 6R HC-mPOF was fabricated in two different diameter sizes maintaining the same geometry ratios, modifying some parameters in the last HC-mPOF drawing stage. Thus, we could be able to compare the FERS performance of three different HC-mPOFs.

In the next sections all the fabrication steps are described, from the design to the LC-mPOF probe for both microstructure geometries and sizes [72].

3.2.1 Design

The first step of a new HC-mPOF is the design, usually aidded by a simulation software. In this case, the software framework was PhotonDesign® (Oxford, United Kingdoom), which allows the calculation of guided modes through different structures and media. Nevertheless, the main goal of the design step is to obtain a geometry which can be replicated in the preform by the chosen technique and is suitable for FERS by MTIR.

However, the agreed geometry design rarely is precisely duplicated in the actual fiber; all the steps involved in the fabrication process alter somehow its geometry. Taking into account this fact, only a remote idea of structure of the fiber can be obtained from the software simulation step, but this rough idea of the geometry design will define all the forthcoming steps and will determine the fabrication parameters, such as the beat dimensions or drawing pressures.

For the first mentioned HC-mPOF geometry, a flower-shape core with a cladding consisting of three rings was developed to ensure the guidance through the core and to remove the undesired surface modes [95]–[97]. The designed geometry is shown in Figure 3.5 (a). Setting the RIs of the core in 1.33 and the RI in the holes in 1, as it will be in the measuring set-up, the guidance in the liquid-core is obtained as it can be seen in Figure 3.5 (b).

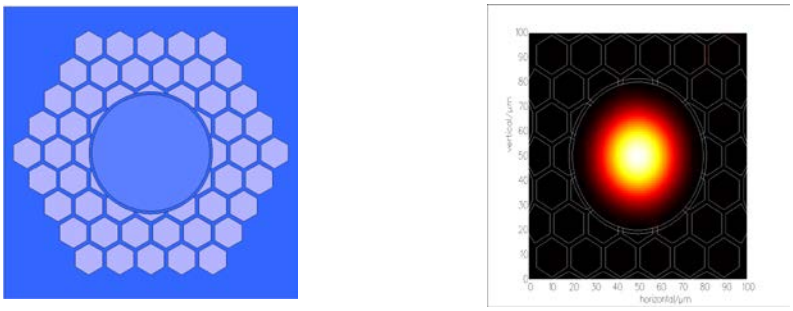

(a) (b)

Figure 3.5 Simulated geometry of the 3R-LC-mPOF with RI=1.33 for the core and RI=1 for the cladding holes. (a) The designed 3R geometry. (b) Intensity distribution of the first guided mode for a 785 nm light source.

Once the 3R HC-mPOF fiber was fabricated and its FERS analyzed, we concluded that the main design idea had to be to enlarge the air-fraction in the cladding region in order to decrease the RI. Besides, in order to simplify the drilling process, it would be better to discard the flower-shape of the core as it was hardly replicated in the actual 3R HC-mPOF. With all these considerations in mind, we designed the 6R HC-mPOF.

3.2.2 Preform fabrication by drilling

Once the design is finished, it has to be replicated in a preform. In the presented case, the drilling technique was employed for both structure geometries. A Computer Numerical Control (CNC) machine was used for this purpose. CNCs provide a great reproducibility, speed and accuracy compared to the main preform fabrication technique in silica microstructured optical fibers, which is the capillary stacking. The drills were made of carbide and they were refrigerated internally. This way, the quality of the holes was improved allowing much faster drilling speed as we prevented the drills from over-heating during all the drilling process.

The chosen structures were drilled in a solid optical quality PMMA rod with a diameter of 60 mm and a length of 120 mm for both structure geometries. In the case of the 3R HC-mPOF (Figure 3.6 (a)), the drill bits were 3 mm wide for the cladding holes and 11

mm for the core. For the 6R HC-mPOF (Figure 3.6 (b)), instead, 3 mm wide drill bit for the cladding holes and 5 mm for the core were used. Afterwards, the preforms were cleaned thoroughly with isopropyl alcohol and stored in low humidity (20 %) and high temperature (80 ^{o}C) conditions for several days with the aim of annealing, to maintain the quality.

(a) (b)

Figure 3.6 Photograph of the preforms. (a) 3R HC-mPOF. (b) 6R HC-mPOF.

3.2.3 Fiber Drawing

In the following step, the drilled preforms were drawn employing a two-step process. In the first one, the preforms were stretched up to a 3 mm wide intermediate cane (Figure 3.7 (a) and (c)), and then, the cane was sleeved with a PMMA tube, obtaining the secondary preform.

In the second step, the secondary preforms were drawn to the desired HC-mPOF dimension (Figure 3.7 (b) and (d)). In this process, many parameters can be tuned in order to modify the resultant geometry of the mPOF, such as the drawing speed or the air pressure proportioned to the cladding and core holes, which can be either positive or negative. By modifying the drawing speed, the higher the speed is, the smaller the obtained fiber diameter. By modifying the air pressure over the holes of the secondary preform, their diameters tend to expand or collapse.

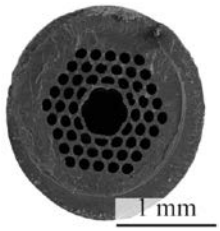

3R HC-mPOF cane.

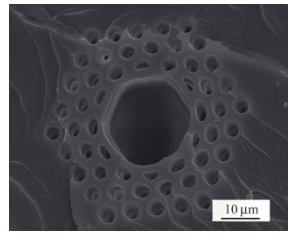

3R HC-mPOF fiber.

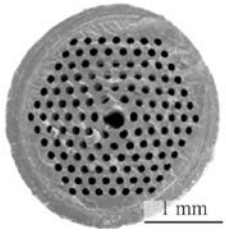

6R HC-mPOF cane.

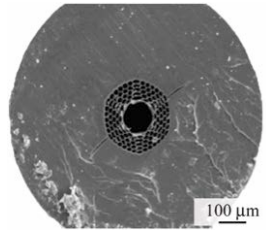

6R HC-mPOF fiber.

Figure 3.7 SEM images of the HC-mPOFs in cane and fiber state.

As mentioned previously, three HC-mPOF microstructure geometries were fabricated. In first instance, the 3R HC-mPOF was drawn (Figure 3.8 (a)). This fiber had a 70 µm hollow-core diameter and a 115 µm wide cladding region with a 1mm external diameter.

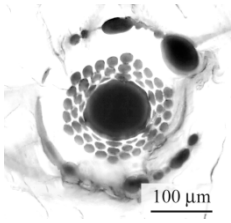

(a) 3R HC-mPOF

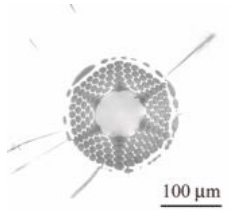

(b) 66 ϕ 6R HC-mPOF

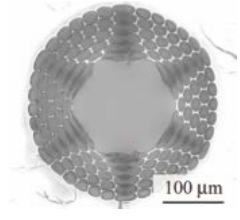

(c) 100 ϕ 6R HC-mPOF

Figure 3.8 Microscope images of the three fibers.

Besides, the 6R HC-mPOF was drawn in two different sizes maintaining the same microstructure design. The small-size 6R HC-mPOF was obtained with higher drawing speed, but lower pressure in the central core, whereas for the big-size 6R HC-mPOF, the speed was lower, but the pressure in the core higher (Figure 3.8 (b) and (c)). The

small-size fiber had a 66 µm diameter central hollow-core and a 660 µm external diameter with a core-cladding ratio of 0.42; in contrast, the big-size fiber had a 100 µm wide central hollow-core and 1 mm external diameter with a core-cladding ratio of 0.47 (almost similar to that of the small-size fiber). From now on, they will be named 66 ϕ and 100 ϕ, respectively.

3.2.4 End-face modification

In order to obtain a LC-mPOF, the hollow-core of the fiber has to be selectively filled. This was achieved, in this case, sealing the holes of the cladding and leaving the hollow-core open. This slight modification on the end-face of the probe was done following the procedure described by [98], [99].

Briefly, an optical adhesive called NOA 65 was solved in isopropyl alcohol 1/4 v/v. Afterwards, a well-cut end-face (Figure 3.9 (a)) of the probe was immersed in the solution for five seconds in the solution and the adhesive was cured with an UV lamp. As the capillary effect filling speed is closely related to the diameter of the hole, the adhesive reached more height in the hollow-core than in the holes of the cladding, so cleaving the fiber between these two distances leaded to a sealed core but an open cladding end-face (Figure 3.9 (b)). Then, this end-face was immersed again in the solution for ten seconds and cured. This time, the solution in the holes of the cladding reached more height than the adhesive previously cured in the hollow-core, so by cleaving the fiber in between, the pursued end-face was obtained (Figure 3.9 (c)). The same exact procedure was replicated for the three HC-mPOF types.

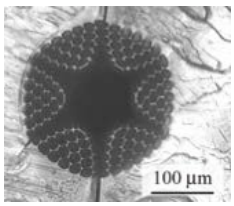

(a) Unmodified end-face

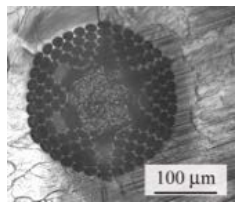

(b) Sealed core but open cladding end-face

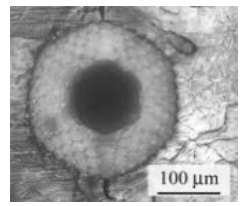

(c) Sealed cladding end-face

Figure 3.9 Microscope images in different steps for the modification of the end-face of the probe for the 100ϕ 6R HC-mPOF.

3.3 Experimental set-up and data-processing

3.3.1 Experimental set-up

Two different set-ups were configured in order to perform the desired measurements. In the first one, with the aim of measuring the Raman spectra of the solution in a traditional set-up, a simple polycarbonate cuvette was filled with the solution containing the target sample and the upper surface was focused with the microscope. Afterwards, the measurement was launched.

In the second one, for the case of LC-mPOF measurements, the unmodified end-face of different probes were held using an ad-hoc holder, and the opposite and modified end-faces were immersed in the solution, as it can be seen in Figure 3.10. The same setup was used for the three fibers (i.e. 3R LC-mPOF, 66 ϕ 6R LC-mPOF, and 100 ϕ LC-mPOF). With this setup, the central hollow-cores of different probes were filled with the target solution by capillary effect in a short period of time (≈ 30 s.). The required volumes for a 10 cm long fiber were 1.4 μl for the 3R LC-mPOF, 1.33 μl for the 66 ϕ fiber, and 3.14 μl for the 100 ϕ fiber. Once the LC-mPOF was completely filled, the launching laser beam was focused in the center of the core, and the experiment performed.

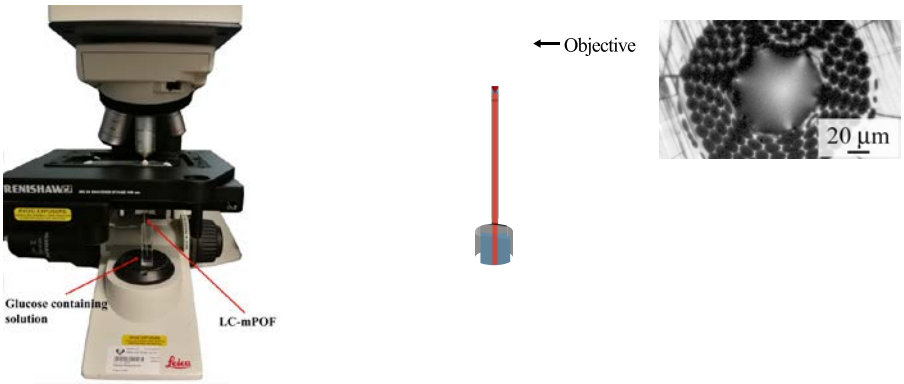

(a) (b)

Figure 3.10 The experimental set-up. (a) Experimental set-up in the Raman microscope. (b) Illustration of the immersion of the modified end-face.

Figure 3.11 shows the correct selective filling in both fiber structures. In both microscope photographs, we can see how the solution containing the target sample fills only the core-hole, from the upper end-face of the fiber.

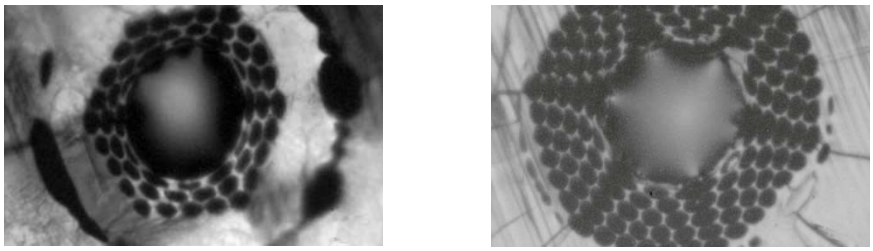

(a) (b)

Figure 3.11 Selectively filled unmodified end-faces. (a) 3R HC-mPOF. (b) 100 ϕ 6R HC-mPOF.

All the measured spectra were recorded using a Renishaw (Gloucestershire, UK) inVia confocal Raman Microscope. A near infrared 785 nm wavelength laser was used as excitation source and only 10 % of the maximum power was launched on the sample (more specifically, 27.61 mW). The acquisition time for each experiment was set to 10 s, in order to avoid any thermal effect either in the solution or in the structure of the LC-mPOF. The spectra were recorded from 100 cm^{-1} to 3200 cm^{-1}. For all the performed measurements, the used objective was a 50 X with a 0.75 NA from Leica (Wetzlar, Germany).

After performing many experiments, we observed that, when high optical powers were launched to the LC-mPOFs, the structure suffered many damages. For instance, an end-face of the 66 □LC-mPOF when 160.27 mW were launched to the core is shown in Figure 3.12. The absorption of aqueous solutions in the infrared region and the poor heat dissipation of the polymer caused the probe burnt. Taking into account this phenomena, we set the launched power to the 10 % (27.61 mW) as it is stated before.

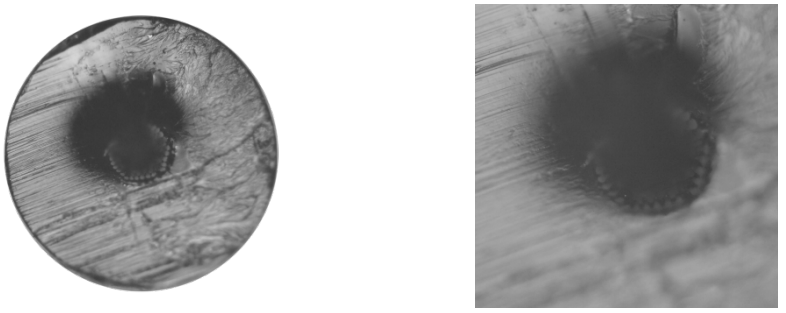

(a) (b)

Figure 3.12 Microscope images of a burnt end-face of the 66 ϕ 6R LC-mPOF. (a) 10 X magnification. (b) 20 X magnification.

3.3.2 Data-processing

In the performed set of measurements, the main target sample is glucose, which is an organic substance of a great interest in many medical fields, as it has been stated in previous chapters. However, the main challenge regarding our set-up is that polymer LC-mPOFs and the target sample glucose are formed by carbon links, so quantifying glucose in PMMA-based fibers is not a straightforward task.

Therefore, we could hide crucial information about the concentration of the target sample by over-processing the measured spectra, so extreme care was taken for the data-processing. For that reason, the baselines of the spectra were only subtracted using the *Fill Peaks* algorithm from the *Baseline* package [100], and any further processing was discarded. The used software was R, which is a free software focused for mathematics and statistics. Additionally, a specially developed package for this software called *hyperSpec* was used for the spectra management [101].

Regarding the Raman spectra of glucose and PMMA, the main peaks of the glucose placed at 917 cm^{-1}, 1066 cm^{-1} and 1127 cm^{-1} [78] interfere with strong peaks corresponding to the background PMMA signal provided by the fiber either when it is hollow or selectively filled with water [102], as it can be seen in Figure 3.13.

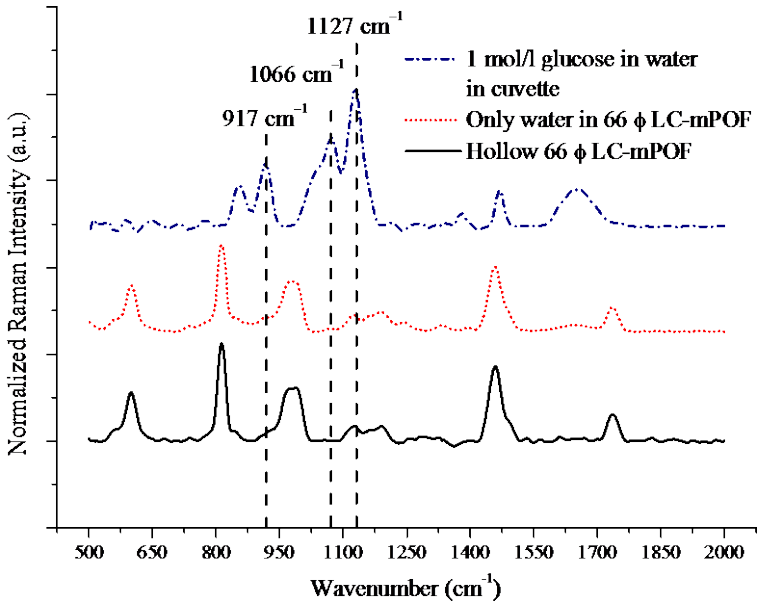

Figure 3.13 Raman spectrum of glucose (1 mol/l concentration) (blue line), background PMMA spectrum of the LC-mPOF when it is filled with water (red line), and background PMMA spectrum of the HC-mPOF (black line).

The chosen approach was to calculate a ratio of areas between specific ranges in the spectra, from now on denoted by area-ratio, as shown in (3.8) and Figure 3.14:

$$Area - ratio = \frac{Area\ from\ 1020\ cm^{-1}\ to\ 1140\ cm^{-1}}{Area\ from\ 1140\ cm^{-1}\ to\ 1300\ cm^{-1}}. \quad (3.8)$$

As a consequence, measurements obtained from a solution without glucose will result in a low area-ratio. However, the area-ratio will increase with higher glucose concentrations as the area from 1020 cm^{-1} to 1140 cm^{-1} will be larger caused by the contribution of glucose peaks.

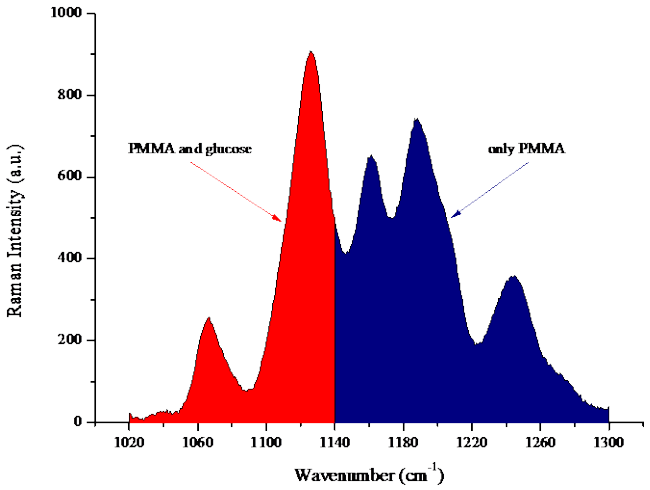

Figure 3.14 The areas used for the area-ratio calculations

In the first attempt using the 3R HC-mPOF, we concluded that it was not possible to determine SNR only with glucose. For that reason, $K_3[Fe(CN)_6]$ was added to the solutions in the second attempt as internal standard control element, which was only measured for 6R HC-mPOFs. For all these new measurements, we took as reference signal the peak located at 2140 cm^{-1}, since it corresponds only to the $K_3[Fe(CN)_6]$ and there is no interference from any other substance [103]. This peak was Gaussian fitted and the SNR was calculated following (3.9):

$$SNR = \frac{Intensity\ at\ 2140\ cm^{-1}}{\sigma^2\ (non-signal\ region)}, \tag{3.9}$$

where σ is the standard deviation of a range in the spectra without peaks, i.e. its mean value is equal to zero.

Furthermore, when a calibration curve is obtained, we can calculate the LOD and the LOQ with the well-known formulas given by (3.10) and (3.11) [104]:

$$LOD = 3\sigma^2/S, \tag{3.10}$$

$$LOQ = 10\sigma^2/S, \tag{3.11}$$

where σ is the standard deviation of the linear fitting and S is the slope.

3.4 Results and discussion

The description of the results is shown in two different sections, following the chronologic order in which they were obtained. The first measurements were performed using the 3R HC-mPOF and the obtained feedback allowed us to design the 6R geometry, focusing on some parameters which previously were not taken into account.

Afterwards, in order to overcome the lacks of the first measurement collection, we designed a wider set of measurements for the 6R LC-mPOFs. One of the measuring targets was to calculate the enhancement provided by the inclusion of the fiber in the measuring platform. As mentioned before, $K_3[Fe(CN)_6]$ was added to the solutions and the SNR measured for both 6R HC-mPOF fiber diameters and the traditional cuvette set-ups. Besides, studies according to the fiber length and how much the glucose affects the SNR are also presented. Lastly, measurements of aqueous low concentration glucose measurements are charted in the region of the SGLT2 inhibitor therapy. Patients suffering daily glucose losses between 70-120 g are common and Tahara et al. reported urinary glucose concentrations varying from 5 mmol/l (100 mg/dl) to 17 mmol/l (300 mg/dl) approximately after 6 hours of SGLT2-inhibitor ingestion [105].

3.4.1 3R HC-mPOF measurements

Six different glucose concentrations in water, ranging from 0 up to 1000 mmol/l, were measured using the 3R HC-mPOf firstly. The obtained spectra were processed as described in section 4.2, and the obtained results are shown in Figure 3.15.

With the measurements shown in Figure 3.15, we concluded that solutions with concentrations higher than 250 mmol/l did not show higher area-ratio. According to (3.7), this behavior is expected since the *D* parameter is worse for high concentration as the dispersion losses are higher.

Another important note to take into account from this experiment bench is that the variation of these fibers for 100 mmol/l is extremely high and we would never achieve the required sensitivity for the proposed goals. For that reason, the 3R HC-mPOF was

discarded for further tests and, therefore, new HC-mPOF geometries were tested in following experiments.

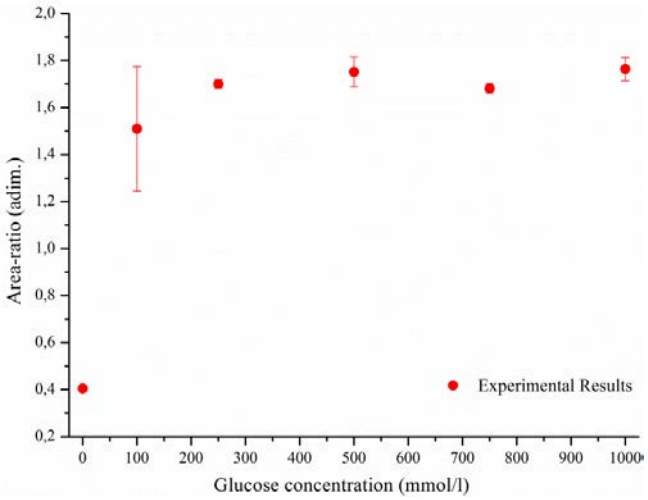

Figure 3.15 Experimental area-ratio measurements for the analyzed glucose concentrations for the 3R LC-mPOF.

3.4.2 6R HC-mPOF measurements

The following measurement set was made using the 6R LC-mPOF, and the measurements were designed in order to measure the FERS effect among other parameters. In the first place, the enhancement factor was calculated by adding a particular additive to the solutions. Once the enhancement factor was calculated, the optimum length of the probe was also searched and the influence of the enhancement factor according to different glucose concentrations analyzed. Afterwards, different measurements were done with glucose in low concentration solutions.

3.4.2.1 SNR enhancement and fiber probe length

To measure the SNR, we prepared solutions with six different concentrations of glucose, ranging from 0 mmol/l to 25 mmol/l in steps of 5 mmol/l, and a reference concentration of 25 mmol/l of $K_3[Fe(CN)_6]$. The objective was to quantify the

enhancement provided by the use of different diameter 6R LC-mPOFs in first instance, and to check whether the enhancement depends on the glucose concentration and/or the length of the probe, in second and third instances, respectively.

For both LC-mPOF fiber sizes, the precise focusing of the launching beam on the fiber-core is critical for FERS measurements to be valid. For that purpose, SNR threshold values were defined. Acquisitions with SNR values below 1000 were discarded for the 66 ϕ LC-mPOF, and SNR values below 500 for the 100 ϕ LC-mPOF. Discards were made under the assumption that, in those cases, the incident spot was not properly focused on the core.

Table 3.1 shows the SNR values obtained from all valid measurements for the cuvette and both 6R fiber sizes regarding the Raman peak of $K_3[Fe(CN)_6]$ at 2140 cm^{-1}.

Table 3.1 SNR of the different set-ups.

Set-up	SNR
Cuvette	32 ± 1
66 ϕ LC-mPOF	1220 ± 40
100 ϕ LC-mPOF	680 ± 20

From the SNR values we can observe that the best Raman signal enhancement is achieved with the 66 ϕ LC-mPOF probe. Besides, we can conclude that, in comparison with the cuvette, and using the same configuration, the enhancement of the SNR values reaches up to 37 times for the 66 ϕ and 21 times for the 100 ϕ LC-mPOF. This behavior can be seen in the average intensities of the peak located in 2140 cm^{-1} for the different set-ups (Figure 3.16).

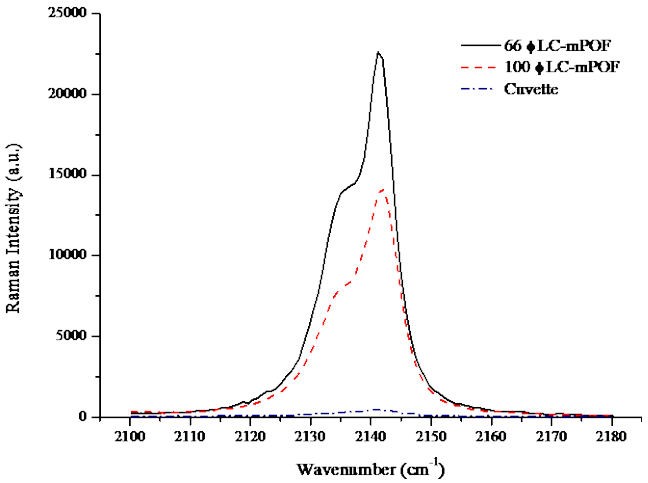

Figure 3.16 Comparison of the Raman average spectra around 2140 cm^{-1} for the cuvette and both fiber sizes.

Afterwards, we split the performed SNR measurements of the LC-mPOFs taking into account the glucose concentration. Detailed results can be seen in Figure 3.17 (the vertical bars denote the uncertainty associated with each measurement).

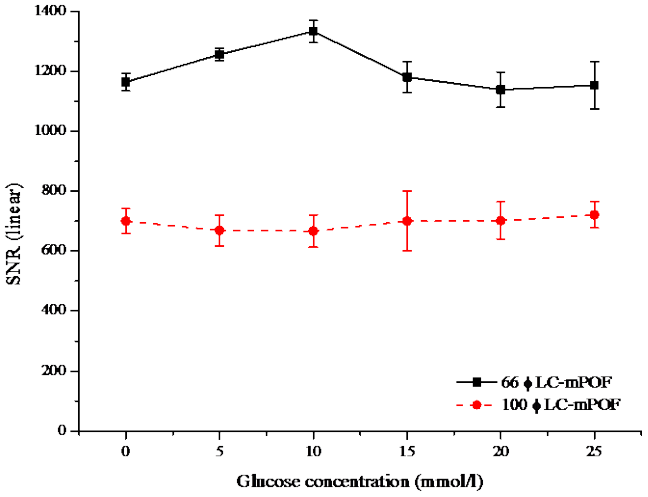

Figure 3.17 SNR values according to the glucose concentration.

From this chart, it can be concluded that the different glucose concentrations do not affect the peak of $K_3[Fe(CN)_6]$ intensity peak, nor the SNR values as expected. The standard deviation of the SNR values measured for the solution of different glucose concentration is lower than 10 % for both fiber diameters (notice that the $K_3[Fe(CN)_6]$ concentration is always the same in all these measurements). The slight variations observed in Figure 3.16 may be attributed to focusing divergences and/or to slight variations on the concentration due to preparation uncertainties.

Finally, different fiber lengths were measured. At this point, it has to be said that, for the 100 ϕ LC-mPOF, it was not possible to fill the core by capillary effect for lengths exceeding 10 cm, as the dimensions were too big. For the 66 ϕ LC-mPOF, lengths from 6 cm up to 15 cm were measured. The obtained results are displayed in Figure 3.18.

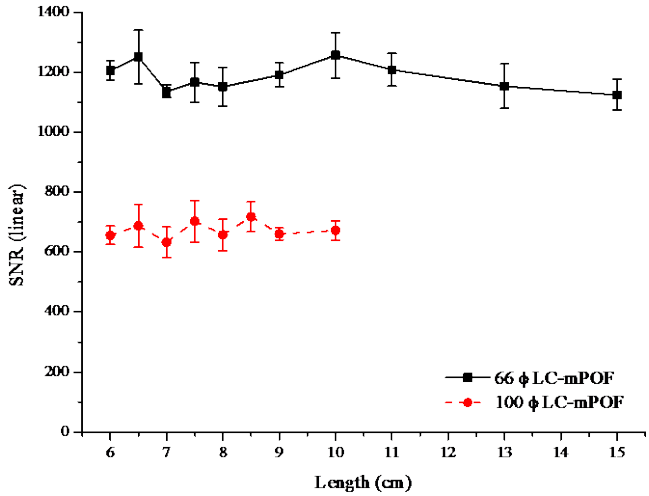

Figure 3.18 SNR values as a function of the fiber probe length.

The obtained results show that the SNR does not improve at all with the length, indicating that, for longer interaction distances, fiber losses go against the contributions in the Raman spectra intensity. The standard deviation in this range is of 3.88 % for the 66 ϕ and of 4.53 % for the 100 ϕ 6R LC-mPOF. In accordance with the results, the glucose concentration measurements shown in the forthcoming section will be performed with 10

cm long fiber probes, since such a length provides easy-to-handle probes and, at the same time, reasonably low solution volumes have to be used.

3.4.2.2 Glucose concentration measurements

With the aim of testing the efficiency of the 6R LC-mPOF-based FERS platform as a glucose sensor in a clinically relevant range, measurements with 66 ϕ and 100 ϕ 6R LC-mPOF were performed for 0, 5, 10, 15, 20, and 25 mmol/l glucose solutions, together with 25 mmol/l of $K_3[Fe(CN)_6]$.

For each glucose concentration, at least three high SNR measurements were performed and the area-ratio calculated for each of the two diameter fiber probes using (3.8). From the averaged measured spectra, we can observe an increase of the intensity of the peaks at 1127 cm^{-1} and 1066 cm^{-1} corresponding to glucose, whereas the peak for the only-PMMA at 1190 cm^{-1} is constant. The ratio of these regions is charted in Figure 3.19. It is also remarkable that these glucose concentrations could not be measured using the cuvette set-up.

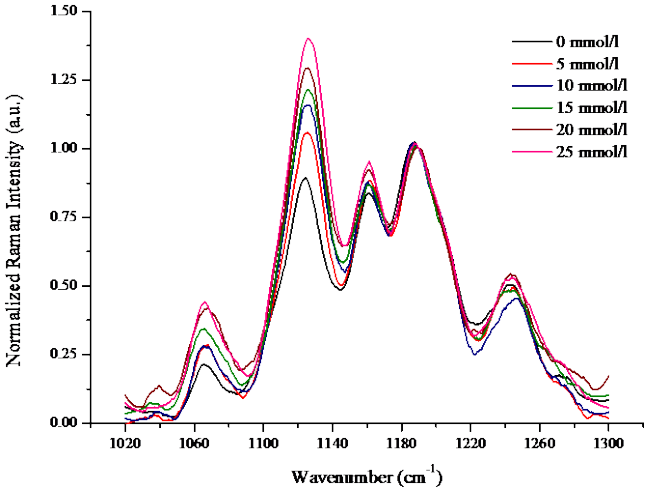

Figure 3.19 Processed Raman average spectra normalized for the peak at 1190 cm^{-1} for different glucose concentrations measured in 10 cm length 66 ϕ LC-mPOF.

From these spectra, it can be observed that even slight variations of 5 mmol/l in the glucose concentration are detected. Figure 3.20 and Figure 3.21 show the area-ratio for

experimental results and the linear fitting for the 66 ϕ LC-mPOF and the 100 ϕ LC-mPOF, respectively.

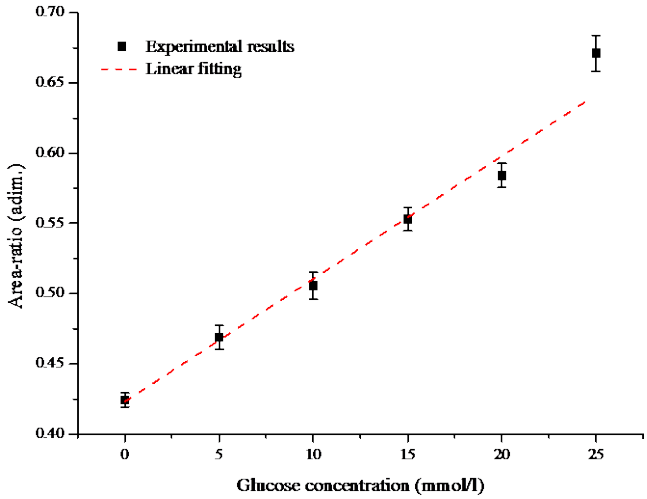

Figure 3.20 Experimental area-ratio measurements and linear calibration curve for the analyzed glucose concentrations for the 66 ϕ LC-mPOF.

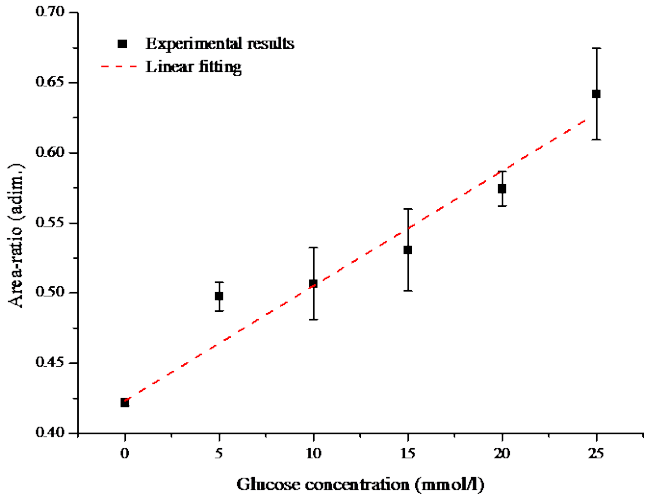

Figure 3.21 Experimental area-ratio measurements and linear calibration curve for the analyzed glucose concentrations for the 100 ϕ LC-mPOF.

From the experimental results, we could demonstrate that a minimum sensitivity threshold of 5 mmol/l was measured for the 66 ϕ LC-mPOF with our sensing platform. For the 100 ϕ LC-mPOF case, whose higher standard deviations for different measurements made it less suitable for our purposes, we were not able to ensure the sensitivity. The values of the Pearson correlation coefficient (r) for the linear fitting were 0.992 for the 66 ϕ LC-mPOF and 0.975 for the 100 ϕ LC-mPOF.

For the 66 ϕ LC-mPOF, the calculated LOD was 0.183 mmol/l and the LOQ was 0.612 mmol/l. For the case of the 100 ϕ LC-mPOF, the LOD was 0.338 mmol/l and the LOQ was 1.129 mmol/l. These results demonstrated the feasibility of this novel and easily affordable LC-mPOF-based FERS platform to monitor glucose in aqueous media in clinically relevant concentration range. Thus, this sensing platform has great potential for further studies in biological fluids such as urine, pawing a way for a potential therapeutic SGLT2 inhibitor monitoring device.

3.5 Conclusions

All along this chapter, the FERS approach for measuring glucose in low concentrations is described. Firstly, a deep analytical study of the effect has been described. Afterwards, and with the aim of achieving low LOD and LOQ values, three different HC-mPOFs have been fabricated and tested. The entire fabrication process, from the design to the end-face modification has deeply been described and shown. The designed set-up provides a Raman signal enhancement above one order of magnitude compared to conventional cuvette. These results indicate the detection and quantification of low glucose concentrations, with a LOQ value of 0.621 mmol/l and a LOD value of 0.186 for the 6R LC-mPOF with a 66 µm diameter core. Thus, this platform enables the detection and quantification of clinically relevant low glucose concentrations, showing great potential for urinary glucose monitoring during SGLT2 inhibitor therapy. The volume of solution necessary for the measurements is 1.33 µl for the LC-mPOF with a 66 µm diameter core and a length of 10 cm, which makes this sensing platform an ideal candidate for bio-sensing applications.

Chapter 4 / 4. Kapitulua

General Conclusions and Future Work for the improvement of the developed Biosensing platforms

Ondorio Orokorrak eta Etorkizuneko Atazak garaturiko Biosentsore plataformen hobekuntzarako

Abstract—The aim of this chapter is to describe the possible improvements of the sensing and detection systems described in previous chapters. For that purpose, we give a general overview of the state-of-art of biosensors mentioning the herein developed platforms. In addition, new challenges and required specifications for biosensors are listed. Hence, we describe many applications in which the developed platforms could be implemented. Besides, some first measurements of real applications are shown.

Laburpena— Kapitulu honen asmoa aurreko ataletan erakutsi diren sentsore eta neurketa sistemen etorkizuneko hobekuntza aukerak azaltzea da. Horretarako, biosentsoreen gaur egungo egoeraren ikuspegi orokorra deskribatzen da, tesian zehar garatu diren plataformak aipatuz. Horretaz gain, biosentsoreen erronka berriak eta hauek bete beharko dituzten ezaugarriak zerrendatzen dira. Honenbestez, garaturiko plataformak ezarri daitezkeen hainbat aplikazio azaltzen dira. Gainera, zenbait aplikazio errealetako lehen neurketak aurkezten dira.

Biosentsoreen ikerkuntza, erabilpena eta garapena azken urteotan areagotu egin da. Testuinguru honetan, glukosa detektatzeko bi paradigma ezberdin aurkeztu dira aurreko kapituluetan, biak ere PZOetan oinarrituak. Hala ere, aurkezturiko sistemek bizitza

errealeko aplikazio klinikoetan erabiliak izatera iristeko aurrerapauso batzuk behar dituzte. Hori dela eta, garapen hauen noranzkoa zehazteaz gain, biosentsoreen eskaerak zehaztuko dira kapitulu honetan.

Substantzia kimikoak detektatu eta neurtzeko erabiltzen diren gailu hauen etorkizuna oparoa dela jakina da, baina berauen ezarpen hedatua eman dadin, hainbat ezaugarri bermatu behar dituzte. Erabiltzaile edo bezeroen lehen eskakizuna, noski, neurketa sistemen kostu baxua da, baina badira beste hainbat, sinpletasuna edo azkartasuna, besteak beste. Gainera, sentikortasun handikoak eta egoera ezberdinetan fidagarriak izan behar dira, sistema irmoak direla bermatuz.

Nahiz eta deskribatu diren ezaugarriak nahiko orokorrak izan, PZOetan oinarrituriko sistemek eskaerak ia osotasunean betetzen dituztela esan behar da. Hori dela eta, gaur egun oso zabalduta daude medikuntza, farmakologia edo osasungintza eremuetan [106]. Aurkezturiko sistemak, U formako detekzio sistemak zein NH-PZOm sistemak, kostu baxukoak, hautakorrak, muntaia sinpleekin eraikiak izateko eta momentuan emaitza jakiteko diseinatu dira. Raman espektroskopia jorratzen duenak gainera, sentikortasun handia eskaintzen du glukosaren kontzentrazioa erabakitzeko orduan, eta Raman espektroskopiari esker, fidagarritasun handia bermatzen du.

Dena den, analisi klinikoetarako edo beste edozein motako aplikaziotan erabili ahal izateko, sentsore sistemak, etorkizuneko eskaerak edo joerak betetzeko helburuz garatu egin behar dira. Joera hauen artean, biosentsoreen multiplexazioa aurkitzen da [107]. Biosentsore bakarra erabiliz hainbat substantzia kimiko ezberdin aldi berean neurtzea da helburua. Bestetik, teknika ezberdinen garapenek sentikortasuna handitzea dakarte, molekula bakarraren detekzioraino. Honela, modu zuzenean zelulak banaka aztertu ahal izango dira erreakzio denborak laburtuz.

Beste garapen korronte bat epe luzerako sentsore adimenduena da. Sentsore hauek giza gorputzean inplantatu ahal izango dira eta, erabiltzaileak erabakitzean, neurketa konkretu bat egin ahal izango dute. Eredu honek hainbat gaixotasunen garapen historikoa izaten lagun dezake, bizi-parametroen monitorizazio jarraitua ahalbidetuz. Sistema hauek, ordea, hainbat arazo aurkezten dituzte, etikoak besteak beste. Izan ere, epe luzerako diseinaturiko monitorizazio sistemek norbanakoaren intimitateari eraso diezaizkiela

ondorioztatu baitaiteke. Tesi honetan zehar aurkezturiko sistemek une bakarreko neurketak egitea dutenez helburu, auzi etikoak ekiditen dira.

Gaur egungo biosentsoreek izan behar dituzten ezaugarriak definituta eta etorkizuneko joerak laburbilduta, hurrengo ataletan tesian zehar garaturiko bi sentsore sistemen hobekuntza posibleak aurkeztuko dira. Aplikazio eremuak aztertu eta eremu posible horietan erabilgarriak izateko beharko lituzketen hobekuntza edo modifikazioak azaltzen dira. Gainera, zenbait neurketa egin dira ingurune fisiologiko errealetan.

4.1 U forma eta funtzionalizaturiko gainazala duten PZO eta uhin ebaneszentearen xurgapenean oinarrituriko sistema

4.1.1 Ondorioak

U formako PZO eta uhin ebaneszentearen xurgapenean oinarrituriko sistemek biosentsore gisa izan ditzaketen erabilerak aztertu dira bigarren kapituluan. Bertan, glukosa detekziorako egokia den sistema bat aurkeztu da PZOaren gainazala funtzionalizatuz. Berauen abantailen artean, produkzio kostu baxuak eta erakutsitako hautakortasun handia ditugu. Izan ere, glukosa 0.1 mol/l-ko kontzentrazioan detektatu da hiru ingurune ezberdinetan, eta horretarako, gainazala funtzionalizatzeko errezeta bat egokitu da. Glukosarako duen eraginkortasuna erakusteaz gain, mota honetako sentsore plataformea beste zenbait eremutan erabiltzeko jakituria lortu da, ekarpen garrantzitsuena hau izanik.

Bestalde, hainbat desabantaila ere aurkezten dituzte, sentikortasun falta besteak beste, muga handiena sortzen duena hau izanik. Hala ere, badira zenbait aplikazio eremu non aurkezturiko detekzio sistemaren ezaugarriak desiragarriak izan daitezkeen.

4.1.2 Hobekuntza posibleak

Bigarren kapituluan lorturiko 0.1 mol/l-ko sentikortasuna ez da nahikoa plataforma hau medikuntza eremuan erabiltzeko, sentikortasun altuagoa eskatzen ohi

baitzaie neurketa sistemei. Hala ere, beste eremuetan erabilgarria izatea gerta liteke. Esate baterako, detekzio sistema hau 0-ala-1 gisako sistemetan erabil daiteke, elikagaien industrian adibidez. Bertan prozesatzen diren elikagai likidoek glukosa kontzentrazio jakin bat baino baxuagoa duten ala ez monitorizatzeko erabil daiteke, zenbait estandar bete ahal izateko. Horretarako, ordea, muntaia eramangarri bat garatu beharko litzateke; osagai batzuk trukatuz lor daitekeen ataza.

Ideia bera mantenduz baina funtzionalizazioa aldatuz, gisa honetako sistema bat denbora eta bolumen handiko neurketetan erabil daiteke, esaterako, ur-edangarrian bakteria berezi bat aurkitzen den ala ez detektatzeko. Adibidez, *Escherichia coli* bakteriaren detekziorako hainbat sentsore-eredu eraiki dira eta tesi honetan aurkeztutakoak bete-betean betetzen ditu honelako sentsore baten eskaerak, hain zuzen ere [57], [62], [108].

Azkenik, detekzio plataforma hau antigorputzen jarduera ikuskatzeko ere erabil daiteke. Kasu honetan, gainazalean finkatu diren antigorputzek sorturiko xurgapena gainbegiratuz, hauen jarduera kontrola daiteke. Eredu honetan, zuntzaren gainazala antigorputzen aktibitatea monitorizatzeko substratua litzateke. Eginiko lehen neurketak 4.1 irudian ageri dira. Bertan, hidrolizaturiko U formako zunda bati antigorputz eta jomuga-proteina espezifiko bat erantsi zaizkio, *IgG goat anti-rabbit* antigorputza, *Alexa fluor 647*-arekin markatua dagoena, hain zuzen ere. Gainazaleko modifikazio hauek IMG Pharma Biotech S.L. (Derio, Bizkaia) enpresak gauzatu ditu.

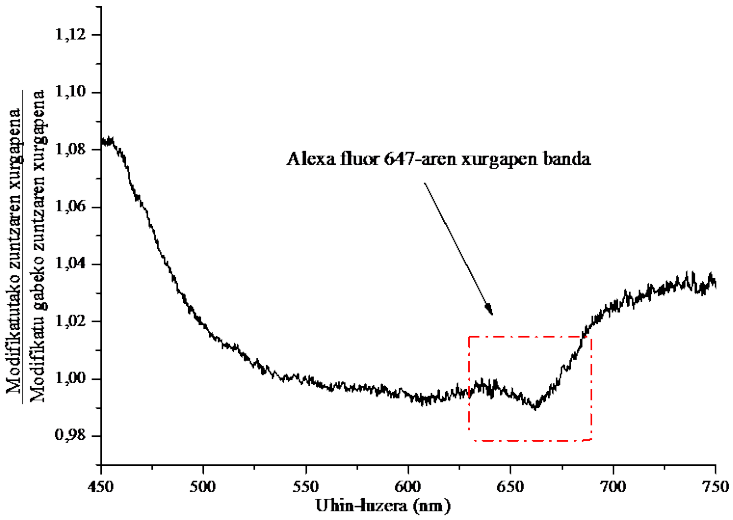

4.1 irudia. U formako zunden xurgapen espektroak Alexa fluor 647-arekin markatua dauden IgG goat anti-rabbit antigorputzekin.

Uhin ebaneszentearen xurgapen neurketa honetan, proteinari atxikitu zaion *Alexa 647* fluoforoaren xurgapen eta emisio bandak ikus daitezke, ikusgaiena 665 nm-tan aurkitzen den xurgapen banda izanik. Modu honetan frogatua geratzen da *IgG goat anti-rabbit* antigorputzari eginiko tratamendua arrakastatsua izan dela, xurgapen banda egokia ikusten baita. Lehen neurketa hauek kontzeptuzko froga bat izanik, neurketa sistema honen bideragarritasuna baieztatzen dute.

4.2 Sei eraztuneko NH-PZOm

4.2.1 Ondorioak

Tesi honetako hirugarren kapituluan aurkezturiko glukosa sentsore plataformak hainbat ekarpen ahalbidetu ditu. Horien artean garrantzitsuena NH-PZOm diseinu zehatz bat fabrikatu eta honen desiragarritasuna frogatzea izan da. Aurkikuntza honek hemendik aurrera egingo diren diseinu berrien edo helburu-molekula berrien azterketa egiteko lehen mugarri sendoa ezarri du. Aurkezturiko kasuan, glukosa 5 mmol/l-ko sentikortasunarekin

zenbatu da eta honek, medikuntza munduan interes handia duen SGLT2 inhibitzaile terapian giza gernuko glukosa monitorizatzea ahalbidetzen du.

4.2.2 Hobekuntza posibleak

Hasieratik tesi honen asmoa, disoluzio ezberdinen Raman espektroa hobetu eta anplifikatzeko asmotan, NH-PZOm-en erabilera uztartzea izan da. Nahiz eta orain arte lorturiko lorpenak hirugarren kapituluan azaldu, egin daitezkeen hainbat hobekuntza eta egokitzapen azalduko dira atal honetan.

Hauen artean lehena, argi-transmisioa NH-PZOm-etan zehar aztertzea da. Izan ere, sei eraztuneko geometria honek airean argia transmititzeko gaitasuna baduela ikusi da *band-gap* efektuaren bitartez; horregatik, geometria eta transmitituriko banden arteko erlazioa modu sakonago batean aztertu behar da. Arlo honetan lan asko geratzen da egiteke, biosentsore eredu berriak jorratzeko. Paraleloan jorra daitekeen beste ikerkuntza ildoa hirugarren kapituluan garatu den sistema giza gernua aztertzeko erabiltzea da, hau baitzen asmoa hasieratik. Horretarako, lehen neurketa batzuk burutu dira ondoren ikusiko den moduan.

4.2.2.1 Band-gap efektuan oinarritutako neurketak

Helburu-molekularen Raman dispertsioak eta erabiltzen dugun kitzikapen-iturriak zuntz mikroegituratuaren transmisio bandetan aurkitu behar dira, bestela, Raman espektroaren anplifikazioa ezinezkoa izango da. Premisa hau kontuan hartuta, PZOm-en transmisio espektroa aztertzeak garrantzi handia du. Hala ere, transmisio espektroa neurtzerakoan Raman neurketak egiteko erabiliko den konfigurazioa hartu behar da kontuan. Horrek hurrengoa esan nahi du: *band-gap* efektuan oinarrituriko anplifikazioa neurtu nahi bada, NH-PZOm-aren egiturako zulotxo guztiak disoluzioz bete behar dira.

Lehen neurketa gisa, 66 ϕ NH-PZOm-aren transmisio espektroa neurtu da zulotxo guztiak eta nukleoa airez beteta daudelarik. 4.2 irudian ikus daitekeen moduan, mikroegituraren geometria eta dimentsio horiekin, infragorri eremuan nukleotik zehar transmisioa lortzen da. Neurketa osagarri gisa, zuntza *supercontinuum* argi-iturriarekin

kitzikatzean lortzen den potentzia banaketa espaziala ere neurtu da, potentzia optikoa nukleo-hutsean kontzentratzen dela ziurtatzeko (4.3 irudia).

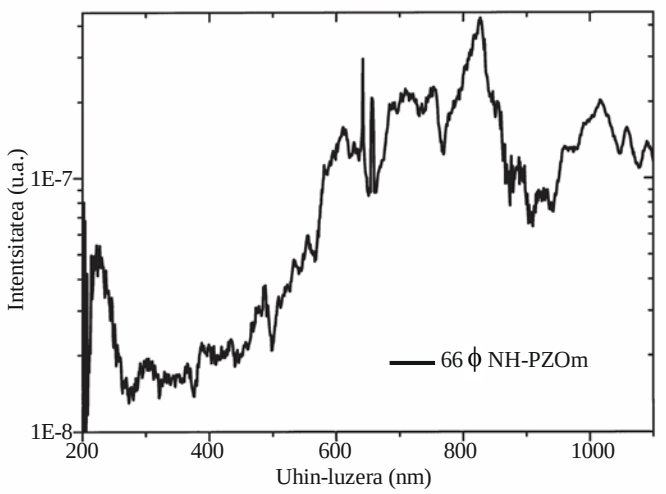

4.2 irudia. 66 ϕ NH-PZOm-aren argi transmisioaren espektroa hutsean *Supercontinuum* argiarekin kitzikatzean.

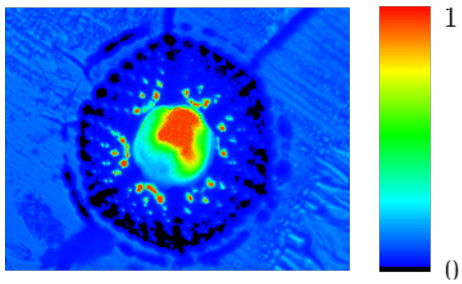

4.3 irudia. 66 ϕ NH-PZOm-aren eremu hurbileko irudia.

Erakutsi den kasuan 6 eraztuneko NH-PZOm-aren zulo guztiak airez beteta zeuden. Disoluzioekin lan egiterako orduan, ordea, ZBARE neurketak bi modutan lor daitezke. Batetik, hirugarren kapituluan azaltzen den ABIO bitartez, non zuntzaren muturretako bat eraldatu behar den disoluzioarekin nukleoa bakarrik bete dadin. Bestetik, *band-gap* efektu bidez ZBARE efektua lortu ahal da zuntzaren zulo guztiak disoluzioz beteta. Bigarren eredu honetan kritikoa da transmisio espektroa neurtzea, transmitituriko

banden desplazamendua gertatzen baita zuntza hutsean edo disoluzioz beteta dagoenean. Disoluzioez gain, airean transmititzeko gai diren zuntzek gasen Raman espektroa neurtzea ahalbidetzen dute, hainbat aplikaziorentzat ezaugarri oso erakargarria izanik.

Raman espektroak jorratzeaz gain, NH-PZOm-ek hainbat sentsore eredu jorratzeko aukera eskaintzen dute. Xurgapen sentsoreak edo egiturako zuloak bigarren atalean aipatu den hazkuntza substratu gisa erabil baitaitezke.

4.2.2.2 Glukosa neurketak giza gernuan

Hirugarren kapituluan aurkeztutako sistemarekin SGLT2 inhibitzaile terapiaren monitorizazioa egin genezake, gutxieneko zenbatze-eskaera betetzen baita [105], [109], [110]. Honenbestez, hurrengo pausua zuntz berberak erabiliz giza gernua disolbatzaile edo bitarteko gisa erabiltzea litzateke. Horretarako egokiena, prozedura berdina errepikatuz beste kalibrazio kurba bat egitea litzateke.

Hala ere, hori egin baino lehen, gernuaren espektroa aztertu behar da, posible baita gernuaren xurgapenak edo gernuan aurkitzen den beste substantzia baten Raman tontorrek zailtasunak sortzea glukosa zenbatzerako orduan. Horregatik, 4.4irudian ikus daitekeen moduan, lehenik kubetan giza gernu hutsa (marra gorria) eta giza gernua 1 mol/l glukosarekin (marra urdina) neurtu dira. Bi espektro hauez gain, 1 mol/l glukosa uretan (marra beltza) ere irudikatu da.

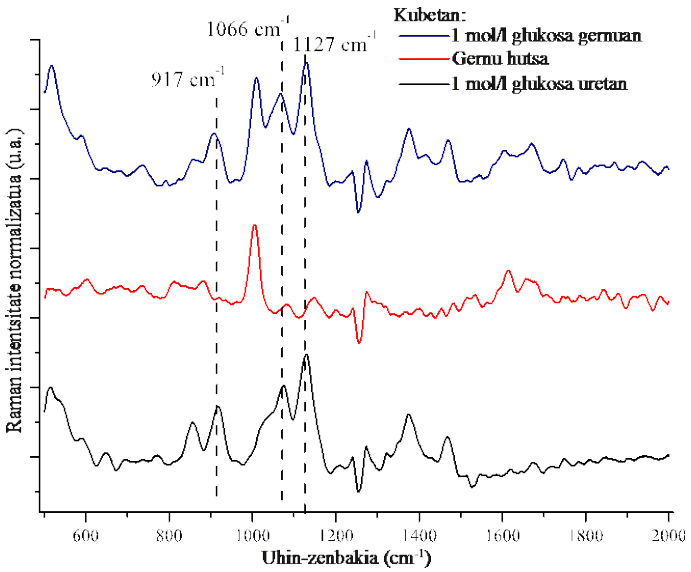

4.4 irudia. Gernuaren neurketak kubetan.

Hiru espektro hauen konparaketatik gernuak 1000 cm^{-1} uhin-zenbakiaren inguruan tontor garrantzitsu bat erakusten duela ikusten da. Tontor hau giza gernuan aurkitzen den kreatinaren eta, batez-ere, urearen ekarpenei dagokie [91], [111]. Hala ere, tontor nagusi honek ez ditu glukosari dagozkionak estaltzen, glukosaren hiru tontor nagusiak ikusgaiak baitira, gernuari 1 mol/l glukosa gehitu zaion disoluzioaren Raman espektroak erakusten duen moduan.

Giza gernuaren Raman espektroak aztertuta, glukosaren kontzentrazioa jaitsi eta uraren kasuan eginiko neurketak errepikatzea izan da hurrengo pausua. Neurketa hauek, noski, LBN-PZOm-arekin egin behar dira, kubetaren kasurako kontzentrazio baxuak ezin baitira neurtu. 4.5irudian ikus daitezke 6 eraztuneko 66 eta 100 μm-ko nukleoa duten zuntz birekin neurturiko ZBARE emaitzak.

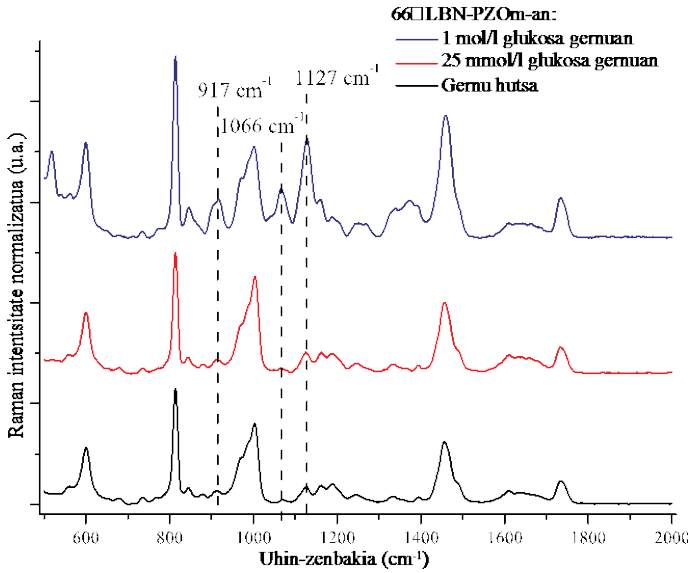

66 ϕ LBN-PZOm-an neurturiko Raman espektroak.

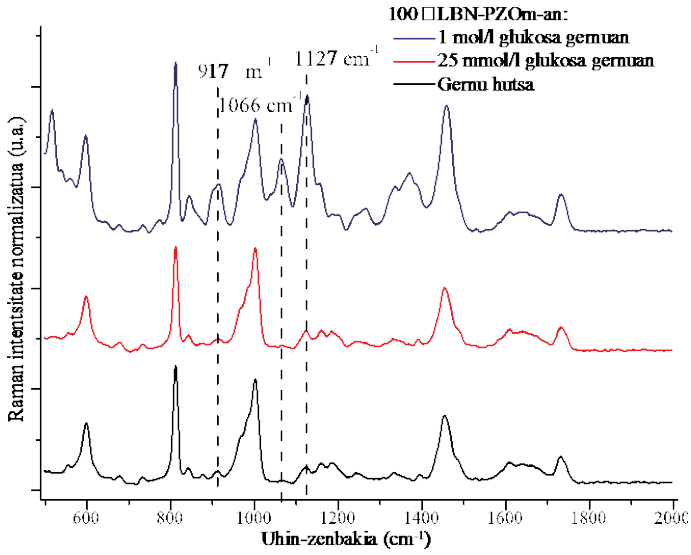

100 ϕ LBN-PZOm-an neurturiko Raman espektroak.

4.5 irudia. Giza gernuan eta glukosa kontzentrazio ezberdinetan eginiko ZBARE neurketak.

Neurtu diren bi dimentsioetako zuntzen kasuan, begi bistaz ikus daitezke 1 mol/l-ko kasurako glukosaren piko nagusiak. 25 mmol/l-ko kontzentrazioaren kasuan ordea, hirugarren kapituluan deskribaturiko azalera-erlazioa kalkulatuz, glukosaren presentzia baieztatu daiteke. Hirugarren kapituluan deskribaturiko kondizio bertsuetan neurturiko azalera-erlazioak azaltzen dira 4.1 taulan.

4.1 taula. Azalera-erlazioa giza gernuan neurtua.

Zuntza	Glukosa gabe	25 mmol/l glukosa	1000 mmol/l glukosa
66 ϕ LC-mPOF	0.48 ± 0.01	0.56 ± 0.03	2.02 ± 0.01
100 ϕ LC-mPOF	0.45 ± 0.02	0.59 ± 0.08	2.34 ± 0.07

Emaitza hauetatik ondorio positiboak besterik ezin daitezke atera. Nahiz eta giza gernuak ura baino ezaugarri okerragoak izan argi-transmisiorako, 25 mmol/l-ko kontzentrazioa detektatu da. Honenbestez, giza gernuan glukosa detektatzeko sistema sendoa dela esan dezakegu. Betiere, detekzio limitea zein kuantifikazio muga zein diren ezagutzeko neurketa gehiago egin beharko lirateke. Honekin batera eta ahalik eta lagin bolumen txikiena erabiltzeko helburuarekin, luzera eraginkorra berriz kalkulatu beharko litzateke.

4.3 Etorkizuneko hobekuntza posibleak

Aurreko ataleko emaitzak aztertuz, NH-PZOm-ek garapen-ahalmen itzelak aurkezten dituzte; sentikortasun, hautakortasun eta balioaniztasun handiak eskaintzen baitituzte. Hori kontuan izanda eta glukosa detekziorako erabili den plataforma oinarritzat hartuta, etorkizunerako beste zenbait hobekuntza posible aurkezten dira ondoren.

4.3.1 Gainazal funtzionalizazioa

Polimerozko gainazala funtzionalizatua duten NH-PZOm-etan oinarrituriko neurketa sistemek abantaila aunitz eskainiko lituzkete. Aurrez esan den moduan, likido fisiologiko gehienek hainbat substantzia izaten dituzte helburu-molekulaz gain. Horregatik, neurketaren asmoa substantzia edo helburu-molekula zehatz hori aztertzea bada, hau isolatu egin beharko da lehenik eta behin. Sistemaren hautakortasuna ahalik eta hoberena

izan dadin, nukleoa osatzen duen zuloaren gainazalak funtzionalizatzea da helburua atal honetan. Modu horretan, nukleoko zulotik diharduen likido fisiologikoaren helburu-molekulak nukleoko gainazalean atxikituta geratuko dira eta beste substantzia ez-desiragarriak, berriz, atera egingo dira 4.6 irudian ikus daitekeen moduan. Ondoren, neurketa burutu eta helburu-molekularen informazioa aztertzeko prest izango da plataforma.

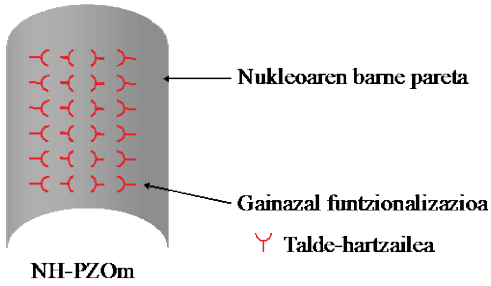

Nukleoko barne-paretak funtzionalizaturik dituen NH-PZOm-a.

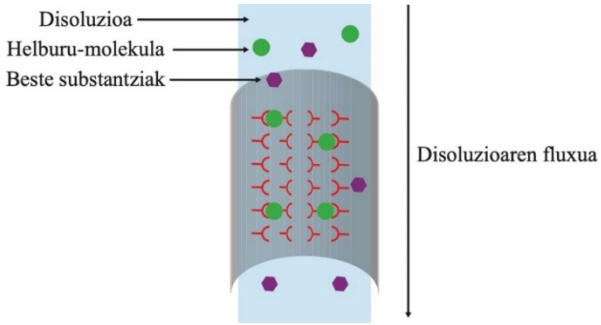

Disoluzioaren fluxua NH-PZOm-an zehar.

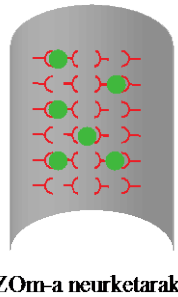

NH-PZOm-a neurketarako prest.

4.6 irudia. Gainazala funtzionalizatua duten zuntzen neurketa sistemaren azalpena.

Eredu honek neurketa plataformaren balioaniztasuna nabarmentzen du, hainbat eremutan ezartzeko aukera eskaintzen baitu. Likido fisiologiko ezberdinetan glukosa kontzentrazioa neurtzeaz gain, hainbat medizinen eraginkortasuna, odoleko osagaien kontzentrazioa edota zenbait gasen kontzentrazioa zehaztasun handiz neurtzera irits gintezke.

Atal honetan beste ideia bat ere aipa genezake. Izan ere, nukleoko pareten gainazala urrezko edo zilarrezko nanopartikulekin funtzionalizatuz, GBARE efektua modu kontrolatuan sor baitaiteke eta horrela, sistemaren sentikortasuna areagotu. Hala ere, sistemari metalezko nanopartikulak gehitzeak produkzio kostuak areagotuko lituzke eta ezarpen konplexuagoa eskatuko luke, nanopartikulen hainbat ezaugarri kontuan hartu beharko liratekeelako (geometria, tamaina, erresonantzia eta xurgapen bandak, …).

4.3.2 Geometria ezberdinen erabilera

6 eraztuneko NH-PZOm-aren kasuan, disoluzioen ZBARE neurketak egiteko geometria berarekin bi dimentsio ezberdinetan fabrikatu diren zuntzak erabili dira. Hala ere, Fotonika Aplikatuaren Taldeak (FAT) PZOm fabrikazio dorre bat duenez, hainbat mikroegitura geometria diseinatu eta fabrikatu ahal dira. Geometria berrien garapenerako simulazio erreminta sendo baten laguntzaz hornitu beharko ginateke; Photon Design edo Lumenical adibidez. Era honetan zuntzen fabrikazioak dakartzan buruhausteak ekidin ahal izango dira. Bestetik, luzaketa prozesuaren ondorioz aurreforman eginiko zuloek pairatzen dituzten aldaerak sakonean aztertu beharko lirateke, diseinatutako PZOm-ek eta fabrikaturikoek geometria ahalik eta bertsuena izan dezaten. Modu honetan, geometria ezberdinek eskainitako anplifikazioa neurtu eta aplikazio bakoitzeko mikroegitura-diseinu optimoa gara daiteke.

4.3.3 Materialen ikerkuntza

Atal honetan gainazalaren funtzionalizazioa azaldu duen sekzioarekin antza handia duen ideia jorratzen da, ezberdintasun handi batekin: gainazala funtzionalizatu ordez, PZOm-en substratu materialak eraldatzea aztertuko da efektu jakin batzuk eragiteko asmoz. PZOm-etan gehien erabili ohi den substratu materiala PMMA da eta koloratzaile organiko ezberdinekin oso erraz dopa daiteke [112]. Koloratzailearen fluoreszentzia eta igorpen bandak aztertuz, sentsore ezberdinak gara daitezke; NH-PZOm onenetan ere transmititzen den argiak substratu materialarekin interakzio handia baitu. Nahiz eta fluoreszentzia efektua Raman espektroskopiaren arerio nagusietakoa izan (fluoreszentziak Raman tontorrak estaltzen ditu), dopatze hauek beste neurketa ereduetan oso erabilgarriak

izan litezke. Ideia hau kontuan izanik, NH-PZOm-en ekarpen espezifikoa ondorengoan oinarrituko da: lagina eta argiaren arteko interakzio handiak eta efektua jasan duen argiaren transmisioa.

Esparru honetan lehen saiakera gisa nukleo hutsezko eta 500 μm-ko diametroa duten PZOak 6G errodamina koloratzailearekin dopatzea lortu da, eta gainera, denboran zehar dopatzailearen irismena kontrolatzea. Kasu honetan, 10 ^{o}C-tako tenperaturan, 6G errodamina metanolean disolbatu eta zuntza bertan hainbat ordutan murgildu da. 4.7 irudian ikus daitekeen gisa, dopatzailea noraino iritsi den oso modu sinplean kontrola daiteke.

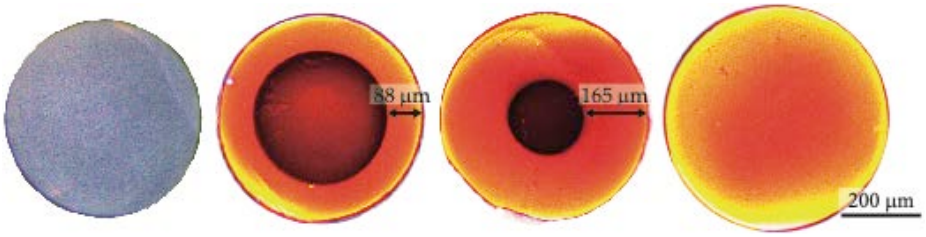

4.7 irudia. 6G errodamina *dye*-arekin dopaturiko PZOak denboran zehar.

Irudian erakutsitako kasuetan, murgilketa denborak 0, 8, 16 eta 24 ordukoak izan dira. Azken kasuan, dopatzailea zuntz osoan zehar barreiatu dela ikusten da. 8 eta 16 orduz murgildu diren zuntzen kasuan berriz, dopatzailea ez da zuntz osoan zehar hedatu; horregatik, metanola eta dopatzailea noraino iritsi diren gezien bitartez zehaztu da. Hurrengo pausua dopatzaile honekin NH-PZOm-ak dopatzea litzateke.

4.4 Ondorioak

PZOetan oinarrituriko sentsore plataformak garatu dira tesi guztian zehar, hauek eskainitako abantailak direla eta. Honenbestez, kapitulu honetan zehar aurreko kapituluetan garaturiko neurketa sistemen hobekuntza posibleak aurkeztu eta aztertu dira. Gainera, plataforma hauek biosentsoreen garapenaren testuinguruan kokatu dira. Sistema hauen malgutasuna, produkzio kostu baxuak eta hautakortasuna kontuan izanik, etorkizun oparoa duen biosentsore merkatuan leku garrantzitsua izango dutela esan daiteke.

Horretaz gain, etorkizun oparoa antzematen zaion uhin ebaneszentearen xurgapenean oinarrituriko sistema hobetu da. Jatorrizko aplikaziotik abiatuz, antigorputzen aktibitatearen monitorizazioa egiteko sistema hau substratu moduan erabili da, lehen neurketak aurkeztuz. Hala ere, arrakastarako esperantzarik handiena NH-PZOm-etan kokatzen da. Izan ere, argia airean transmititzeko gaitasunak edo glukosa neurketetan lorturiko sentikortasunak ahalmen handiko eredua dela erakusten baitute. Beraz, etorkizunean geometria eta helburu-molekula ezberdinak edo pareten funtzionalizazioa jorratuko dira

Chapter 5 / 5. Kapitulua

Contributions

Ekarpenak

Abstract—Herein, we enumerate the articles published in several journals and proceedings, which have been derived as a result of the present work.

Laburpena— Azken kapitulu honetan tesian zehar eginiko lanaren ondorioz osatu diren zenbait aldizkari eta konferentziatan argitaratutako artikuluak aipatzen dira.

Many of the results obtained during the progress of the research have led to the publication of many papers in both international and national high impact journals, as well as in the proceedings of different conferences. In this chapter we enumerate these contributions by separating them into different categories and by presenting them in chronological order. This way we have ensured the correct diffusion of the contributions we made.

5.1 Publications in international journals

We have published five papers in four different high-impact international journals. In the engineering field, the journals situated in the first or second quartile in the *JCR ranking* are considered high-impact publications. Additionally, one of them was chosen to be the cover of the volume in which was published. Moreover, a new contribution is in publication process currently.

- ***Study of the Influence of Various Stress-Based Mechanisms on Polarization of an SM mPOF for the Development of Useful Devices.***
  - Journal: Journal of Lightwave Technology. (ISSN: 0733-8724).
  - Publication date: 15 July 2017.
  - Impact factor: 3.65.
  - Category ranking: Optics 13/94 (Q1).

A polarimetric system sensible to the bending was presented in this article based on the properties of the light transmission through the mPOF. The change in the angle of polarization of the linearly polarized transmitted light provoked by the bending allowed designing and implementing a stress sensor. The angle of polarization in the fiber was modified proportionally by the stress suffered in it, making a novel polarimetric sensor.

Considering that the employed technique used for the measurements required great accuracy, my contribution consisted in building the set-up and performing the measurements. From this work, we obtained the knowhow of the manipulation of mPOFs, as we were able to fabricate single-mode mPOFs in the drawing tower, being the first step of the research developed in my PhD.

- ***Characterization of Chromatic Dispersion and Refractive Index of Polymer Optical Fibers.***
  - Journal: Polymers (ISSN: 2073-4360).
  - Publication date: 20 December 2017.
  - Impact factor: 2.93.
  - Category ranking: Polymer science 19/87 (Q1).

The chromatic dispersion and the refractive index of PMMA-based POFs were characterized in this work by using a femtosecond laser and a Streak Camera.

In order to compare the subtract material in the two POFs analyzed along the article, an exhaustive Raman spectroscopy study was made. My main contribution in this article was to ascertain that both fibers were made of exactly the same material. For that purpose, we used Raman spectroscopy, as this technique suits perfectly to this aim. The feedback obtained from this research was the wide database of the Raman spectra of different POF materials used during my PhD research.

- ***U-Shaped and Surface Functionalized Polymer Optical Fiber Probe for Glucose Detection.***
  - Journal: Sensors (ISSN: 1424-8220).

- Publication date: 25 December 2017.
- Impact factor: 2.47.
- Category ranking: Instrument & instrumentation 16/61 (Q2).

In this work we showed an evanescent wave absorption POF probe for glucose detection in different physiological media. High selectivity was achieved by functionalizing the surface of an only-core PMMA POF with phenilboronic groups. Besides, its sensitivity was noticeably enhanced by using a U-shaped geometry.

This article was the first important milestone of this PhD as we were able to make a novel glucose detection system. We adapted a surface functionalization recipe to POF surfaces, and besides, we fabricated U-shaped POFs in our drawing tower. By joining both achievements we implemented the glucose detection system and performed measurements in various media. We would also like to highlight the teamwork with Labquimac research group, since the conception of this article was the result of a strong collaboration between us.

- ***Polymers beyond standard optical fibres–fabrication of microstructured polymer optical fibres.***
  - Journal: Polymer International (ISSN: 1097-0126).
  - Publication date: 31 March 2018.
  - Cover photo assigned to this article (Figure 5.1).
  - Impact factor: 2.35.
  - Category ranking: Polymer science 27/87 (Q2).

This paper reported the overall fabrication process of mPOFs.

Herein, we reported all the acquired expertise from the different POF fabrications carried out in our facilities. This article may be considered as a transversal contribution obtained from different research works made while we were focused on developing biosensing platforms. The accuracy of only-core 500 μm diameter fibers or the fabrication of the first HC-mPOFs were reported in it among many other achievements.

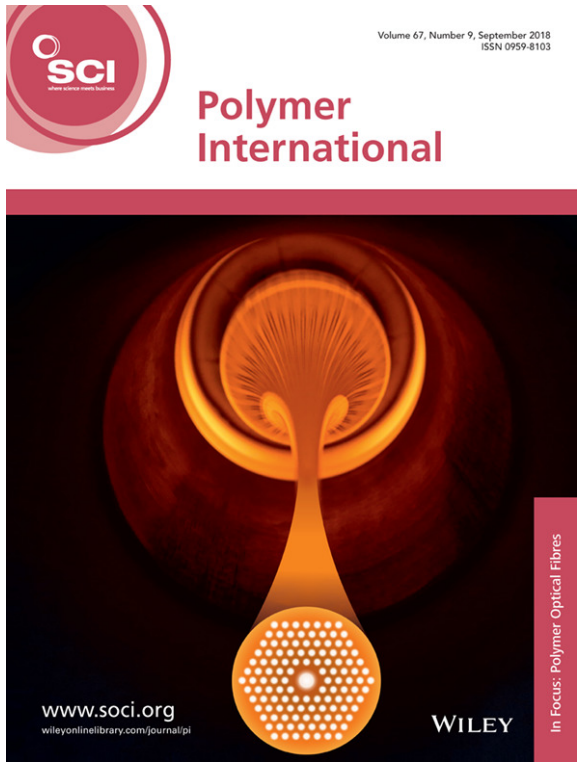

Figure 5.1 Cover image of Polymer international journal.

- ***Fabrication of Active Polymer Optical Fibers by Solution Doping and Their Characterization.***
  - Journal: Polymers (ISSN: 2073-4360).
  - Publication date: 31 December 2018.
  - Impact factor: 2.93.
  - Category ranking: Polymer science 19/87 (Q1).

In this article we doped only-core POFs by immersing them into the dopant-containing solution in order to fabricate active POFs. By this way, the dopant molecules were directly incorporated into the only-core fibers.

In order to research on active fibers, and taking advantage of all the knowledge obtained from previous publications, we decided to fabricate our own active POFs in our laboratories. The understanding of

the subtract material and the implementation of the doping technique were required in order to carry out this work, and I worked mostly on it.

- ***Liquid-Core Microstructured Polymer Optical Fiber as Fiber Enhanced Raman Spectroscopy Probe for Glucose Sensing.***
  - Journal: Journal of Lightwave Technology. (ISSN: 0733-8724).
  - Submission date: 26 November 2018.
  - Impact factor: 3.65.
  - Category ranking: Optics 13/94 (Q1).

Herein, we designed and fabricated two LC-mPOF of different sizes for FERS. The main aim was to detect glucose in aqueous solutions in a clinically relevant range for SGLT2 inhibitor therapy.

This paper, *which is still in publication process*, was conceived during my stay at the Leibniz Institute for Photonic Technologies (IPHT). As a result of this strong collaboration, we were able to detect a target molecule improving an already known technique such as the Raman spectroscopy. For that purpose, we fabricated two novel HC-mPOFs and implemented a simple algorithm to calculate the glucose concentration. Additionally, we exposed the first measurements in real human urine.

5.2 Publications in Basque language journals

We have contributed with two papers in a national journal named Ekaia. With these contributions, apart from showing the latest scientific results, we have ensured the development of the Basque language in science.

- ***Polimero akrilikoak oftalmologian. Degradazio-prozesuaren analisia.***
  - Journal: Ekaia (ISSN: 0214-9001).
  - Publication year: 2017.

In this article we analyzed different polymers used in ophthalmology. A historical review of different contact lens designs and materials was widely explained. Additionally, the thermic degradation

and the kinetics of three different polymers (PMMA, poly(benzyl methacrylate) and poly(tert-butyl acrylate)) were analyzed.

The main contribution to this review consisted in measuring the degradation process of the aforementioned polymers, as it was the perfect opportunity to train in the chemistry laboratory. Besides, the analysis of these polymers was of big interest, as they are the most common materials in POFs.

- ***Poli(metilmetakrilatoa)ren gainazal eraldaketa. Sentsore adimendunak.***
  - Journal: Ekaia (ISSN: 0214-9001).
  - Publication year: 2017.

This paper summarized the different methods to functionalize the surface of different polymers in order to design and implement smart sensing platforms. Specifically, the possibilities of the PMMA and the most used characterization techniques for this purpose were studied, along with some results.

A deep bibliography review was made to write this article. The most common surface functionalization methods and characterization techniques were studied as well as their suitability for our main aim. However, the main contribution was to make the first functionalization attempts in plain PMMA samples.

5.3 Publications in proceedings of international conferences

We have contributed with three papers to the proceedings of several international conferences:

- ***Analysis of light scattering in SI-POFs by using side-illumination technique.***
  - Conference: Photonics West 2015 (SPIE).
  - Date: January 2015.

- Peer-reviewed.

The aim of this work was to compare two different methods for measuring scattered light in SI-POF by using the side-illumination technique. On the one hand, scattered intensity and far-field patterns at a single wavelength were measured by varying the following launching conditions: position of the excitation spot in the fiber and incidence angle. On the other hand, we measured the spectral distribution of the scattered light in SI-POFs by exciting the fiber with a supercontinuum source.

My efforts were focused on performing the measurements in the laboratory.

- ***High reproducibility SERS sensing platform using Hollow-Core microstructured Polymer Optical Fibers.***
  - Conference: 24th International Conference on Polymer Optical Fiber (POF 2015).
  - Date: September 2015.

A reproducible and time-stable experimental platform suitable for measuring the Raman spectrum of 2-Naphtalenethiol was reported in this work. For that purpose Kagome lattice HC-mPOFs were used.

This contribution described the first SERS measurements that were made entirely in our facilities. I worked on sample preparations and measurements.

- ***A novel liquid-filled microstructured polymer optical fiber as bio-sensing platform for Raman spectroscopy.***
  - Conference: Photonics West 2018 (SPIE).
  - Date: January 2018.
  - Peer-reviewed.

In order to optimize the Raman spectra of glucose dissolved in water, the core of the HC-mPOF was filled with this solution, enabling in this way the MTIR guiding mechanism. Experimental Raman measurements were performed and their results were discussed.

In this conference it was the first time a HC-mPOF made entirely in our drawing tower was shown. My contribution in this work involved all the steps and processes.

5.4 Publications in proceedings of national conferences

We have also contributed with two different papers to the proceedings of several national conferences:

- ***Raman Espektroskopian Oinarrituriko Biosentsorea Zuntz Optikoa Erabiliz.***
  - Conference: IkerGazte 2015.
  - Publication date: May 2015.

  In this work, employing *Kagome* lattice HC-mPOFs, we reported a reproducible and time-stable experimental Raman spectra of *Methylene Blue*.

  I contributed in this work performing the experiments and writing the contribution. Moreover, this work was the very first step in this PhD as we settled the measuring parameters. In order to do that, we made a deep training in the Raman equipment of our facilities.
- ***Biosensor Raman y SERS utilizando Fibras Microestructuradas de Polímero de Núcleo Hueco.***
  - Conference: IX Reunión Española de optoelectrónica (OPTOEL 2015).
  - Publication date: July 2015.
  - Finalist on the best poster award category.

  We presented a robust, feasible and reproducible sensing platform using a HC-mPOF for Raman spectroscopy measurements in this work.

  Many attempts were made in order to obtain such platform. All the experimental measurements and the signal processing was made in our facilities, except for the fibers, which were imported. Therefore, all my efforts were focused in performing the measurements.

Tesi honen garapenean zehar eginiko ikerkuntzaren emaitzak inpaktu altua duten zenbait aldizkaritan, bai nazioartekoetan bai nazionaletan, argitaratu dira eta baita kongresu ezberdinetako liburuxketan ere. Kapitulu honetan ekarpen horiek zerrendatzen dira, kategoria ezberdinetan bananduz eta ordena kronologikoa errespetatuz. Ekarpen hauek direla eta, tesian zehar eginiko aurkikuntzen eta emaitzen hedapen egokia bermatu da.

5.5 Nazioarteko aldizkarietako argitalpenak

Bost artikulu argitaratu dira inpaktu handiko nazioarteko lau aldizkari ezberdinetan. Ingeniaritza eremuan, lehen eta bigarren laurdenetan kokaturiko argitalpenak kontsideratzen dira inpaktu handiko aldizkariak, *JCR sailkapenari* helduz beti ere. Gainera, hauetako bati aldizkariaren azala esleitu zitzaion. Honetaz gain, gaur egun, bada seigarren artikulu bat argitaratzeko prozesuan dena.

- ***Study of the Influence of Various Stress-Based Mechanisms on Polarization of an SM mPOF for the Development of Useful Devices.***
    - Aldizkaria: Journal of Lightwave Technology. (ISSN: 0733-8724).
    - Argitalpen data: 2017ko uztailaren 15a.
    - Inpaktu-indizea: 3.65.
    - Sailkapena kategorian: Optika 13/94 (Q1).

    Artikulu honetan PZOm baten argi-transmisioaren ezaugarrietan oinarrituz tolesdurari erantzuten zion polarizazio sistema bat aurkeztu zen. Honela, sarreran igortzen zen linealki polarizaturiko argiaren polarizazio angelua tolesdurak eraldatzen zuen, estres sentsore baten diseinu eta muntaia ahalbidetuz. Polarizazio angelua zuntzak jasandako tentsioak modu proportzionalean eraldatzen zuen, honelako sentsore polarimetrikoa aurkezten zen lehenengo aldia izanik.

    Neurketak egin ahal izateko erabili zen teknikak sistema zehatz baten beharra eskatzen zuenez, honen muntaian eta neurketetan oinarritu zen nire ekarpena. Lan honetatik PZOm-ak manipulatzen ikasi genuen. Gainera, modu bakarreko PZOm-ak gure fabrikazio dorrean fabrikatzeko

gai izan ginen, tesi honetan burututako ikerkuntzaren lehen pausua izanik.

- ***Characterization of Chromatic Dispersion and Refractive Index of Polimer Optical Fibers.***
  - Aldizkaria: Polymers (ISSN: 2073-4360).
  - Argitalpen data: 2017ko abenduaren 20a.
  - Inpaktu-indizea: 2.93.
  - Sailkapena kategorian: Polimeroen zientzia 19/87 (Q1).

PMMAn oinarrituriko PZOen dispertsio kromatikoa zein errefrakzio indizea karakterizatu ziren femtosegundozko laser eta *Streak Camera* bat erabiliz ataza hauek burutzeko.

Artikulu guztian zehar aztertzen ziren bi PZOen susbstratu materialaren konparazioa egin ahal izateko Raman espektroskopia ikerketa sakon bat egin zen. Nire ekarpenik garrantzitsuena artikulu honetan konparaturiko bi zuntzak material berberaz eginda zeudela ziurtatzea izan zen. Helburu horretarako, Raman espektroskopia erabili zen, teknika hau asmo honetarako ederki egokitzen baitzen. Ikerkuntza honetatik lorturiko emaitza PZO materialen Raman espektroen datu-base andana izan zen, nire tesi osoan zehar oso erabilia izan zena.

- ***U-Shaped and Surface Functionalized Polimer Optical Fiber Probe for Glucose Detection.***
  - Aldizkaria: Sensors (ISSN: 1424-8220).
  - Argitalpen data: 2017ko abenduaren 25a.
  - Inpaktu-indizea: 2.47.
  - Sailkapena kategorian: Instrumentu eta instrumentazioa 16/61 (Q2).

Lan honetan uhin ebaneszentearen xurgapena neurtzen zuen PZO zunda bat aurkezten zen, ingurune fisiologiko ezberdinetan aurkitzen zen glukosa detektatzeko. Nukleo hutsezko PMMAzko PZOaren gainazala fenil-boriko taldeekin funtzionalizatuz hautakortasun handia lortu zen. Gainera, zundaren sentikortasuna nabari hobetu zen zundari U forma emanaz.

Artikulu hau tesiko lehen mugarri garrantzitsutzat jo liteke glukosa detekzio sistema berri bat aurkezteko gai izan baikinen. Gainazala funtzionalizatzeko errezeta bat PZOentzako egokitu genuen, eta gainera, U formako zundak fabrikatu geure fabrikazio dorrean. Bi lorpen hauek batuz glukosa detekzio sistema ezarri genuen eta hainbat ingurumenetan neurketak burutu genituen. Gainera, Labquimac taldearekin eginiko elkarlana azpimarratu nahi da, artikulu hau bi taldeen arteko elkarlanaren emaitza izan baitzen.

- ***Polimers beyond standard optical fibres–fabrication of microstructured polimer optical fibres.***
    - Aldizkaria: Polymer International (ISSN: 1097-0126).
    - Argitalpen data: 2018ko martxoaren 31a.
    - Azal-argazkia esleitua artikulu honi (5.2 irudia)
    - Inpaktu-indizea: 2.35.
    - Sailkapena kategorian: Polimeroen zientzia 27/87 (Q2).

Artikulu honek PZOm-en fabrikazio prozesu orokorra deskribatzen du.

Kasu honetan gure instalazioetan PZOak fabrikatzean lorturiko jakintza guztia azaldu zen. Artikulu hau, beste biosentsore plataformak garatzean jasotako jakituriarekin osaturiko zeharkako ekarpen gisa ere uler daiteke. Bertan, nukleo hutsezko eta 500 $\pm$10 nm zuntzaren diametroaren zehaztasun itzela, edota lehenengo NH-PZOm-en fabrikazioa agertzen dira, beste aurkikuntzen artean.

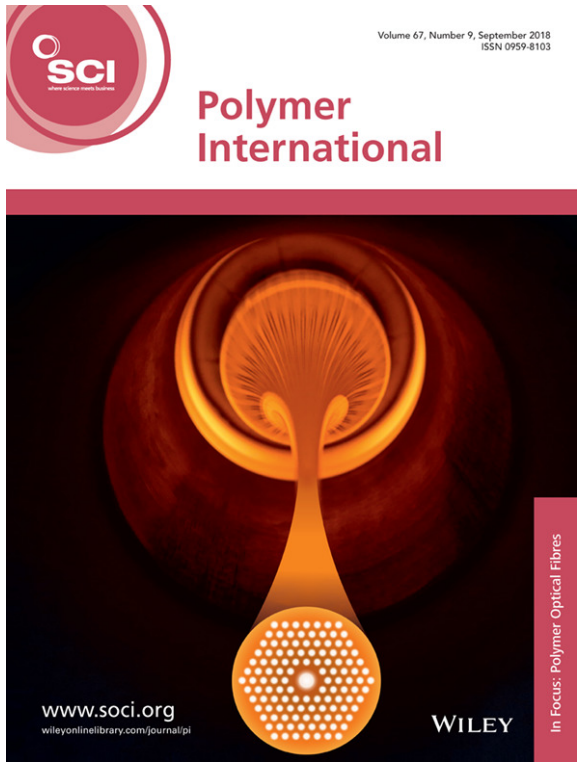

5.2 irudia. Polymer international aldizkariko azal-argazkia.

- ***Fabrication of Active Polimer Optical Fibers by Solution Doping and Their Characterization.***
  - Aldizkaria: Polymers (ISSN: 2073-4360).
  - Argitalpen data: 2018 abenduaren 31a.
  - Inpaktu-indizea: 2.93.
  - Sailkapena kategorian: Polimeroen zientzia 19/87 (Q1).

Artikulu honetan nukleo hutsezko PZOak dopatu ziren, horretarako PZOak dopatzailea zeukan disoluzioan murgilduz, PZO aktiboak fabrikatzeko asmotan. Honela, molekula dopatzaileak zuzenean gehitu ziren nukleo hutsezko zuntzetara.

Zuntz aktiboetan ikertzeko asmotan, eta aurrez eginiko argitalpenetatik lorturiko jakintzarekin batera, gure laborategietan PZO aktiboak fabrikatzea otu zitzaigun. Lan hau aurrera eramateko, zuntzen

substratu materialaren ulermena eta dopaketa teknikaren gauzatzea behar izan ziren, eta horretan jardun nuen gehien.

- ***Liquid-Core Microstructured Polimer Optical Fiber as Fiber Enhanced Raman Spectroscopy Probe for Glucose Sensing.***
  - Aldizkaria: Journal of Lightwave Technology. (ISSN: 0733-8724).
  - Igorpen data: 2018ko azaroaren 26a.
  - Inpaktu-indizea: 3.65.
  - Sailkapena kategorian: Optika 13/94 (Q1).

Bertan, ZBARErako tamaina ezberdinetako LBN-PZOm bi diseinatu eta fabrikatu genituen. Helburu nagusia glukosa disoluzio urtsuetan eta SGLT2 inhibitzaile terapian esanguratsua zen kontzentrazioetan detektatzea izan zen.

Artikulu hau, *oraindik argitalpen prozesuan aurkitzen dena*, Leibnizko Institute for Photonic Technologies (IPHT) zentroan eginiko egonaldiaren ondorio dugu. Elkarlan estu hau dela eta, helburu-molekula detektatzeko gai izan ginen gaur egun ezaguna den Raman espektroskopia teknika hobetuz. Horretarako, NH-PZOm bi fabrikatu ziren lehenengo aldiz, eta algoritmo sinple baten bitartez glukosa kontzentrazioa kalkulatu zen. Gainera, giza gernuan eginiko lehen neurketak azaldu genituen.

5.6 Euskarazko aldizkarietako argitalpenak

Ekaia izeneko aldizkarian bi artikulu argitaratu dira. Argitalpen hauekin, lorturiko azken zientzia emaitzak azaltzeaz gain, euskararen garapen zuzena bermatu dugu zientzia-munduan ere.

- ***Polimero akrilikoak oftalmologian. Degradazio-prozesuaren analisia.***
  - Aldizkaria: Ekaia (ISSN: 0214-9001).
  - Argitalpen urtea: 2017.

Artikulu honetan oftalmologian erabilitako hainbat polimero aztertu ziren. Ukipen-lenteetan erabilitako material eta diseinuen garapen historikoa azaldu zen. Horrez gain, hiru polimero ezberdinen (PMMAa, poli(bentzilakrilato)-a eta poli(tert-butilakrilato)-a) degradazio termikoak eta beren zinetikak aztertu ziren.

Artikulu honi eginiko ekarpen nagusia aipatzen diren polimeroen degradazioa neurtzea izan zen, kimika laborategian trebatzeko aukera ezin hobea izanik. Polimero hauek aztertzea, gainera, interes handikoa gertatu zen, hauek baitira PZOetan gehien erabiltzen diren materialak.

- ***Poli(metilmetakrilatoa)ren gainazal eraldaketa. Sentsore adimendunak.***
    - Aldizkaria: Ekaia (ISSN: 0214-9001).
    - Argitalpen urtea: 2017.

Artikulu honek polimero ezberdinen gainazala funtzionalizatzeko aukerak laburtzen ditu, sentsore plataforma adimendunak diseinatu eta gauzatzeko asmoz. Bereziki PMMAren aukerak eta karakterizazio teknika erabilienak azaldu ziren, zenbait emaitzekin batera.

Artikulu hau idazterako orduan bibliografia ikerketa sakona egin genuen. Polimero gainazalak funtzionalizatzeko teknika erabilienak eta karakterizazio metodoak aztertu genituen eta gure kasurako egokienak zein izan zitezkeen aztertu. Hala ere, ekarpenik garrantzitsuena PMMA lagin lauetan lehen funtzionalizazio saiakerak egitea izan zen.

5.7 Nazioarteko kongresu liburuxketako argitalpenak

Nazioarteko hainbat kongresutako liburuxketan hiru artikulu argitaratu dira:

- ***Analysis of light scattering in SI POFs by using side-illumination technique.***
    - Kongresua: Photonics West 2015 (SPIE).
    - Kongresuaren data: 2015eko urtarrila.

- Parekazko zuzenketarekin.

Lan honen helburua MI-PZOetan gertatzen zen argi-dispertsioa neurtzeko bi sistema ezberdin konparatzea izan zen, alboko argiztapenaren teknika erabiliz. Batetik, uhin-luzera bakarra erabiliz, dispertsaturiko intentsitatea eta eremu urruneko patroiak neurtu ziren eraso puntua eta angelua zuntzaren luzeran zehar aldatuz. Bestetik, MI-PZOetako argi dispertsioaren banaketa espektrala neurtu zen zuntza *supercontinuum* motako argi-iturri batez kitzikatuz.

Nire esfortzuak laborategiko esperimentuak burutzean zentratu nituen.

- ***High reproducibility SERS sensing platform using Hollow-Core microstructured Polimer Optical Fibers.***
  - Kongresua: 24th International Conference on Polymer Optical Fiber (POF 2015).
  - Kongresuaren data: 2015eko iraila.

Denboran zehar egonkorra eta errepikagarria zen 2-Naphtalenethiol-aren Raman espektroa neurtzeko plataforma sentsore bat deskribatu zen lan honetan. Asmo horretarako *Kagome* saretako NH-PZOm-ak erabili ziren.

Ekarpen honek gure laborategian egin ziren lehen GBARE neurketak deskribatu zituen. Laginen prestakuntzan eta neurketetan aritu nintzen kasu honetan.

- ***A novel liquid-filled microstructured polimer optical fiber as bio-sensing platform for Raman spectroscopy.***
  - Kongresua: Photonics West 2018 (SPIE).
  - Kongresuaren data: 2018ko urtarrila.
  - Parekazko zuzenketarekin.

Uretan disolbaturiko glukosaren Raman espektroa optimizatzeko asmotan, NH-PZOm-en nukleoko zuloa disoluzio honekin bete zen, modu honetan ABIO gidapen mekanismoa ahalbidetuz. Hainbat Raman espektroskopia gauzatu eta horien emaitzak eztabaidatu ziren.

Kongresu honetan gure fabrikazio dorrean erabat gauzaturiko NH-PZOm-ak aurkeztu ziren lehenengo aldiz. Lan honetan eginiko ekarpena prozesu eta etapa guztietara zabaltzen da.

5.8 Kongresu nazionaletako liburuxketako argitalpenak

Nazio mailan antolatzen diren hainbat kongresu ezberdinetako liburuxketan ere bi artikulu argitaratu dira:

- ***Raman Espektroskopian Oinarrituriko Biosentsorea Zuntz Optikoa Erabiliz.***
  - Kongresua: IkerGazte 2015.
  - Kongresuaren data: 2015eko maiatza.

  Lan honetan *Kagome* sareta zuten NH-PZOm-ak erabiliz, denboran zehar egonkorra eta errepikagarria zen *Methylene Blue*-aren Raman espektroskopia neurtu zen.

  Nire ekarpena lan honetan artikuluaren idazketan eta esperimentuen gauzaketan zetzan. Gainera, lan hau aurkezten den tesi-lanaren lehen pausutzat uler daiteke, Raman ekipoan neurketak egiteko parametroak adostu baikenituen. Hori dela eta, gure laborategiko Raman ekipamenduan ikasketa sakon bat egiteko erabilgarria izan zen.
- ***Biosensor Raman y SERS utilizando Fibras Microestructuradas de Polímero de Núcleo Hueco.***
  - Kongresua: IX Reunión Española de optoelectrónica (OPTOEL 2015).
  - Kongresuaren data: 2015eko uztaila.
  - Poster onenaren sari bereziko finalista.

  Raman espektroskopia neurketak egiteko NH-PZOm-etan oinarritzen zen plataforma sentsore irmo, errepikagarri eta erabilgarri bat aurkeztu zen lan honetan.

  Hainbat saiakera egin behar izan ziren mota honetako plataforma bat gauzatu arte. Neurketa esperimental guztiak gure laborategietan gauzatu ziren, zuntzak izan ezik, hauek kanpotik ekarriak

izan baitziren. Honenbestez, nire esfortzuak neurketak gauzatzean zentratu ziren.

References

Bibliografia

[1] Y. Koike, “High-bandwidth graded-index polymer optical fibre,” *Polymer* ., vol. 32, no. 10, pp. 1737–1745, Jan. 1991.

[2] Y. Koike, E. Nihei, N. Tanio, and Y. Ohtsuka, “Graded-index plastic optical fiber composed of methyl methacrylate and vinyl phenylacetate copolymers,” *Appl. Opt.*, vol. 29, no. 18, p. 2686, Jun. 1990.

[3] Y. Ohtsuka, E. Nihei, and Y. Koike, “Graded -index optical fi
methacrylate ndwidth, Appl copolymer with lo
Phys. Lett., vol. 57, no. 2, pp. 120–122, Jul. 1990.

[4] B. Lee, “Review of the present status of optical fiber sensors,” *Opt. Fiber Technol.*, vol. 9, no. 2, pp. 57–79, Apr. 2003.

[5] J. Zubia, I. Garcia, J. Villatoro, M. A. Illarramendi, J. Mateo, and C. Vazquez, “Polymer optical fiber sensors for aircraft structural and engine health monitoring,” in *2017 19th International Conference on Transparent Optical Networks (ICTON)*, 2017, pp. 1–1.

[6] World Health Organization.” [Online]. Available: https://www.who.int/home. [Accessed: 15-Feb-2019].

[7] “International Union of Pure and Applied Chemistry.” [Online]. Available: https://iupac.org/. [Accessed: 15-Feb-2019].

[8] F. Davis and Z. Altintas, *General introduction to biosensors and recognition receptors*. 2018.

[9] I. Palchetti and M. Mascini, “Biosensor technology: a brief history,” *Sensors and Microsystems*, vol. 91, pp. 15–23, 2011.

[10] L. Clark, “Monitor and control of blood and tissue oxygen tensions," Transactions of the American Society for Artificial Internal Organs, v. 2, 1956.

[11] L. C. Clark and C. Lyons, “Electrode Systems For Continuous Monitoring In Cardiovascular Surgery,” *Ann. N. Y. Acad. Sci.*, vol. 102, no. 1, pp. 29–45, Dec. 1962.

[12] S. J. Updike and G. P. Hicks, “The Enzyme Electrode,” *Nature*, vol. 214, no. 5092, pp. 986–988, Jun. 1967.

[13] G. G. Guilbault and J. G. Montalvo, “Urea-specific enzyme electrode,” *J. Am. Chem. Soc.*, vol. 91, no. 8, pp. 2164–2165, Apr. 1969.

[14] A. E. G. Cass, G. Davis, G. D. Francis, H. A. O. Hill, W. J. Aston, I. J. Higgins, E. V. Plotkin, L. D. L. Scott, and A. P. F. Turner, "Ferrocene-mediated enzyme electrode for amperometric determination of glucose," *Anal. Chem.*, vol. 56, no. 4, pp. 667–671, Apr. 1984.

[15] E.- Korotkaya-, "Biosensors: Design, Classification, and Applications in the Food Industry," *Foods Raw Mater.*, vol. 2, no. 2, pp. 161–171, Sep. 2014.

[16] A. P. F. Turner, I. Karube, and G. S. Wilson, *Biosensors : fundamentals and applications*. Oxford University Press, 1987.

[17] B. R. Eggins, *Chemical sensors and biosensors*. J. Wiley, 2002.

[18] H. Murofushi., "Low loss perfluorinated POF," in *Proceedings of the fifth international conference on plastic optical fibres and applications- POF*, 1996, pp. 17–23.

[19] J. Arrue, "Propagation in straight and bent plastic optical fibres, ap- plied to the design of optical links, sensors and couplers," Univ. Basque Country (UPV/EHU), 1999.

[20] J. Zubia and J. Arrue, "Plastic optical fibers: An introduction to their technological processes and applications," *Opt. Fiber Technol.*, vol. 7, no. 2, pp. 101–140, 2001.

[21] Y. Koike and M. Asai, "The future of plastic optical fiber," *NPG Asia Mater.*, vol. 1, no. 1, pp. 22–28, Oct. 2009.

[22] T. Kaino, K. Jinguji, and S. Nara, "Low loss poly(methylmethacrylate -d8) core optical fibers," *Appl. Phys. Lett.*, vol. 42, no. 7, pp. 567–569, Apr. 1983.

[23] W. Groh and A. Zimmermann, "What is the lowest refractive index of an organic polymer?," *Macromolecules*, vol. 24, no. 25, pp. 6660–6663, Dec. 1991.

[24] Asahi Glass Company, "Lucina: Graded Index-Cytop Optical Fiber," Tokyo. [Online]. Available: www.agc.com/en/ [Accessed: 15-Feb-2019]

[25] Y. Koike., "High Bandwidth, Low-Loss Polymer Fibres," in *18th Euro- pean Conference on Optical Communication (ECOC'92)*, 1992.

[26] Y. Koike, "High-Speed Multimedia POF Network," in *3rd International Conference on Plastic Optical Fibres and Applications (POF'94)*, 1994.

[27] R. V. Y. G. Giaretta, M. Wegmueller, *Proc. Optical Fiber Commun. Conf. PD-14*, 1999.

[28] Y. Koike, "Design of POF for Gigabit Transmission," in *12th International Conference on Plastic Optical Fibres (POF'94)*, 2003.

[29] A. M. J. Koonen, C. Okonkwo, E. Tangdiongga, F. Breyer, H. Yang, H. P. A. van den Boom, S. C. J. Lee, and S. Randel, "47.4 Gb/s Transmission Over 100 m

Graded-Index Plastic Optical Fiber Based on Rate-Adaptive Discrete Multitone Modulation," *J. Light. Technol. Vol. 28, Issue 4, pp. 352-359*, vol. 28, no. 4, pp. 352–359, Feb. 2010.

[30] O. Ziemann et al., in *Proc. Int. Conf. POF*, 2008.

[31] "Breyer, S. Randel, H. van den Boom, T. Koonen J. Lee," in *Proc. Int. Conf. POF*, 2008.

[32] G. Yabre, "Theoretical Investigation on the Dispersion of Graded-Index Polymer Optical Fibers," *J. Light. Technol. Vol. 18, Issue 6, pp. 869-*, vol. 18, no. 6, p. 869, Jun. 2000.

[33] G. Yabre, "Comprehensive Theory of Dispersion in Graded-Index Optical Fibers," *J. Light. Technol. Vol. 18, Issue 2, pp. 166-*, vol. 18, no. 2, p. 166, Feb. 2000.

[34] R. F. Shi, C. Koeppen, G. Jiang, J. Wang, and A. F. Garito, "Origin of high bandwidth performance of graded-index plastic optical fibers," *Appl. Phys. Lett.*, vol. 71, no. 25, pp. 3625–3627, Dec. 1997.

[35] L. Jacomme, "Modal dispersion in multimode graded-index fibers," *Appl. Opt.*, vol. 14, no. 11, p. 2578, Nov. 1975.

[36] Mitsubishi Rayon Co. Ltd., "Eska-Miu." [online]. Available: https://www.pofeska.com/ [Accessed:3-Mar-2019].

[37] S. Lee, U.-C. Paek, and Y. Chung, "Bandwidth enhancement of plastic optical fiber with multi-step core by thermal diffusion," *Microw. Opt. Technol. Lett.*, vol. 39, no. 2, pp. 129–131, Oct. 2003.

[38] J. Zubia, G. Aldabaldetreku, G. Durana, J. Arrue, C.-A. Bunge, and H. Poisel, "Geometric Optics Analysis of Multi-Step Index Optical Fibers," *Fiber Integr. Opt.*, vol. 23, no. 2–3, pp. 121–156, Jan. 2004.

[39] S. T. H. Munekuni, S. Katsuta, "Plastic optical fiber for high-speed transmisssion," in *Proceedings of the third international conference on plastic optical fibers and applications-POF'94*, 1994.

[40] P. Russell, "Photonic crystal fibers.," *Science*, vol. 299, no. 5605, pp. 358–62, Jan. 2003.

[41] M. van Eijkelenborg, M. Large, A. Argyros, J. Zagari, S. Manos, N. Issa, I. Bassett, S. Fleming, R. McPhedran, C. M. de Sterke, and N. A. Nicorovici, "Microstructured polymer optical fibre," *Opt. Express*, vol. 9, no. 7, p. 319, Sep. 2001.

[42] R. F. Cregan, B. J. Mangan, J. C. Knight, T. A. Birks, P. S. J. Russell, P. J. Roberts, and D. C. Allan, "Single-Mode Photonic Band Gap Guidance of Light in Air," *Science*, vol. 285, no. 5433, pp. 1537–1539, Sep. 1999.

[43] M. Large, *Microstructured polymer optical fibres*. Springer, 2007.

[44] S. W. J. Mak, "Raman Characterization of Colloidal Nanoparticles using Hollow-core Photonic Crystal Fibers," Dec. 2011.

[45] C. V. Raman and K. S. Krishnan, "A New Type of Secondary Radiation," *Nature*, vol. 121, no. 3048, pp. 501–502, Mar. 1928.

[46] M. S. Amer, "Chapter 2: Raman Spectroscopy; the Diagnostic Tool.," in *In Raman spectroscopy, Fullerenes and Nanotechnology*, UK: Royal., 2010, pp. 43–108.

[47] J. R. Ferraro, K. Nakamoto, and C. W. Brown, *Introductory Raman spectroscopy*. Academic Press, 2003.

[48] J. J. Stevenson, C. L., Vo-Dinh, T., & Laserna, *Modern Techniques in Raman Spectroscopy*, John Wiley. 1996.

[49] R. Aroca, *Surface-Enhanced Vibrational Spectroscopy*. John Wiley & Sons, 2006.

[50] N. S. Punjabi, J. Satija, and S. Mukherji, "Evanescent Wave Absorption Based Fiber-Optic Sensor - Cascading of Bend and Tapered Geometry for Enhanced Sensitivity," *Smart Sensors, Meas. Instrum.*, vol. 11, pp. 201–221, 2015.

[51] J. Satija, N. S. Punjabi, V. V. R. Sai, and S. Mukherji, "Optimal design for U-bent fiber-optic LSPR sensor probes," *Plasmonics*, vol. 9, no. 2, pp. 251–260, 2014.

[52] D. V. Lim, "Detection of microorganisms and toxins with evanescent wave fiber-optic biosensors," *Proc. IEEE*, vol. 91, no. 6, pp. 902–907, Jun. 2003.

[53] N. Zhong, Q. Liao, X. Zhu, M. Zhao, Y. Huang, and R. Chen, "Temperature-independent polymer optical fiber evanescent wave sensor," *Sci. Rep.*, vol. 5, p. 11508, Jun. 2015.

[54] S. Korposh, H. Okuda, T. Wang, S. W. James, and S.-W. Lee, "U-shaped evanescent wave optical fibre sensor based on a porphyrin anchored nanoassembled thin film for high sensitivity ammonia detection," *Proc. SPIE - Int. Soc. Opt. Eng.*, vol. 9655, pp. 1–4, 2015.

[55] T. Kundu, V. V. R. Sai, R. Dutta, S. Titas, P. Kumar, and S. Mukherjee, "Development of evanescent wave absorbance-based fibre-optic biosensor," *Pramana - J. Phys.*, vol. 75, no. 6, pp. 1099–1113, 2010.

[56] S. N. Elias, N. Arsad, and S. Abubakar, "Nitrite detection using plastic optical fiber (POF); an early stage investigation towards the development of oral cancer sensor using POF," *Opt. - Int. J. Light Electron Opt.*, vol. 126, no. 21, pp. 2908–2911, 2015.

[57] K. Miyajima, T. Koshida, T. Arakawa, H. Kudo, H. Saito, K. Yano, and K. Mitsubayashi, "Fiber-Optic Fluoroimmunoassay System with a Flow-Through Cell for Rapid On-Site Determination of Escherichia coli O157:H7 by Monitoring

Fluorescence Dynamics," *Biosensors*, vol. 3, no. 1, pp. 120–131, Mar. 2013.

[58] A. Messica, A. Greenstein, and A. Katzir, "Theory of fiber-optic, evanescent-wave spectroscopy and sensors," *Appl. Opt.*, vol. 35, no. 13, p. 2274, 1996.

[59] R. Gravina, G. Testa, and R. Bernini, "Perfluorinated plastic optical fiber tapers for evanescent wave sensing," *Sensors*, vol. 9, no. 12, pp. 10423–10433, 2009.

[60] B. D. Gupta, H. Dodeja, and A. K. Tomar, "Fibre-optic evanescent field absorption sensor based on a U-shaped probe," *Opt. Quantum Electron.*, vol. 28, no. 11, pp. 1629–1639, Nov. 1996.

[61] F. De-Jun, L. Guan-Xiu, L. Xi-Lu, J. Ming-Shun, and S. Qing-Mei, "Refractive index sensor based on plastic optical fiber with tapered structure," *Appl. Opt.*, vol. 53, no. 10, p. 2007, 2014.

[62] G. Wandemur, D. Rodrigues, R. Allil, V. Queiroz, R. Peixoto, M. Werneck, and M. Miguel, "Plastic optical fiber-based biosensor platform for rapid cell detection," *Biosens. Bioelectron.*, vol. 54, pp. 661–666, 2014.

[63] A. W. Snyder and J. D. Love, *Optical Waveguide Theory*. Boston, MA: Springer US, 1984.

[64] S. F. Memon, E. Lewis, M. M. Ali, J. T. Pembroke, and B. S. Chowdhry, "U-bend evanescent wave plastic optical fibre sensor for minute level concentration detection of ethanol corresponding to biofuel production rate," in *2017 IEEE Sensors Applications Symposium (SAS)*, 2017, pp. 1–5.

[65] G. Springsteen and B. Wang, "A detailed examination of boronic acid - diol complexation," *Tetrahedron*, vol. 58, pp. 5291–5300, 2002.

[66] G. Springsteen and B. Wang, "Alizarin Red S. as a general optical reporter for studying the binding of boronic acids with carbohydrates," *Chem. Commun.*, no. 17, pp. 1608–1609, 2001.

[67] A. Matsumoto, H. Matsumoto, Y. Maeda, and Y. Miyahara, "Simple and robust strategy for potentiometric detection of glucose using fluorinated phenylboronic acid self-assembled monolayer," *Biochim. Biophys. Acta - Gen. Subj.*, vol. 1830, no. 9, pp. 4359–4364, Sep. 2013.

[68] X. Wu, Z. Li, X.-X. Chen, J. S. Fossey, T. D. James, and Y.-B. Jiang, "Selective sensing of saccharides using simple boronic acids and their aggregates," *Chem. Soc. Rev.*, vol. 42, no. 20, p. 8032, 2013.

[69] J. Yan, G. Springsteen, S. Deeter, and B. Wang, "The relationship among pKa, pH, and binding constants in the interactions between boronic acids and diols—it is not as simple as it appears," *Tetrahedron*, vol. 60, no. 49, pp. 11205–11209, Nov. 2004.

[70] S. Himmelein and B. J. Ravoo, “A Self-Assembled Sensor for Carbohydrates on the Surface of Cyclodextrin Vesicles,” *Chem. - A Eur. J.*, vol. 23, no. 25, pp. 6034–6041, May 2017.

[71] S. Schumacher, T. Nagel, F. W. Scheller, and N. Gajovic-Eichelmann, “Alizarin Red S as an electrochemical indicator for saccharide recognition,” *Electrochim. Acta*, vol. 56, no. 19, pp. 6607–6611, Jul. 2011.

[72] E. Arrospide, G. Durana, M. Azkune, G. Aldabaldetreku, I. Bikandi, L. Ruiz-Rubio, and J. Zubia, “Polymers beyond standard optical fibres - fabrication of microstructured polymer optical fibres,” *Polym. Int.*, vol. 67, no. 9, pp. 1155–1163, Sep. 2018.

[73] N. Fortin and H. A. Klok, “Glucose monitoring using a polymer brush modified polypropylene hollow fiber-based hydraulic flow sensor,” *ACS Appl. Mater. Interfaces*, vol. 7, no. 8, pp. 4631–4640, 2015.

[74] P. C. Chen, L. S. Wan, B. B. Ke, and Z. K. Xu, “Honeycomb-patterned film segregated with phenylboronic acid for glucose sensing,” *Langmuir*, vol. 27, no. 20, pp. 12597–12605, 2011.

[75] X. Yu, D. Yong, and Y. Zhang, “Photonic Crystal Fiber-Based Biosensors,” in *Handbook of Photonics for Biomedical Engineering*, Dordrecht: Springer Netherlands, 2017, pp. 61–86.

[76] X. Yu, Y. Zhang, Y. C. Kwok, and P. Shum, “Highly sensitive photonic crystal fiber based absorption spectroscopy,” *Sensors Actuators B Chem.*, vol. 145, no. 1, pp. 110–113, Mar. 2010.

[77] Wei Chang Wong, Chi Chiu Chan, Jia Liang Boo, Zi Yong Teo, Zhi Qiang Tou, Hong Bin Yang, Chang Ming Li, and Kam Chew Leong, “Photonic Crystal Fiber Surface Plasmon Resonance Biosensor Based on Protein G Immobilization,” *IEEE J. Sel. Top. Quantum Electron.*, vol. 19, no. 3, pp. 4602107–4602107, May 2013.

[78] J. Shao, M. Lin, Y. Li, X. Li, J. Liu, J. Liang, and H. Yao, “In Vivo Blood Glucose Quantification Using Raman Spectroscopy,” *PLoS One*, vol. 7, no. 10, pp. e48127–e48127, Oct. 2012.

[79] J. L. Lambert, C. C. Pelletier, and M. Borchert, “Glucose determination in human aqueous humor with Raman spectroscopy,” *J. Biomed. Opt.*, vol. 10, no. 3, p. 031110, 2005.

[80] O. Lyandres, J. M. Yuen, N. C. Shah, R. P. VanDuyne, J. T. Walsh, M. R. Glucksberg, and M. R. Glucksberg, “Progress toward an in vivo surface-enhanced Raman spectroscopy glucose sensor,” *Diabetes Technol. Ther.*, vol. 10, no. 4, pp. 257–265, Aug. 2008.

[81] D. Yan, J. Popp, M. W. Pletz, and T. Frosch, “Fiber enhanced Raman sensing of

levofloxacin by PCF bandgap-shifting into the visible range," *Anal. Methods*, vol. 10, no. 6, pp. 586–592, 2018.

[82] D. Yan, J. Popp, M. W. Pletz, and T. Frosch, "Highly sensitive broadband Raman sensing of antibiotics in step-index hollow-core photonic crystal fibers," *ACS Photonics*, vol. 4, no. 1, pp. 138–145, 2017.

[83] F. M. Cox, A. Argyros, M. C. J. Large, and S. Kalluri, "Surface enhanced Raman scattering in a hollow core microstructured optical fiber.," *Opt. Express*, vol. 15, no. 21, pp. 13675–13681, Oct. 2007.

[84] D. Qi and A. J. Berger, "Quantitative analysis of Raman signal enhancement from aqueous samples in liquid core optical fibers," *Appl. Spectrosc.*, vol. 58, no. 10, pp. 1165–1171, 2004.

[85] R. Altkorn, I. Koev, and M. J. Pelletier, "Raman performance characteristics of Teflon-AF 2400 liquid-core optical-fiber sample cells," *Appl. Spectrosc.*, vol. 53, no. 10, pp. 1169–1176, 1999.

[86] M. J. Pelletier and R. Altkorn, "Raman sensitivity enhancement for aqueous protein samples using a liquid-core optical-fiber cell," *Anal. Chem.*, vol. 73, no. 6, pp. 1393–1397, 2001.

[87] Y. Tian, L. Zhang, J. Zuo, Z. Li, S. Gao, and G. Lu, "Raman sensitivity enhancement for aqueous absorbing sample using Teflon-AF 2400 liquid core optical fibre cell," *Anal. Chim. Acta*, vol. 581, no. 1, pp. 154–158, 2007.

[88] B. J. Marquardt, P. G. Vahey, R. E. Synovec, and L. W. Burgess, "A Raman waveguide detector for liquid chromatography," *Anal. Chem.*, vol. 71, no. 21, pp. 4808–4814, 1999.

[89] R. Altkorn, I. Koev, and A. Gottlieb, "Waveguide capillary cell for low-refractive-index liquids," *Appl. Spectrosc.*, vol. 51, no. 10, pp. 1554–1558, 1997.

[90] R. Altkorn, M. D. Malinsky, R. P. Van Duyne, and I. Koev, "Intensity considerations in liquid core optical fiber Raman spectroscopy," *Appl. Spectrosc.*, vol. 55, no. 4, pp. 373–381, 2001.

[91] D. Qi and A. J. Berger, "Quantitative concentration measurements of creatinine dissolved in water and urine using Raman spectroscopy and a liquid core optical fiber," *J. Biomed. Opt.*, vol. 10, no. 3, p. 031115, 2005.

[92] D. Yan, C. Domes, R. Domes, T. Frosch, J. Popp, M. W. Pletz, and T. Frosch, "Fiber enhanced Raman spectroscopic analysis as a novel method for diagnosis and monitoring of diseases related to hyperbilirubinemia and hyperbiliverdinemia," *Analyst*, vol. 141, no. 21, pp. 6104–6115, 2016.

[93] S. Schlücker, *Surface Enhanced Raman Spectroscopy: Analytical, Biophysical and Life Science Applications*. Weinheim, Germany: Wiley-VCH Verlag GmbH & Co.

, 2010.

[94] T. Frosch, D. Yan, and J. Popp, "Ultrasensitive Fiber Enhanced UV Resonance Raman Sensing of Drugs," *Anal. Chem.*, vol. 85, no. 13, pp. 6264–6271, Jul. 2013.

[95] J. A. West, C. M. Smith, N. F. Borrelli, D. C. Allan, and K. W. Koch, "Surface modes in air-core photonic band-gap fibers," *Opt. Express*, vol. 12, no. 8, p. 1485, Apr. 2004.

[96] H. K. Kim, M. J. F. Digonnet, G. S. Kino, J. Shin, and S. Fan, "Simulations of the effect of the core ring on surface and air-core modes in photonic bandgap fibers," *Opt. Express*, vol. 12, no. 15, p. 3436, 2004.

[97] M. J. F. Digonnet, Hyang Kyun Kim, G. S. Kino, and Shanhui Fan, "Understanding air-core photonic-bandgap fibers: analogy to conventional fibers," *J. Light. Technol.*, vol. 23, no. 12, pp. 4169–4177, Dec. 2005.

[98] Y. Huang, Y. Xu, and A. Yariv, "Fabrication of functional microstructured optical fibers through a selective-filling technique," *Appl. Phys. Lett.*, vol. 85, no. 22, pp. 5182–5184, Nov. 2004.

[99] K. Nielsen, D. Noordegraaf, T. Sørensen, A. Bjarklev, and T. P. Hansen, "Selective filling of photonic crystal fibres," *J. Opt. A Pure Appl. Opt.*, vol. 7, no. 8, pp. L13–L20, 2005.

[100] K. H. Liland, "baseline: Baseline Correction of Spectra," crane.r-project, 2018. [Online]. Available: https://cran.r-project.org/ [Accessed: 15-Feb-2019].

[101] C. S. Beleites Valter, "hyperSpec: a package to handle hyperspectral data sets in R," *cran.r-project*, vol. R package, 2018. [Online]. Available: https://cran.r-project.org/ [Accessed: 15-Feb-2019].

[102] K. J. Thomas, M. Sheeba, V. P. N. Nampoori, C. P. G. Vallabhan, and P. Radhakrishnan, "Raman spectra of polymethyl methacrylate optical fibres excited by a 532 nm diode pumped solid state laser," *J. Opt. A Pure Appl. Opt.*, vol. 10, no. 5, p. 55303, May 2008.

[103] Z. Iqbal, "Raman scattering and the electronically-induced phase transition in K3Fe(CN)6 at 130K," *J. Phys. C (Solid State Physics)*, vol. 10, no. 18, pp. 3533–3543, Sep. 1977.

[104] A. Shrivastava and V. Gupta, "Methods for the determination of limit of detection and limit of quantitation of the analytical methods," *Chronicles Young Sci.*, vol. 2, no. 1, p. 21, 2011.

[105] A. Tahara, T. Takasu, M. Yokono, M. Imamura, and E. Kurosaki, "Characterization and comparison of sodium-glucose cotransporter 2 inhibitors in pharmacokinetics, pharmacodynamics, and pharmacologic effects," *J Pharmacol Sci*, vol. 130, no. 3, pp. 159–169, 2016.

[106] R. Correia, S. James, S. W. Lee, S. P. Morgan, and S. Korposh, "Biomedical application of optical fibre sensors," *J. Opt. (United Kingdom)*, vol. 20, no. 7, 2018.

[107] S. Vigneshvar, C. C. Sudhakumari, B. Senthilkumaran, and H. Prakash, "Recent Advances in Biosensor Technology for Potential Applications – An Overview," *Front. Bioeng. Biotechnol.*, vol. 4, no. February, pp. 1–9, 2016.

[108] R. Bharadwaj, V. V. R. Sai, K. Thakare, A. Dhawangale, T. Kundu, S. Titus, P. K. Verma, and S. Mukherji, "Evanescent wave absorbance based fiber optic biosensor for label-free detection of E. coli at 280nm wavelength," *Biosens. Bioelectron.*, vol. 26, no. 7, pp. 3367–3370, Mar. 2011.

[109] S. Chaplin, "SGLT2 inhibitors and risk of genitourinary infections," *Prescriber*, vol. 27, no. 12, pp. 26–30, 2016.

[110] F. Gomez-Peralta, C. Abreu, A. Lecube, D. Bellido, A. Soto, C. Morales, M. Brito-Sanfiel, and G. Umpierrez, "Practical Approach to Initiating SGLT2 Inhibitors in Type 2 Diabetes," *Diabetes Ther*, vol. 8, no. 5, pp. 953–962, 2017.

[111] P. W. A. Willems, W. Peter Vandertop, R. M. Verdaasdonk, C. F. P. Van Swol, and G. H. Jansen, "Urine analysis by laser Raman spectroscopy," *Lasers Surg. Med.*, vol. 28, no. 4, pp. 330–334, 2001.

[112] I. Ayesta, M. Azkune, E. Arrospide, J. Arrue, G. Durana, J. Zubia, M. Illarramendi, G. Durana, and J. Zubia, "Fabrication of Active Polymer Optical Fibers by Solution Doping and Their Characterization," *Polymers (Basel).*, vol. 11, no. 1, p. 52, Dec. 2018.